AWARD NUMBER: W81XWH-16-1-0400

TITLE: Powering Up Mitochondrial Functions to Treat Mitochondrial Disease

PRINCIPAL INVESTIGATOR: Liming Pei, Ph.D.

CONTRACTING ORGANIZATION: Children's Hospital of Philadelphia, Philadelphia, PA 17104

REPORT DATE: October 2018

TYPE OF REPORT: Annual

PREPARED FOR: U.S. Army Medical Research and Materiel Command
Fort Detrick, Maryland 21702-5012

DISTRIBUTION STATEMENT: Approved for Public Release;
Distribution Unlimited

REPORT DOCUMENTATION PAGE

Form Approved
OMB No. 0704-0188

1. REPORT DATE	2. REPORT TYPE	3. DATES COVERED
October 2018	Annual	30 Sep 2017 - 29 Sep 2018

4. TITLE AND SUBTITLE

Powering Up Mitochondrial Function to Treat Mitochondrial Disease

5a. CONTRACT NUMBER

5b. GRANT NUMBER
W81XWH-16-1-0400

5c. PROGRAM ELEMENT NUMBER

6. AUTHOR(S)
Liming Pei, Ph.D.

E-Mail: peil@email.chop.edu

5d. PROJECT NUMBER

5e. TASK NUMBER

5f. WORK UNIT NUMBER

7. PERFORMING ORGANIZATION NAME(S) AND ADDRESS(ES)
Children's Hospital of Philadelphia, The
3615 Civic Center Blvd
Philadelphia, PA 19104-4318

8. PERFORMING ORGANIZATION REPORT NUMBER

9. SPONSORING / MONITORING AGENCY NAME(S) AND ADDRESS(ES)

U.S. Army Medical Research and Materiel Command
Fort Detrick, Maryland 21702-5012

10. SPONSOR/MONITOR'S ACRONYM(S)

11. SPONSOR/MONITOR'S REPORT NUMBER(S)

12. DISTRIBUTION / AVAILABILITY STATEMENT

Approved for Public Release; Distribution Unlimited

13. SUPPLEMENTARY NOTES

14. ABSTRACT

We proposed that induction of the ERRα/γ signaling pathway can enhance mitochondrial function in both cell and animal models of mitochondrial disease. Our major findings include;

1) We recently compared in detail the different mitochondrial disease animal models (under review in Cell Metabolism). We found that the compound Ant1-/-ND6 mutant mouse model exhibited the earliest and strongest mitochondrial cardiomyopathy phenotype and therefore provided the best therapeutic window for our proposed intervention research strategy.
2) We discovered that GDF15 is a heart-derived hormone whose serum level correlates positively with the severity of mitochondrial cardiomyopathy (recently published with DOD grant support acknowledged), and it can be used as a biomarker in our studies.

15. SUBJECT TERMS
Mitochondria, mitochondrial disease, cardiomyopathy, estrogen-related receptor, transcriptional regulation, mitochondrial biogenesis, signaling, iPSCs, heart disease,

16. SECURITY CLASSIFICATION OF:			17. LIMITATION OF ABSTRACT	18. NUMBER OF PAGES	19a. NAME OF RESPONSIBLE PERSON
a. REPORT	b. ABSTRACT	c. THIS PAGE			USAMRMC
Unclassified	Unclassified	Unclassified	Unclassified	54	19b. TELEPHONE NUMBER *(include area code)*

Table of Contents

Page

1. **INTRODUCTION:** We recently identified that two transcription factors, estrogen related receptor alpha (ERRα) and gamma (ERRγ), are critical transcriptional regulators of mitochondrial biogenesis and function. Loss of both cardiac ERRα and ERRγ in mice results in severe mitochondrial cardiomyopathy, heart failure and death within the first month of life. This is because that ERRα and ERRγ are both sufficient and required to induce the transcription of many genes crucial for normal mitochondrial function and biogenesis. Overexpression of ERRα and ERRγ increases mitochondrial biogenesis and function in cells. Therefore, we hypothesize that induction of the ERRα/ERRγ signaling pathway (with both genetic and pharmacological approaches) can enhance mitochondrial function in both cells and tissues, thus providing a general approach for treating a broad spectrum of mitochondrial diseases. We propose to test our hypothesis using novel animal models of mitochondrial disease we recently developed.

2. **KEYWORDS:** Mitochondria, mitochondrial disease, cardiomyopathy, estrogen related receptor, transcriptional regulation, mitochondrial biogenesis, signaling, iPSCs, heart disease

3. **ACCOMPLISHMENTS:**

- **What were the major goals of the project?**

Specific Aim 1 (specified in proposal)	**Timeline**	**% complete**
Major Task 1	**Months**	
Subtask 1: Treat mitochondrial cardiomyopathy in ND6 mutant mice	1-36	60%; **Wallace lab** has generated mice; **Pei lab** has generated virus
Subtask 2: Treat mitochondrial cardiomyopathy in CO1 mutant mice	1-36	60% **Wallace lab** has generated mice; **Pei lab** has generated virus
Milestone(s) Achieved: Successful completion of subtasks 1 and 2.	36	On track
IACUC Approval	1	100% August 09, 2016 **Wallace and Pei**
Milestone Achieved: HRPO/ACURO Approval	1	100% October 24, 2016 **Wallace and Pei**

	Specific Aim 2 (specified in proposal)		
	Major Task 2		
Subtask 1: Treat mitochondrial cardiomyopathy in Ant1-/- mice		1-36	60% **Wallace lab** has generated mice; **Pei lab** has generated virus
Milestone(s) Achieved: Successful completion of subtask 1.		36	On track
	Specific Aim 3 (specified in proposal)		
	Major Task 3		
Subtask 1: Improve mitochondrial and cellular functions in human Ant1-/- patient iPSCs-derived cardiomyocytes		13-36	50% **Pei lab**
Milestone(s) Achieved: Successful completion of subtask 1		36	On track

- **What was accomplished under these goals?**

1) Major activities: Overall we are on track to achieve our major research goals.

Aims 1 and 2: the **Wallace lab** recently published the detailed comparison of the different mitochondrial disease animal models (Mitochondrial DNA Variation Dictates Expressivity and Progression of Nuclear DNA Mutations Causing Cardiomyopathy. McManus MJ, Picard M, Chen HW, De Haas HJ, Potluri P, Leipzig J, Towheed A, Angelin A, Sengupta P, Morrow RM, Kauffman BA, Vermulst M, Narula J, **Wallace** DC. Cell Metab. 2018 Aug 23. pii: S1550-4131(18)30503-5. PMID: 30174309 also see Appendices). Based on these latest results we decided to prioritize our research efforts on the compound Ant1-/-ND6 mutant mouse model, because this model exhibited the earliest and strongest mitochondrial cardiomyopathy phenotype and therefore provided the best therapeutic window for our proposed intervention research strategy. We devoted our efforts in this model in Year 1 and 2. The **Wallace lab** have maintained breeding colonies that have generated the several cohorts of compound Ant1-/-ND6 mutant mice for our experiments. The **Pei lab** has generated the AAV9-ERRγ virus and the **Pei lab** has injected Ant1-/-ND6 mutant mice with AAV9-ERRγ virus. We are currently measuring cardiac functions in these mice. We are also injecting more mice to reach to cohort number as we originally planned.

In order to determine the most reliable and earliest outcome measure for treatment, detailed analysis of the Ant1-/-ND6 mutant heart has been performed in mice between 1.5 and 9 months of age. Results from echocardiography are shown in Table 1 and Figure 1.

	ANT1-/- ND6						
	1.5 months old (n=4)	2 months old (n=4)	2.5 months old (n=4)	3 months old (n=4)	4 months old (n=3)	7.5 months old (n=4)	9 months old (n=5)
IVS;d (mm)	1.12 ± 0.06	1.00 ± 0.05	0.98 ± 0.04	1.05 ± 0.06	1.14 ± 0.09	1.27 ± 0.06	1.11 ± 0.11
IVS;s (mm)	1.60 ± 0.08	1.42 ± 0.06	1.42 ± 0.52	1.26 ± 0.10	1.17 ± 0.13	1.42 ± 0.12	1.31 ± 0.11
LVID;d (mm)	3.57 ± 0.04	4.00 ± 0.04	4.04 ± 0.13	4.25 ± 0.05	4.58 ± 0.18	4.57 ± 0.24	5.05 ± 0.25
LVID;s (mm)	2.23 ± 0.12	2.84 ± 0.11	2.79 ± 0.07	3.49 ± 0.09	3.90 ± 0.12	3.88 ± 0.20	4.53 ± 0.28
LVPW;d (mm)	0.94 ± 0.15	0.95 ± 0.06	0.88 ± 0.07	1.21 ± 0.15	0.90 ± 0.05	1.29 ± 0.13	1.15 ± 0.09
LVPW;s (mm)	1.35 ± 0.16	1.22 ± 0.03	1.18 ± 0.08	1.41± 0.06	1.04 ± 0.11	1.38 ± 0.13	1.23 ± 0.11
CO (LV Trace) (ml/min)	17.85 ± 1.29	18.66 ± 1.35	16.87 ± 1.06	17.02 ± 1.40	15.24 ± 1.44	14.76 ±1.30	15.25 ± 2.39
EF (%)	67.75 ± 4.91	56.02 ± 4.29	59.01 ± 2.56	37.34± 3.02	31.49 ± 3.41	31.81 ±1.21	22.55 ± 4.34
FS (%)	37.42 ± 3.98	29.05 ± 2.82	30.96 ± 1.82	17.87 ± 1.63	14.84 ± 1.79	14.96 ± 0.63	10.48 ± 2.13
LV Mass (mg)	140.65 ± 11.86	155.54 ± 11.37	145.82 ± 4.02	210.06 ± 14.70	206.88 ± 22.44	280.27 ± 16.17	277.92 ± 25.54
LV Mass (Corrected) (mg)	112.52 ± 9.46	124.44 ± 9.09	116.66 ± 3.22	168.05 ± 11.76	165.50 ± 17.95	224.22 ± 12.93	222.33 ± 20.43
LV Vol;d (mm)	53.24 ± 1.45	70.05 ± 1.48	72.19 ± 5.52	80.88 ± 2.06	96.86 ± 8.95	96.90 ± 12.24	122.84 ± 13.55
LV Vol;s (mm)	17.00 ± 2.23	30.76 ± 2.86	29.35± 1.89	50.72± 2.96	66.03 ± 5.08	66.07 ± 8.28	95.96 ± 14.12
SV (LV Trace) (ul)	39.54 ± 2.76	43.08 ± 3.41	42.50 ± 4.17	36.50 ± 3.96	33.10 ± 3.57	32.95 ± 3.10	33.66 ± 5.48

•Control:	Ctrl		
	2.5 months old (n=5)	3 months old (n=5)	4 months old (n=5)
IVS;d (mm)	0.8 ± 0.03	0.84 ± 0.07	0.92 ± 0.08
IVS;s (mm)	1.10 ± 0.05	1.29 ± 0.14	1.23 ± 0.09
LVID;d (mm)	4.27 ± 0.17	4.03 ± 0.06	4.34 ± 0.12
LVID;s (mm)	3.17 ± 0.17	2.56 ± 0.12	3.29 ± 0.10
LVPW;d (mm)	0.72 ± 0.10	0.76 ± 0.06	0.76 ± 0.03
LVPW;s (mm)	1.03 ± 0.09	1.17 ± 0.11	1.00 ± 0.07
CO (LV Trace) (ml/min)	15.61 ± 1.34	22.40 ± 3.13	20.36 ± 2.55
EF (%)	50.93 ± 3.13	66.30 ± 3.79	48.14 ± 1.70
FS (%)	25.83 ± 1.91	36.50 ± 2.97	24.07 ± 1.03
LV Mass (mg)	121.48 ± 7.32	120.81 ± 12.83	144.78 ± 12.94
LV Mass (Corrected) (mg)	97.18 ± 5.86	96.65 ± 10.27	115.83 ± 10.35
LV Vol;d (mm)	82.32 ± 7.66	71.48 ± 2.63	85.16 ± 5.71
LV Vol;s (mm)	40.77 ± 5.14	24.07 ± 2.85	44.22 ± 3.59
SV (LV Trace) (ul)	45.20 ± 2.82	50.33 ± 3.74	47.01 ± 4.34

Table 1. Echocardiography Results. A) Results from Ant1-/-ND6 mutant mice at given ages. B) Results from control mice (C57B6J) at given ages. IVS;d=interventricular septal end diastole, IVS;s=interventricular septal end systole, LVID;d=left ventricular internal diameter end diastole, LVID;s= left ventricular internal diameter end diastole, LVPW;d=Left ventricular posterior wall end diastole, LVPW;s=Left ventricular posterior wall end systole, CO=cardiac output, EF=ejection fraction, FS=fraction shortening, LV Vol;d= left ventricular volume diastolic, , LV Vol;s= left ventricular volume systolic, SV= Stroke volume

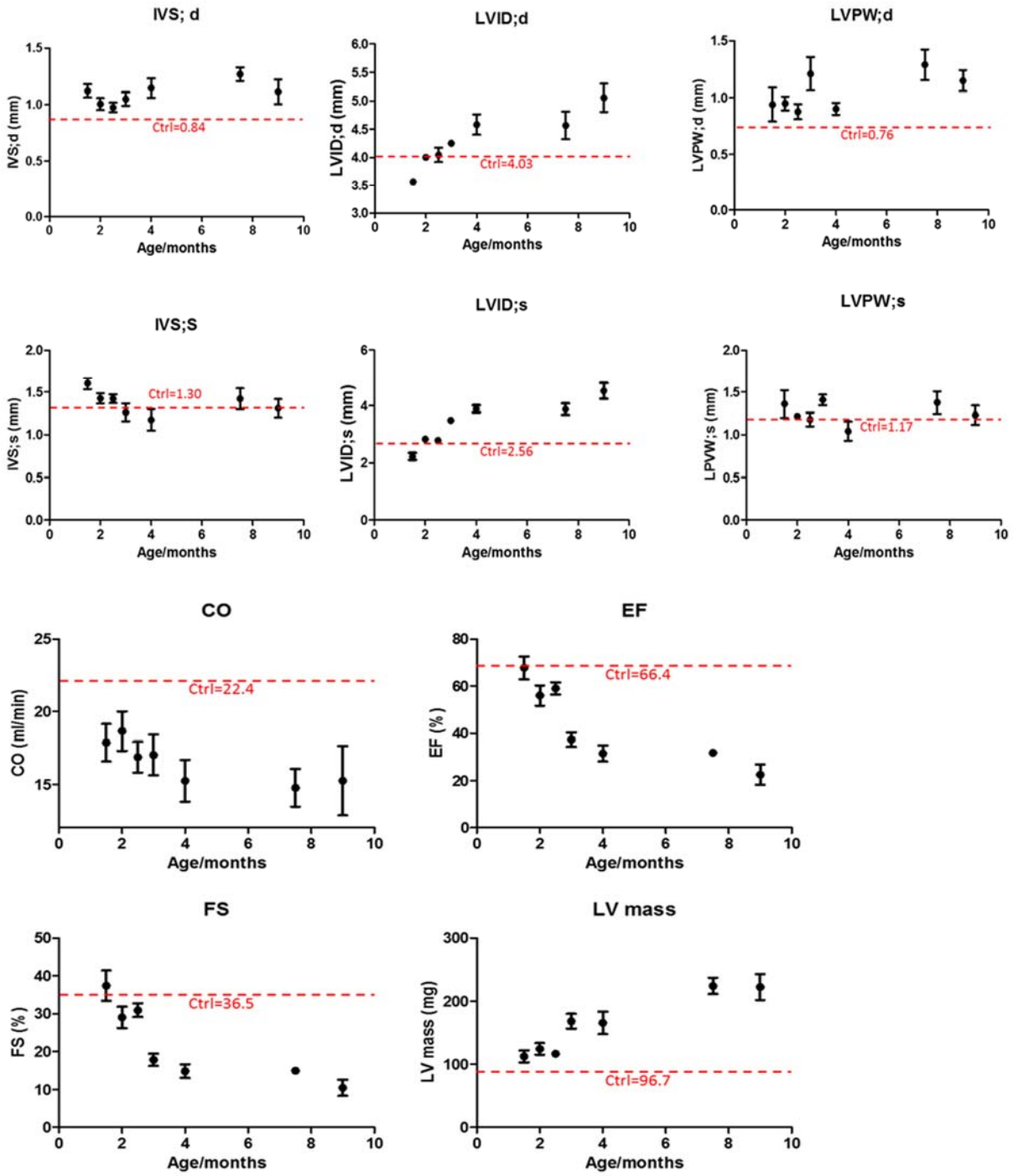

Figure 1. Echocardiography of Ant1-/-ND6 mutant mice. IVS;d=interventricular septal end diastole, IVS;s=interventricular septal end systole, LVID;d=left ventricular internal diameter end diastole, LVID;s= left ventricular internal diameter end diastole, LVPW;d=Left ventricular posterior wall end diastole, LVPW;s=Left ventricular posterior wall end systole, CO=cardiac output, EF=ejection fraction, FS=fraction shortening, LV Vol;d= left ventricular volume diastolic, LV Vol;s= left ventricular volume systolic, SV= Stroke volume

These experiments demonstrate that the Ant1-/-ND6 mutants present with cardiac changes by three months of age. These results have informed the therapeutic experiments, and the Pei lab is now injecting AAV9-ERRγ into control and Ant1-/-ND6 mutant mice at 2 time points: 1 month of age via ultrasound-assisted injection, and 3 days of age via direct pericardial injection. We expect to complete all studies in Aim 1 and 2 by end of Year 3.

Aim 3: **Pei lab** has initiated studies in Aim 3 using Ant1-/- iPSC-derived cardiomyocytes. We have measured and evaluated mitochondrial functions in control and ERRγ overexpressed cardiomyocytes. Our initial results show that ERRγ increases mitochondrial membrane potential (Figure 2) and calcium signaling (Figure 3), supporting our hypothesis that ERRγ may increase mitochondrial functions in Ant1-/- cells. We are currently completing experiments to measure other aspects of mitochondrial functions (respiration, morphology, etc) as we originally proposed. We expect to complete all studies in Aim 3 by end of Year 3.

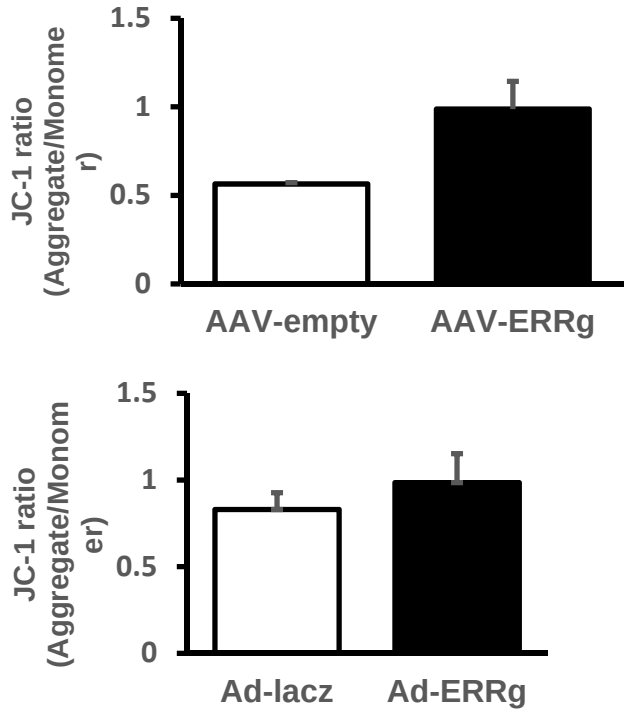

Figure 2. Membrane potential in Ant1-/- iPSCs transduced with AAV9-ERRγ. Membrane potential in Ant1-/- iPSCs was measured using JC-1 dye.

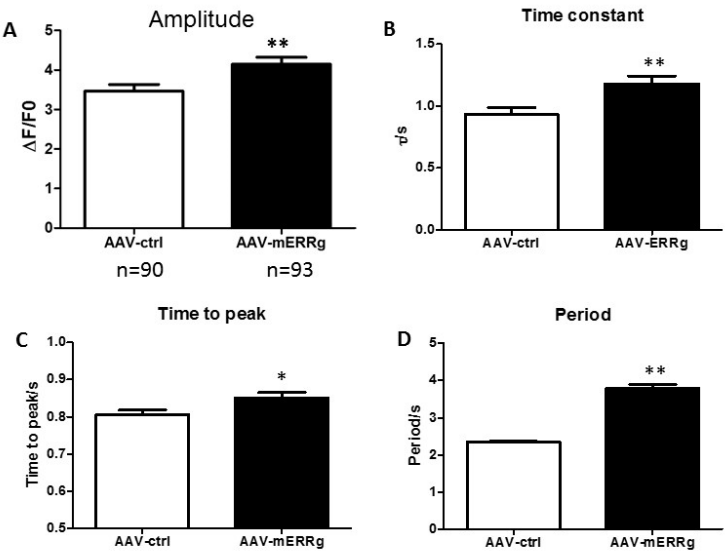

Figure 3. Calcium transients measured in Ant1-/- iPSCs transduced with AAV9-ERRγ. (A) fluorescence normalized to baseline. (B) time constant. (C) time to peak. (D) period. F: fluorescence; Fo: baseline fluorescence

2) Specific objectives: In addition to aforementioned progress in major activities, **Pei and Wallace** together have successfully achieved milestones of institute IACUC protocol and ACURO approvals on time.

3) Significant results and key outcomes:

- **Pei lab** has previously discovered that GDF15 is a heart-derived hormone that regulates body growth. Circulating GDF15 level correlates positively with the severity of mitochondrial cardiomyopathy and can be used as a serum biomarker for our mitochondrial disease studies. **Pei lab** has further identified the molecular mechanism of GDF15 upregulation in mitochondrial cardiomyopathy. This work was just published (see appendices) and the DOD grant support was acknowledged. We will take advantage of these new findings and monitor serum GDF15 level as an additional, more convenient and less invasive method to determine whether mitochondrial cardiomyopathy was ameliorated by ERRγ overexpression and activation (Aims 1 and 2). **Pei lab** has also published a paper discovering that ERRγ is important to maintain mitochondrial functions in the kidney, another organ often affected in mitochondrial disease (see appendices).
- **Wallace lab** recently published results of the different mitochondrial disease animal models (see Appendices). We found that the compound Ant1-/-ND6 mutant mouse model exhibited the earliest and strongest mitochondrial cardiomyopathy phenotype and therefore provided the best therapeutic window for our proposed intervention research strategy.

4) Other accomplishments: Our recent publications in Year 2 that are supported by this DOD grant are attached in the appendices.

- **What opportunities for training and professional development has the project provided?**

  - Training: Dr. Zhao has received one-on-one training in iPSC technology, gene editing and single cell or nucleus RNA-Seq.
  - Professional Development: Dr. **Pei** attended the United Mitochondrial Disease Foundation annual meeting in Nashville, June 27-30, 2018. He met with many fellow researcher in mitochondrial disease. He also met many mitochondrial disease patients and family members and learned more about their life. He is eager to continue to contribute to our cause to cure mitochondrial disease one day.

- How were the results disseminated to communities of interest?

  First, the Pei and Wallace labs have published series of papers on or related to ERRγ and mitochondrial functions:

  - The **Pei lab** has published several papers:
    - Zhao J, Lupino K, Wilkins BJ, Qiu C, Liu J, Omura Y, Allred AL, McDonald C, Susztak K, Barish GD, **Pei L**. (2018) Genomic integration of ERRγ-HNF1β regulates renal bioenergetics and prevents chronic kidney disease. Proceedings of National Academy of Sciences *115*, E4910-E4919. PMID: 29735694.
    - Li J, Liu J, Lupino K, Liu X, Zhang L, **Pei L**. (2018) GDF15 maturation requires proteolytic cleavage by PCSK3, 5 and 6. Molecular and Cellular Biology. PMID: 30104250.
    - Hu P, Liu J, Zhao J, Wilkins BJ, Lupino K, Wu H, **Pei L**. (2018). Single-nucleus transcriptomic survey of cell diversity and functional remodeling in the postnatal developing hearts. Genes & development 32, 1344-1357. PMID: 30254108.
  - The **Wallace lab** has published a manuscript in Cell Metabolism that described the cardiac phenotype of mice with combined mutations in mitochondrial and nuclear genes.
    - Mitochondrial DNA Variation Dictates Expressivity and Progression of Nuclear DNA Mutations Causing Cardiomyopathy. McManus MJ, Picard M, Chen HW, De Haas HJ, Potluri P, Leipzig J, Towheed A, Angelin A, Sengupta P, Morrow RM, Kauffman BA, Vermulst M, Narula J, **Wallace DC**. Cell Metab. 2018 Aug 23. pii: S1550-4131(18)30503-5. PMID:30174309

- Drs. **Pei and Wallace** together published a review of mitochondria and disease:
  - **Pei L**, **Wallace DC** (2018). Mitochondrial Etiology of Neuropsychiatric Disorders. Biological psychiatry 83, 722-730. PMID: 29290371. PMCID: PMC5891364

In addition, Drs. **Pei and Wallace** have been invited to give talks in numerous national/international meetings and in academic institutions about their work on this topic (please see below in "6. PRODUCTS)

- What do you plan to do during the next reporting period to accomplish the goals?

We plan to finish all proposed goals and experiments in all research aims. For Aims 1 and 2, the Pei lab will complete injecting AAV9-ERRγ to all Ant1-/-ND6 mutant mice as planned, and the Pei lab will measure their cardiac functions periodically to determine whether overexpression of ERRγ improves cardiac function in these mice. For Aim 3 the Pei and Wallace labs will complete studies to determine whether ERRγ overexpression has improved mitochondrial functions in Ant1-/- iPSC-differentiated cardiomyocytes.

4. IMPACT:

- What was the impact on the development of the principal discipline(s) of the project?

The **Pei lab** has recently discovered that GDF15 is a heart-derived hormone that regulates body growth. Circulating GDF15 level correlates positively with the severity of mitochondrial cardiomyopathy and can be used as a serum biomarker for our mitochondrial disease studies. The **Pei lab** has further identified the molecular mechanism of GDF15 upregulation in mitochondrial cardiomyopathy. This work was just published (see appendices) and the DOD grant support was acknowledged. We will take advantage of these new findings and monitor serum GDF15 level as an additional, more convenient and less invasive method to determine whether mitochondrial cardiomyopathy was ameliorated by ERRγ overexpression and activation (Aims 1 and 2). **Pei lab** has also published a paper discovering that ERRγ is important to maintain mitochondrial functions in the kidney, another organ often affected in mitochondrial disease (see appendices).

- **What was the impact on other disciplines?**

The **Pei lab** recently discovered that GDF15 is a heart-derived hormone that regulates body growth. Pediatric heart disease induces GDF15 synthesis and secretion by cardiomyocytes. Circulating GDF15 in turn acts on the liver to inhibit growth hormone (GH) signaling and body growth. We demonstrate that blocking cardiomyocyte production of GDF15 normalizes circulating GDF15 level and restores liver GH signaling, establishing GDF15 as a bona fide

heart-derived hormone that regulates pediatric body growth. Importantly, plasma GDF15 is further increased in children with concomitant heart disease and failure to thrive (FTT). Together these studies reveal a new endocrine mechanism by which the heart coordinates cardiac function and body growth. Our results also provide a potential mechanism for the well-established clinical observation that children with heart diseases often develop FTT. The **Pei lab** has further identified the molecular mechanism of GDF15 upregulation in mitochondrial cardiomyopathy. This work was just published (see appendices) and the DOD grant support was acknowledged. We will take advantage of these new findings and monitor serum GDF15 level as an additional, more convenient and less invasive method to determine whether mitochondrial cardiomyopathy was ameliorated by ERRγ overexpression and activation (Aims 1 and 2). The **Pei lab** has also published a paper discovering that ERRγ is important to maintain mitochondrial functions in the kidney, another organ often affected in mitochondrial disease (see appendices).

- **What was the impact on technology transfer?**

Nothing to Report

- **What was the impact on society beyond science and technology?**

Johnson & Johnson named Douglas Wallace, Ph.D. winner of the 2017 Dr. Paul Janssen Award for Biomedical Research, and launched a campaign for champions of science as part of the Dr. Paul Janssen Project – a new year-long, multi-faceted program to recognize the impact of science on humanity. Dr. Wallace won for his pioneering work in the field of mitochondrial genetics, and joined 14 other scientists who have received the Dr. Paul Janssen Award in the past 13 years, including two who went on to win the Nobel Prize. The ceremony included a talk by Dr. Wallace on the importance of the mitochondria in health and disease.

5. CHANGES/PROBLEMS:

- **Changes in approach and reasons for change**

As detailed above, we have prioritized the compound Ant1-/-ND6 mutant mouse model based on our latest research results. This model exhibited the earliest and strongest mitochondrial cardiomyopathy phenotype and therefore provided the best therapeutic window for our proposed intervention research strategy. We devoted our efforts in this model in Year 2 and moving forward. We also prioritized AAV9 to deliver ERRγ using two different approaches

(ultrasound guided injection in adult mice, or pericardial injection in newborn mice) against the pharmacological activation of ERRγ as we are still determining the optimal dose.

- **Changes that had a significant impact on expenditures**

Nothing to report

- **Significant changes in use or care of human subjects, vertebrate animals, biohazards, and/or select agents**

Nothing to report

- **Significant changes in use or care of human subjects**

Nothing to report

- **Significant changes in use or care of vertebrate animals.**

Nothing to report

- **Significant changes in use of biohazards and/or select agents**

Nothing to report

6. PRODUCTS:

- **Publications, conference papers, and presentations**
  - **Journal publications.**

The **Pei lab** has published several papers:

- Zhao J, Lupino K, Wilkins BJ, Qiu C, Liu J, Omura Y, Allred AL, McDonald C, Susztak K, Barish GD, **Pei L**. (2018) Genomic integration of ERRγ-HNF1β regulates renal bioenergetics and prevents chronic kidney disease. Proceedings of National Academy of Sciences *115*, E4910-E4919. PMID: 29735694.
- Li J, Liu J, Lupino K, Liu X, Zhang L, **Pei L**. (2018) GDF15 maturation requires proteolytic cleavage by PCSK3, 5 and 6. Molecular and Cellular Biology. PMID: 30104250.
- Hu P, Liu J, Zhao J, Wilkins BJ, Lupino K, Wu H, **Pei L**. (2018). Single-nucleus transcriptomic survey of cell diversity and functional remodeling in the postnatal developing hearts. Genes & development 32, 1344-1357. PMID: 30254108.

The **Wallace lab** has published a manuscript in Cell Metabolism that described the cardiac phenotype of mice with combined mutations in mitochondrial and nuclear genes.

- Mitochondrial DNA Variation Dictates Expressivity and Progression of Nuclear DNA Mutations Causing Cardiomyopathy. McManus MJ, Picard M, Chen HW, De Haas HJ,

Potluri P, Leipzig J, Towheed A, Angelin A, Sengupta P, Morrow RM, Kauffman BA, Vermulst M, Narula J, **Wallace DC**. Cell Metab. 2018 Aug 23. pii: S1550-4131(18)30503-5. PMID:30174309

Drs. **Pei and Wallace** together published a review of mitochondria and disease:

- **Pei L**, **Wallace DC** (2018). Mitochondrial Etiology of Neuropsychiatric Disorders. Biological psychiatry 83, 722-730. PMID: 29290371. PMCID: PMC5891364

- **Books or other non-periodical, one-time publications.**

Nothing to report

- **Other publications, conference papers, and presentations.**
  - **Liming Pei presentations**
    - 09/2017, Inaugural Canadian Mitochondrial Disease Conference, Toronto, Canada. "A heart-derived hormone that connects failure to thrive to mitochondrial disease"
    - 10/2017, Institute for Diabetes and Obesity (IDO), Helmholtz Zentrum München, Munich, Germany, "Listen to your heart – a heart-derived hormone that regulates body growth"
    - 01/2018, Department of Biochemistry & Molecular Medicine, University of California, Davis. Sacramento, CA. "Listen to your heart – a heart-derived hormone that regulates body growth"
    - 06/2018, Center for Pharmacogenetics, Department of Pharmaceutical sciences, University of Pittsburgh, Pittsburgh, PA. "Listen to your heart – a heart-derived hormone that regulates body growth"
    - 06/2018, Gordon Research Conference – Cardiac Regulatory Mechanism, New London, NH. "Single-nucleus transcriptomic survey of cell diversity and functional maturation in the postnatal mammalian hearts"
    - 08/2018, Department of Molecular Biology, UT Southwestern Medical Center, Dallas, TX. "Cardiac endocrinology – heart-derived hormones in physiology and disease"
    - 09/2018, Molecular Metabolism Seminar Series, David Geffen School of Medicine at UCLA, Los Angeles, CA. "Cardiac endocrinology – heart-derived hormones in physiology and disease"
    - 09/2018, Department of Medicine, Northwestern University, Chicago, IL. "Listen to your heart – a heart-derived hormone that regulates body growth"

Doug Wallace presentations

- Sept, 2017 "Mitochondrial DNA Variation in Human Evolution and Disease", Mitochondrial Evolutionary Genomics Conference Keynote Speaker, Ein Gedi, Israel
- Sep, 2017 "The Mitochondrion: Our Origins – Our Diseases", 2017 Dr. Paul Janssen Award Symposium, New York City, NY
- Sep, 2017 "A Mitochondrial Etiology of Metabolic and Degenerative Diseases", The Canada Mitochondrial Network and MitoCanada Foundation, Toronto, Canada
- Oct, 2017 "The Mitochondrion: Our Origins – Our Diseases", Genetics and Complex Diseases, Harvard Chan School, Boston, MA
- Oct, 2017 "A Mitochondrial Etiology of Complex Diseases", University of Pennsylvania Perelman School of Medicine, Department of Cardiovascular Institute Seminar Series, Philadelphia, PA
- Oct, 2017 "Mitochondria: Our Origins-Our Diseases", Cornell University, Ithaca, NY
- Oct, 2017 "Our Origins-Our Diseases: The Mitochondrial Perspective", Golden Sages Lecture, Bryn Mawr College, Bryn, Mawr, PA
- Oct, 2017 "A Mitochondrial Etiology of Complex Diseases and Associated Inflammation", University of Pennsylvania Perelman School of Medicine, Penn Transplant Institute Research Lecture, Philadelphia, PA
- Oct, 2017 "Mitochondria: Our Origins-Our Diseases", the 12th Annual International Conference in Genomics, Shenzhen, China
- Nov, 2017 "Mitochondrial Variation in Metabolic and Degenerative Diseases, Cancer, & Aging", University of Chicago Cancer Biology Seminar Series, Chicago, IL
- Nov, 2017 "Mitochondrial Genetic Variation in Human Evolution and Disease", Cleveland Clinic, Cleveland, OH
- Dec, 2017 "Mitochondrial Genetics and Disease Risk: What Is the Current Evidence?", Nutrigenomics and the Future of Nutrition-Food Forum Meeting at the National Academy of Sciences, Washington, DC
- Jan, 2018 "A Mitochondrion Etiology of the Common "Complex" Diseases", Rutgers Cancer Center, New Brunswick, NJ
- Jan, 2018 "A Mitochondrial Etiology of Neuroophthalmological Diseases", Basic Science Course in Ophthalmology at Columbia University
- Jan, 2018 "A Mitochondrion Etiology of the Common "Complex" Diseases", 2018 Inaugural Mitochondrial Medicine Distinguished Lecture at Columbia University
- Feb, 2018 "A Mitochondrial Etiology Of The Common 'Complex' Diseases", University of California San Diego at the Rady Children's Hospital of San Diego, San Diego, CA
- March, 2018 "The Enigma of Traditional Eastern Medicine", Bench to Bedside Research Symposium, University of California, Irvine Medical School, Irvine, CA
- April, 2018 "Why Can't We Understand and Cure the Common Diseases? An Energyomics Perspective", Keynote Speaker at the American Council of Life Insurers Genetics Symposium (ACLI), Washington, DC
- April, 2018 "Mitochondrial Genetic Variation in Human Evolution and Disease", the First AsiaEvo Conference, Shenzhen, China
- April, 2018 "Mitochondria from Evolution to Disease: It's in the Genes", the 2018 AUA-IARS Joint Symposium: Mitochondria and Bioenergetics in Health and

Disease: It's Not Just a Power Failure, Chicago, IL

- ❖ May, 2018 "Mitochondrial Etiology of Common Diseases", the University of Arkansas Seminar, Fayetteville, AR
- ❖ May, 2018 "Mitochondrial in the Etiology of Traumatic, Acute, and Chronic Disease", the Center for Injury Research and Prevention Guest Lecture at Children's Hospital of Philadelphia, Philadelphia, PA
- ❖ May, 2018 "Mitochondrial biology in disease and modern medicine", the American Thoracic Society International Conference, San Diego, CA
- ❖ May, 2018 "A Mitohcondrial Etiology of Common "Complex" Diseases", the International Conference on Subcellular Organelles 2018 at the Shanghai International Convention Center, Shanghai, China
- ❖ May, 2018 "A Mitochondrial Etiology of Common Disease", Institute of Genetics Zhejiang University, Huanzhou, China.
- ❖ June, 2018 "Mitochondrial Biophysics and the Etiology of Disease", Britten Chance Symposium, U. Pennsylvania
- ❖ June, 2018 "A Mitochondrial Etiology of Common Diseses", Marsh Lecture in Molecular Medicine, Feinstein Institute of Biomedical Research, Northwell Hospital System, Manhasset, NY.
- ❖ June, 2018 "A Mitochondrial Etiology of Common Diseases" 2018 International Symposium in Biomedical Sciences, China Medical University, Taichung, Taiwan.
- ❖ June, 2018 "Clinical Implication of Mitochondrial Medicine" Changhua Christian Hospital, Taichung, Taiwan.
- ❖ July, 2018 "Clinical Implication of Mitochondrial Medicine" 60th Anniversary Celebration of the Department of Genetics, Stanford University, Palo Alto, CA.
- ❖ August, 2018 "A Mitochondrial Etiology of Cardiovascular Disease", "Clinical Implication of Mitochondrial Medicine", NHLBI, Bethesda, MD
- ❖ August, 2018 "A mitochondrial Etiology of Common Diseases", 20th European Bioenergetics Conference (EBEC2018), Budapest, Hungary.

o

- **Website(s) or other Internet site(s)**

  www.mitomap.org. MITOMAP reports published and unpublished data on human mitochondrial DNA variation. Currently our variant tables report frequencies from 30589 human mitochondrial DNA sequences.

- **Technologies or techniques**

  nothing to report

- **Inventions, patent applications, and/or licenses**

  nothing to report

- **Other Products**

  nothing to report

7. PARTICIPANTS & OTHER COLLABORATING ORGANIZATIONS

- **What individuals have worked on the project?**

Name:	*Douglas C. Wallace, Ph.D.*
Project Role:	*No change*
Name:	*Liming Pei, Ph.D.*
Project Role:	*No change*
Name:	*Deborah G. Murdock, Ph.D.*
Project Role:	*No change*
Name:	*Jesus Tintos Hernandez, Ph.D.*
Project Role:	*Postdoctoral fellow*
Nearest person month worked:	*3*
Contribution to Project:	*Dr. Hernandez has been instrumental in creation and maintenance of iPSCs*
Name:	*Juanjuan Zhao, Ph.D.*
Project Role:	*Postdoctoral fellow*
Nearest person month worked:	*12*
Contribution to Project:	*Dr Zhao has been responsible for designing and producing AAV9-ERR viruses and evaluating cardiac function both in animal (Aims 1 and 2) and cell (Aim 3) models of mitochondrial disease.*
Funding Support:	
Name:	*Katherine Lupino*
Project Role:	*Research technician*

Nearest person month worked:	*10*
Contribution to Project:	*Miss Lupino has provided technical support in maintain mouse colonies and cell cultures. Miss Lupino replaced Caitlin McDonald*
Funding Support:	
Name:	*Arrienne Butic*
Project Role:	*Research technician*
Nearest person month worked:	*1*
Contribution to Project:	*Ms Butic has replaced D Rittenhouse as the research technician responsible for mouse husbandry.*
Funding Support:	
Name:	*Jian Liu*
Project Role:	*Postdoctoral fellow*
Nearest person month worked:	*1*
Contribution to Project:	*Dr. Jian Liu has been responsible for working with and assisting Dr. Juanjuan Zhao in designing and producing AAV9-ERRγ viruses and evaluate cardiac function both in animal (Aims 1 and 2) and cell (Aim 3) models of mitochondrial disease.*

- **Has there been a change in the active other support of the PD/PI(s) or senior/key personnel since the last reporting period?**

  No changes for other active research support for Dr. Liming Pei

Changes for other active research support for Dr. Douglas are:

- 5R01-NS021328-30 (PI D. Wallace) 04/01/13 – 03/31/18 1.2 calendar months
  National Institutes of Health (NIH) $261,528
  Mitochondrial Inborn Errors of Metabolism
  This project will investigate the genetics of maternally inherited neurological diseases.
  Role: PI
  There is no scientific or budgetary overlap. This grant has ended since the last reporting period.

- 100041003 (PI D. Wallace) 10/01/14 – 12/31/17 0.24 calendar months
  GlaxoSmithKline $119,048
  Mitochondria and Chronic Obstructive Pulmonary Disease: A LHON Connection
  This project will investigate how mtDNA cybrids can be used to test the efficacy of increasing antioxidant defenses by activation of Nrf2 of reducing mtDNA oxidative damage by over expression of OGG1.
  Role: PI
  There is no scientific or budgetary overlap. This grant has ended since the last reporting period.

- N/A (PI Atif Towheed/D. Wallace) 07/01/15 – 07/31/18 1.2 calendar months
  United Mitochondrial Disease Foundation $35,000
  Allotopic RNA Rescue of LHON Mouse Models
  This project will investigate the use of a novel gene therapy approach in correcting the mutant phenotype in a LHON mouse model
  Role: Fellowship Grant
  There is no scientific or budgetary overlap. **This grant has been extended**

- **What other organizations were involved as partners?**

Nothing to Report

AMERICAN SOCIETY FOR MICROBIOLOGY | Molecular and Cellular Biology®

RESEARCH ARTICLE

Growth Differentiation Factor 15 Maturation Requires Proteolytic Cleavage by PCSK3, -5, and -6

Jing Jing Li,[a,b] Jian Liu,[a,b] Katherine Lupino,[a,b] Xueyuan Liu,[c] Lili Zhang,[c] Liming Pei[a,b,d]

[a]Center for Mitochondrial and Epigenomic Medicine, Children's Hospital of Philadelphia, Philadelphia, Pennsylvania, USA

[b]Department of Pathology and Laboratory Medicine, Children's Hospital of Philadelphia, Philadelphia, Pennsylvania, USA

[c]Research Vector Core, Center for Cellular and Molecular Therapeutics, Children's Hospital of Philadelphia, Philadelphia, Pennsylvania, USA

[d]Department of Pathology and Laboratory Medicine, Perelman School of Medicine, University of Pennsylvania, Philadelphia, Pennsylvania, USA

ABSTRACT Growth differentiation factor 15 (GDF15) is a secreted protein with pleotropic functions from the transforming growth factor β (TGF-β) family. GDF15 is synthesized as a precursor and undergoes proteolytic cleavage to generate mature GDF15. The strong appetite-suppressing effect of mature GDF15 makes it an attractive therapeutic agent/target for diseases such as obesity and cachexia. In addition, clinical studies indicate that circulating, mature GDF15 is an independent biomarker for heart failure. We recently found that GDF15 functions as a heart-derived hormone that inhibits liver growth hormone signaling and postnatal body growth in the pediatric period. However, little is known about the mechanism of GDF15 maturation, in particular the enzymes that mediate GDF15 precursor cleavage. We investigated which candidate proteases can cleave GDF15 precursor and generate mature GDF15 in cardiomyocytes *in vitro* and mouse hearts *in vivo*. We discovered that three members of the proprotein convertase, subtilisin/kexin-type (PCSK) family, namely, PCSK3, PCSK5, and PCSK6, can efficiently cleave GDF15 precursor, therefore licensing its maturation both *in vitro* and *in vivo*. Our studies suggest that PCSK3, -5, and -6 mediate a crucial step of GDF15 maturation through proteolytic cleavage of the precursor. These results also reveal new targets for therapeutic application of GDF15 in treating obesity and cachexia.

KEYWORDS GDF15, PCSK, heart disease, cardiomyocytes, cardiac endocrinology

Growth differentiation factor 15 (GDF15; also known as MIC-1, NAG-1, PTGFB, PDF, and PLAB) is a distant member of the transforming growth factor β (TGF-β) family (1–7). Basal tissue expression of *Gdf15* is low except in the placenta and prostate, but its expression can be induced in pathological conditions (5, 8). In particular, an elevated serum GDF15 level has been found in heart disease patients and is associated with increased morbidity and mortality. GDF15 is therefore used as an independent biomarker for heart disease, especially heart failure (9, 10). We recently discovered GDF15 as a heart-derived hormone that regulates postnatal body growth (11). Cardiac *Gdf15* expression is highly induced in pediatric heart disease, and circulating GDF15 acts on the liver to inhibit growth hormone signaling and body growth. Plasma GDF15 is increased in children with concomitant heart disease and failure to thrive (FTT), providing a potential explanation for the well-established clinical observation that children with heart diseases often develop FTT. In addition, it was recently shown that GDF15 suppresses appetite via activating its receptor GFRAL in the brain stem (12–17). GDF15 is currently being explored as a potential therapeutic agent or target for a

Received 16 May 2018 **Returned for modification** 1 June 2018 **Accepted** 1 August 2018

Accepted manuscript posted online 13 August 2018

Citation Li JJ, Liu J, Lupino K, Liu X, Zhang L, Pei L. 2018. Growth differentiation factor 15 maturation requires proteolytic cleavage by PCSK3, -5, and -6. Mol Cell Biol 38:e00249-18. https://doi.org/10.1128/MCB.00249-18.

Address correspondence to Liming Pei, lpei@pennmedicine.upenn.edu.

J.J.L. and J.L. contributed equally to this article.

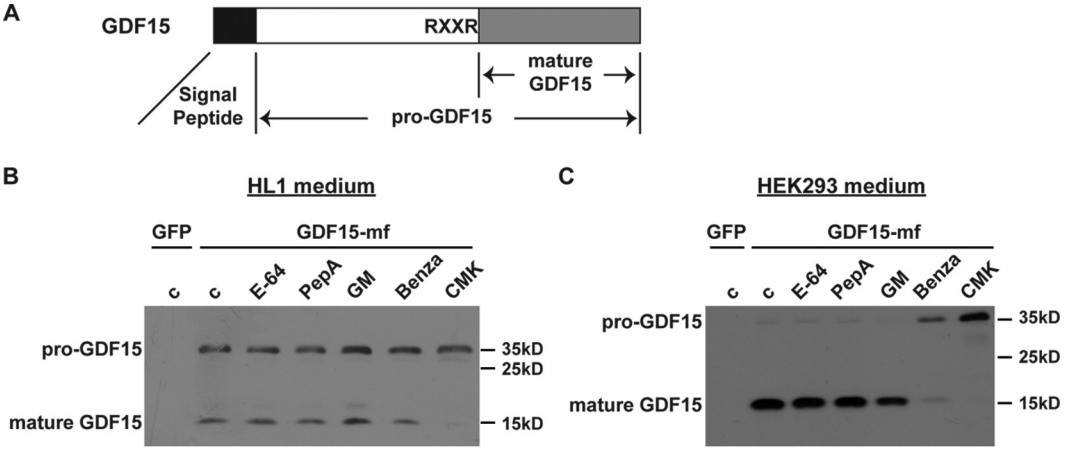

FIG 1 pro-GDF15 is cleaved by the PCSK family of proteases. (A) Schematic diagram of pre-pro-GDF15 with its canonical RXXR cleavage site shown. (B and C) Representative Western blot images showing pro-GDF15 and mature GDF15 in media of HL1 cardiomyocytes (B) and HEK293 cells (C) transfected with GDF15-mf plasmid and treated with different protease inhibitors. GDF15-mf, C-terminal myc-FLAG-tagged pre-pro-GDF15; c, control; PepA, pepstatin A; GM, GM-6001; Benza, benzamidine; CMK, decanoyl-RVKR-CMK.

variety of indications, including obesity, metabolic disease, anorexia, and cancer cachexia.

So far, most studies on GDF15 have focused on its biological function and disease biomarker implications. The biochemical properties of the GDF15 protein itself remain little understood. Like many other protein hormones, GDF15 protein is synthesized as a biologically inactive precursor protein (pre-pro-GDF15), with an N-terminal signal peptide important for its intracellular trafficking and secretion (Fig. 1A). After removal of the signal peptide, the remaining GDF15 propeptide (pro-GDF15; ~30 kDa) undergoes proteolytic cleavage to yield the C-terminal mature GDF15 (~13 kDa), which forms a homodimer as the major secreted form of GDF15 found in serum (18). However, the enzymes responsible for the proteolytic processing and generation of mature GDF15 remain elusive.

The mammalian proprotein convertase, subtilisin/kexin-type (PCSK) proteins are a family of serine proteinases that share homology with bacterial enzyme subtilisin and yeast enzyme kexin (19, 20). Among the nine mammalian PCSK enzymes, PCSK9 is well known for its role in cleaving and degrading low-density lipoprotein receptor (LDLR), which is crucial in cholesterol metabolism (21). Antibodies targeting PCSK9 (Praluent and Repatha) constitute the latest therapy for hypercholesterolemia and heart disease by significantly reducing serum LDL and the risk of cardiovascular events (22). The substrates of PCSK8 (also known as SKI-1/S1P) include sterol-regulated element binding proteins (SREBPs), brain-derived neurotrophic factor (BDNF), and somatostatin. PCSK1 to -7 recognize and cleave right after the basic residues Arg/Lys-X_{2n}-Arg/Lys$\downarrow$ (R/KX_{2n}R/K, where X is any amino acid and $n = 0$ to 3). They are essential for the cleavage and maturation of many secreted proteins, including important hormones (i.e., insulin, glucagon, and adrenocorticotropic hormone [ACTH]). Intriguingly, PCSK3 (also known as furin) has been reported as the major enzyme for TGF-β family proteins TGF-β and bone morphogenetic protein 10 (23, 24). In addition, GDF15 contains the canonical RXXR sequence right before the cleavage site, which can be recognized by PCSK1 to -7. These observations raised the possibility that one or more of the PCSK enzymes are responsible for the cleavage and maturation of GDF15.

In this study, we investigated the mechanisms of GDF15 maturation in cardiomyocytes, in which it is highly induced under the condition of heart disease. We found that PCSK3, PCSK5, and PCSK6 can efficiently cleave pro-GDF15 for maturation both *in vitro* and *in vivo*. These results revealed the long-sought identity of the enzymes responsible

for GDF15 maturation and uncovered novel means for therapeutic application of GDF15 in treating metabolic disease, anorexia, and cachexia.

RESULTS

PCSK3, -5, and -6 cleave pro-GDF15 into the mature form *in vitro*. To determine the enzyme class that cleaves pro-GDF15, we expressed mouse C-terminal myc-FLAG-tagged pre-pro-GDF15 (GDF15-mf) in HL1 mouse cardiomyocytes or HEK293 human embryonic kidney cells. These cells expressed little endogenous GDF15, making them a good system for analysis. We then treated the cells with different classes of protease inhibitors: cysteine protease inhibitor E-64, aspartyl protease inhibitor pepstatin, broad-spectrum matrix metalloprotease inhibitor GM-6001, serine protease inhibitor benzamidine, and pan-PCSK inhibitor decanoyl-RVKR-CMK. Western blot analysis revealed that both benzamidine and CMK could inhibit the processing of pro-GDF15 (decreased ratio of mature GDF15 to pro-GDF15), while the other classes of protease inhibitors had no effect (Fig. 1B and C). These results suggest that GDF15 is cleaved by one or more PCSK family members in these cells.

To determine the specific PCSK protein that cleaves GDF15, we expressed individual PCSK proteins together with pre-pro-GDF15 in HL1 or HEK293 cells. Western blot analysis showed that only PCSK3, PCSK5, and PCSK6 (also known as PACE4) effectively processed pro-GDF15 into mature GDF15 (Fig. 2A). All the other PCSK members exhibited no GDF15-processing capability. To ensure that all PCSK proteins are expressed at comparable levels, we also performed these experiments using tagged PCSK vectors, and we obtained the same results (Fig. 2B). These results suggest that PCSK3, PCSK5, and PCSK6 are cell-type-independent enzymes that process pro-GDF15 into the mature form.

We next investigated whether the PCSK recognition sequence RXXR in pro-GDF15 (ending at position 188 in mouse and position 193 in human pre-pro-GDF15) is essential for its processing. We mutated the last Arg to Gln (R188Q) to disrupt this RXXR motif. While coexpression of PCSK3, PCSK5, or PCSK6 could cleave wild-type (WT) pro-GDF15 into mature GDF15 in both HL1 cell lysate and culture medium, all three PCSK proteins were ineffective against this RXXR motif mutant pro-GDF15 (Fig. 3). These results suggest that PCSK3, PCSK5, and PCSK6 cleave pro-GDF15 at its canonical RXXR sequence.

PCSK3, -5, and -6 catalytic activities are essential for pro-GDF15 cleavage. The so-called catalytic triad Asp-His-Ser forms the catalytic active sites of PCSK enzymes and is conserved from bacterial subtilisin and yeast kexin to mammal PCSK (19, 20). We next investigated whether the catalytic triad of PCSK3, -5, and -6 is essential for pro-GDF15 cleavage. We mutated the individual essential amino acid (Asp to Ala, His to Lys, and Ser to Ala) in the catalytic triad of PCSK3, PCSK5, and PCSK6. These mutations seem to increase the stability of PCSK3 and PCSK6 but not PCSK5 (Fig. 4). While WT PCSK3, PCSK5, or PCSK6 could cleave pro-GDF15 into mature GDF15 in both HL1 cell lysate and culture medium, none of the mutant forms were able to cleave pro-GDF15 (Fig. 4). These results suggest that the catalytic activities of PCSK3, -5, and -6 are essential for pro-GDF15 processing.

PCSK3, -5, and -6 license GDF15 maturation *in vivo*. We next investigated whether PCSK3, PCSK5, or PCSK6 was able to cleave pro-GDF15 in the mouse heart *in vivo*. We generated and performed pericardial injection of adeno-associated virus 9 (AAV9) encoding a cardiac troponin (cTnt) promoter-driven pre-pro-GDF15, in combination with AAV9-cTnt-green fluorescent protein (GFP) (as a control), PCSK3, PCSK5, or PCSK6 into postnatal day 3 to 5 C57BL/6 WT mice and collected the hearts 10 days after injection. We and others have previously shown that pericardial injection of AAV9 achieves stable and cardiac tissue-specific expression of transgenes (11, 25). Quantitative PCR (qPCR) results confirmed the expression of individual genes in the mouse heart (Fig. 5A). GDF15 overexpression alone resulted in increased pro-GDF15 but little change of mature GDF15 protein in the WT mouse hearts (Fig. 5B). In contrast, coexpression of PCSK3, PCSK5, or PCSK6 significantly increased both

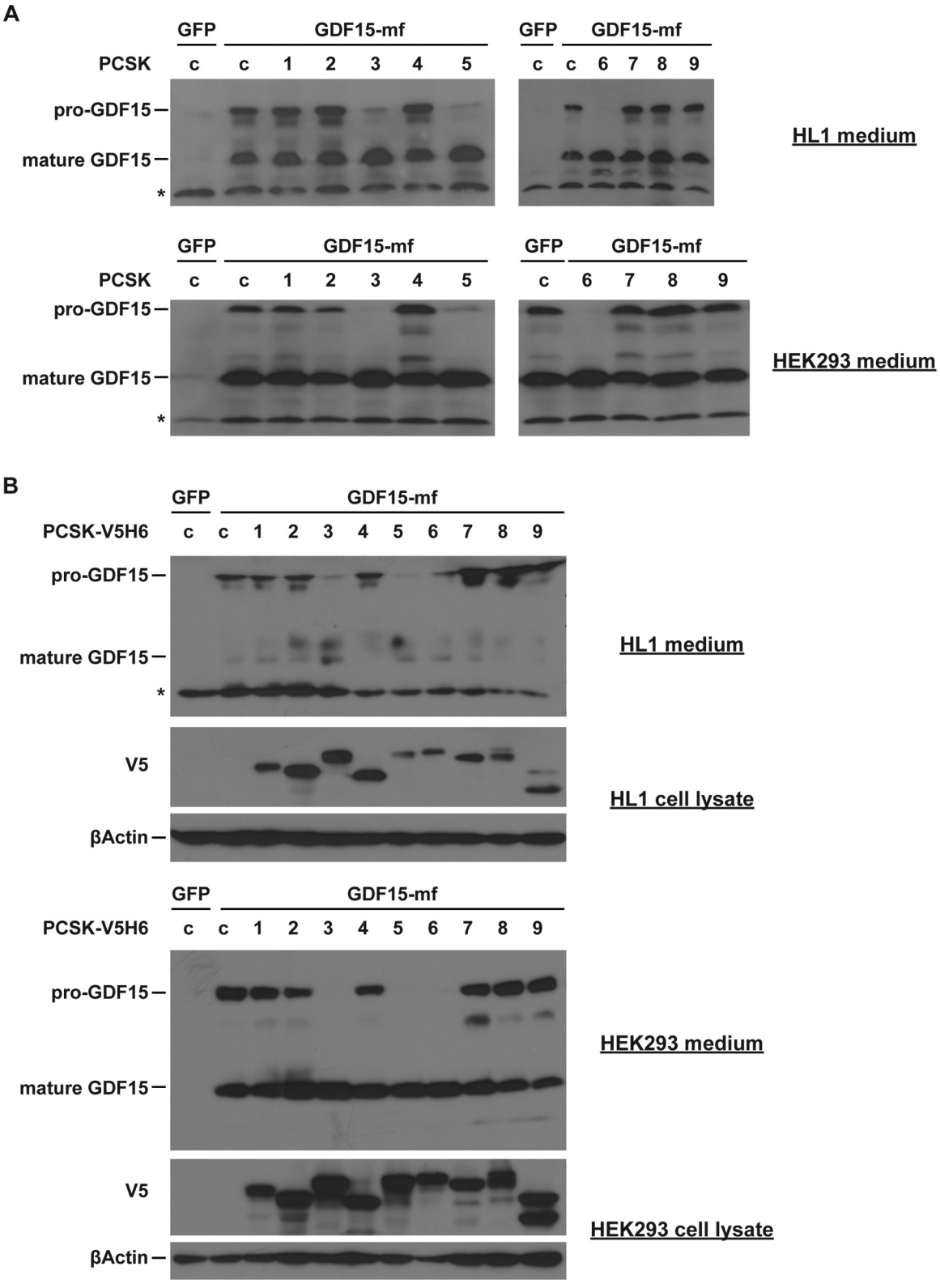

FIG 2 PCSK3, -5, and -6 cleave pro-GDF15 *in vitro*. Representative Western blot images show pro-GDF15 and mature GDF15 in media of HL1 cardiomyocytes and HEK293 cells transfected with GDF15-mf and different PCSK plasmids. (A) Nontagged PCSK; (B) V5H6-tagged PCSK. In panel B, cellular PCSK protein levels were also determined by Western blotting using V5 antibody. β-Actin served as a loading control. *, nonspecific bands.

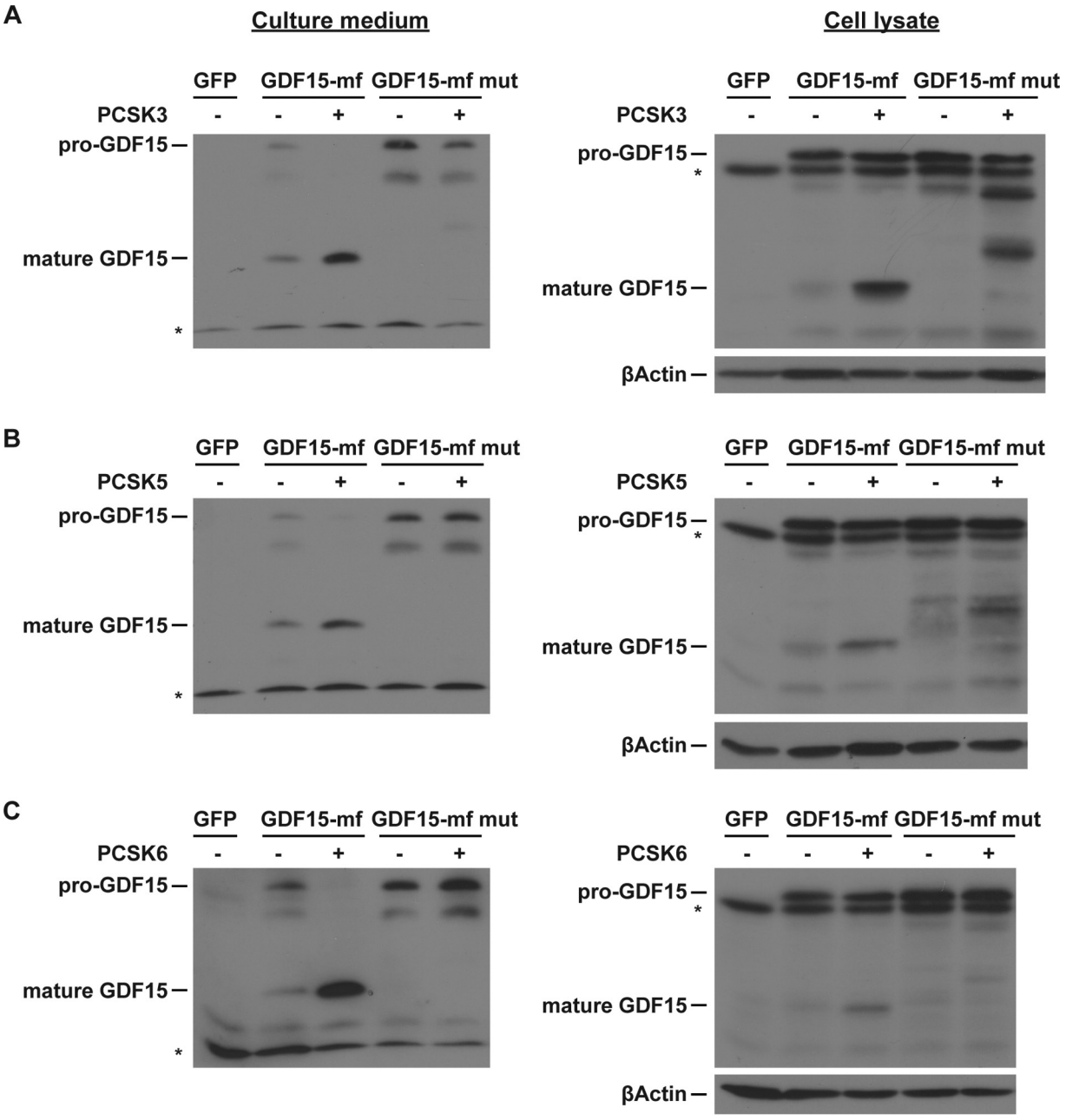

FIG 3 RXXR motif of pro-GDF15 is crucial for PCSK3, -5, and -6-mediated cleavage. Representative Western blot images of HL1 medium and cell lysates are shown. HL1 cardiomyocytes were transfected with WT or R188Q mutant GDF15-mf, with or without an equal amount of plasmid encoding full-length PCSK3 (A), PCSK5 (B), or PCSK6 (C). β-Actin served as a loading control.

pro-GDF15 and mature GDF15, and importantly, the ratio of mature/pro-GDF15. Furthermore, the presence of PCSK3, PCSK5, or PCSK6 doubled the amount of circulating, mature GDF15 (18) (Fig. 5C). Together, these results suggest that PCSK3, PCSK5, and PCSK6 license GDF15 maturation *in vivo*.

We last examined PCSK3, -5, and -6 expression in a mouse model of heart disease. We have previously shown that cardiac loss of two transcription factors essential for normal cardiac metabolism and function, estrogen-related receptor alpha (ERRα) and gamma (ERRγ), results in postnatal cardiomyopathy, heart failure, and FTT (11, 26). *Gdf15* transcription is highly induced in cardiac ERRα/γ knockout (KO) mice, resulting in increased pro-GDF15 and mature GDF15 production in the heart. Circulating GDF15, in turn, inhibits liver growth hormone signaling and pediatric body growth, thereby

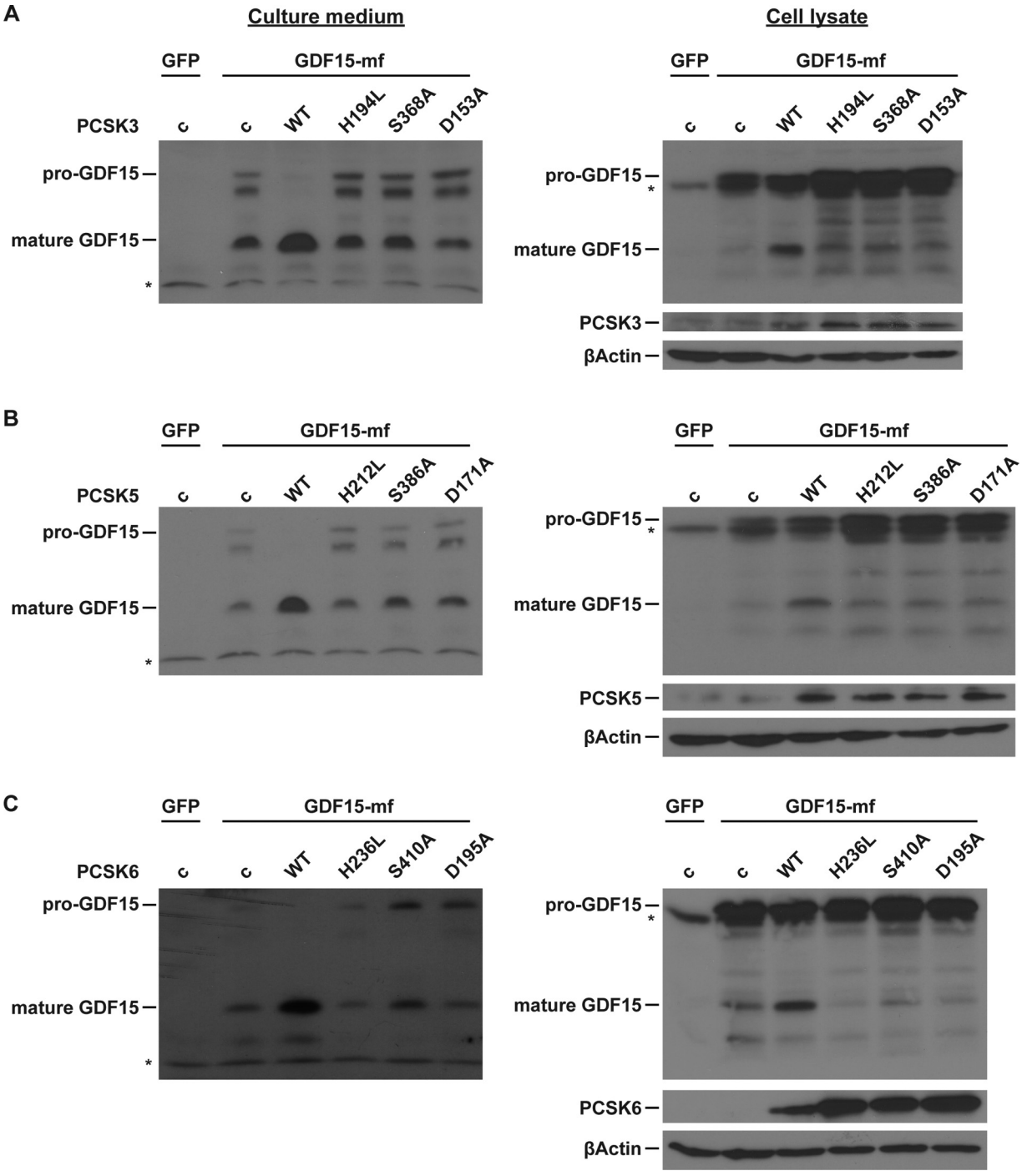

FIG 4 PCSK3, -5, and -6 catalytic activities are essential for pro-GDF15 cleavage. Representative Western blot images of HL1 medium and cell lysates are shown. HL1 cardiomyocytes were transfected with WT GDF15-mf and an equal amount of plasmids encoding WT or mutant PCSK3 (A), PCSK5 (B), or PCSK6 (C). β-Actin served as a loading control.

coordinating body growth rate with cardiac function. We found that PCSK3, -5, and -6 proteins are present in multiple tissues important in metabolism (heart, liver, brown fat, and gastrocnemius muscle [Fig. 6A]). Although PCSK3 and PCSK6 abundance were little changed, both the RNA and protein levels of PCSK5 were significantly increased in cardiac ERRα/γ KO mouse hearts, further supporting significant GDF15 maturation (Fig. 6B and C). Although further investigations are required to determine whether the activities of these PCSK enzymes alter under other physiological or pathological con-

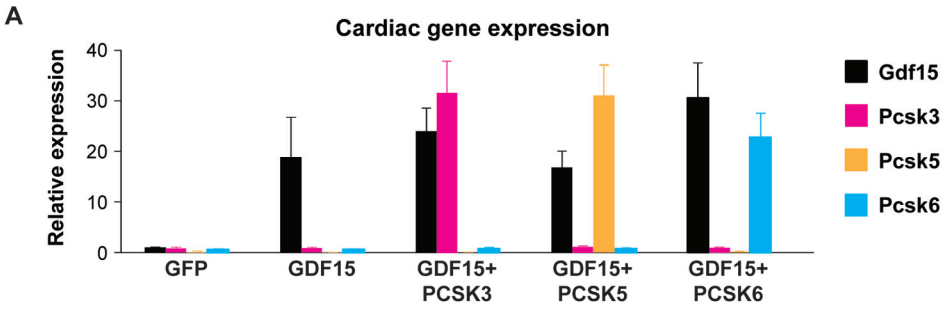

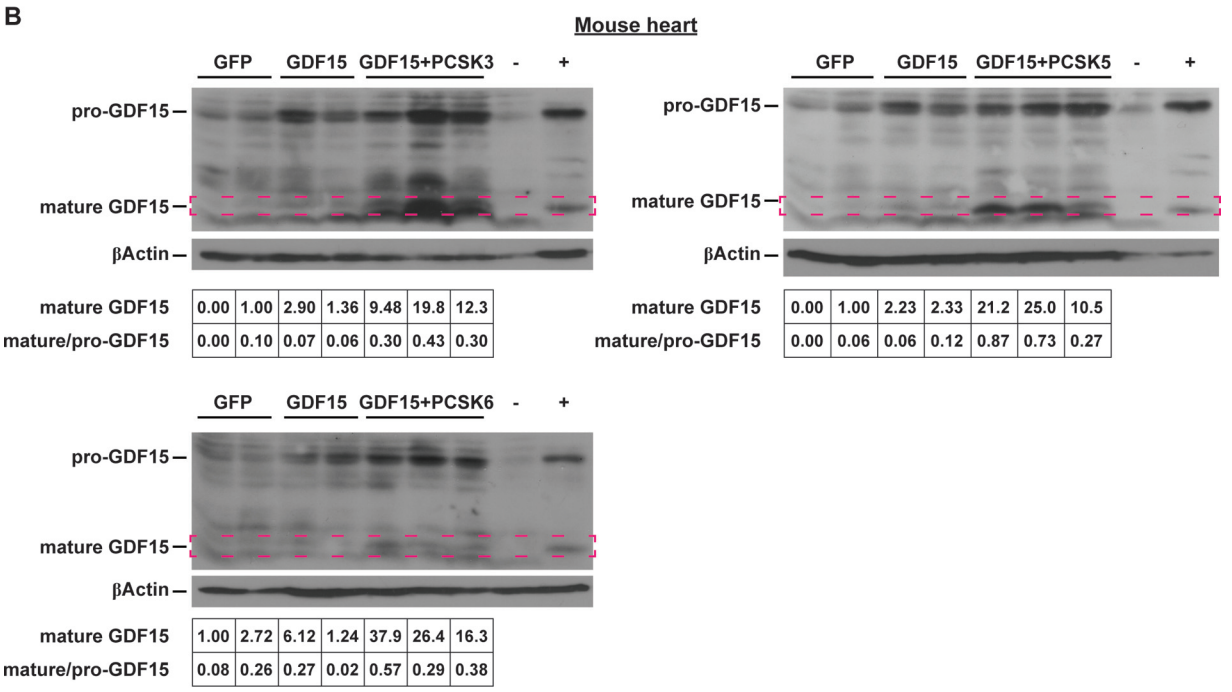

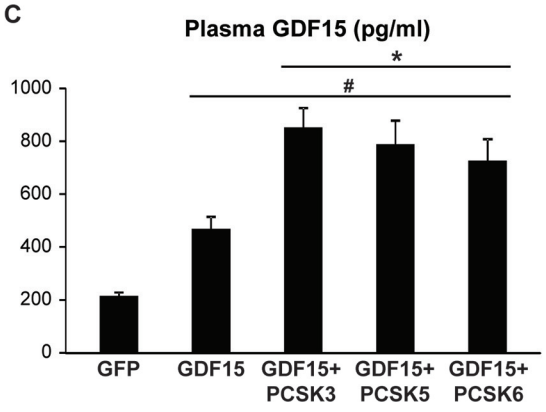

FIG 5 PCSK3, -5, and -6 license GDF15 maturation *in vivo*. (A) Cardiac *Gdf15*, *Pcsk3*, *Pcsk5*, and *Pcsk6* mRNA levels in mice receiving AAV9 pericardial injection. (B) Representative Western blot images of pro-GDF15 and mature GDF15 (framed) in AAV-injected heart lysates. −, negative control (GDF15 KO heart lysate); +, positive control (heart lysates from cardiac ERRα/γ KO mice). β-Actin served as a loading control. Quantification of mature GDF15 band density (normalized to β-actin) and mature versus pro-GDF15 ratio is shown at the bottom. (C) Plasma GDF15 levels in AAV9-injected mice (n = 12 to 18 per group). #, $P < 0.0001$ versus AAV9-GFP; *, $P < 0.01$ versus AAV9-GDF15.

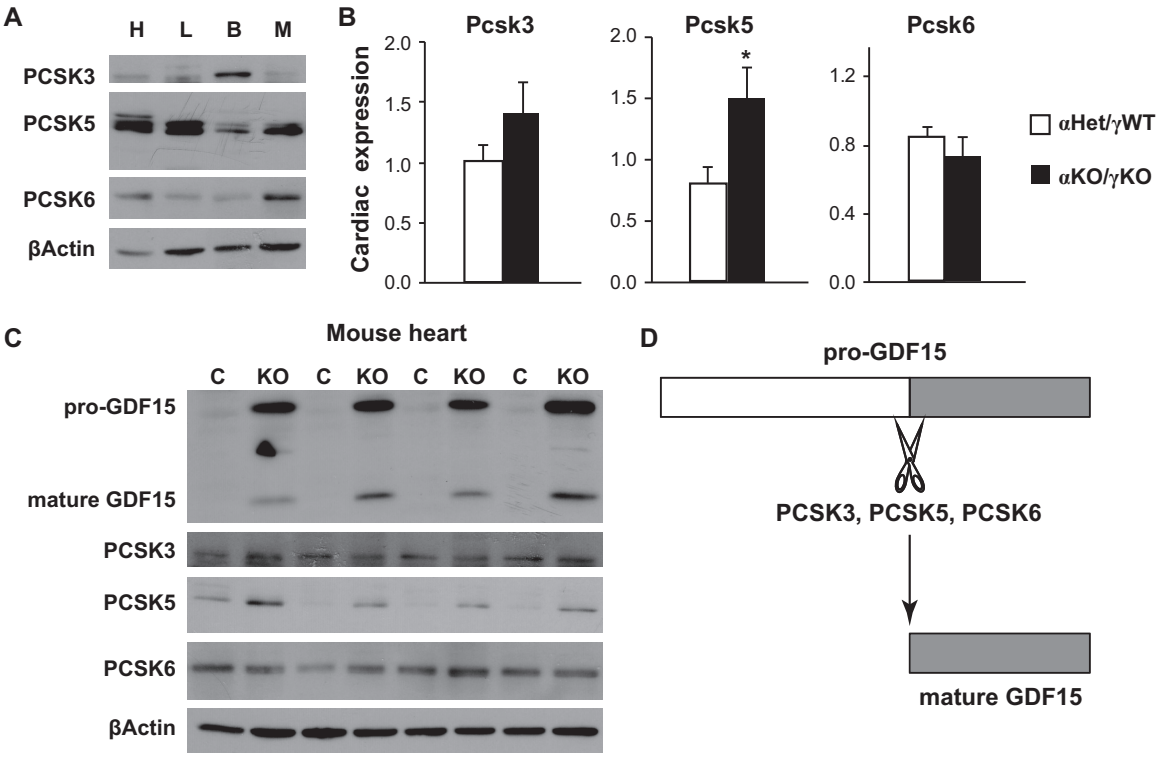

FIG 6 PCSK3, -5, and -6 expression in mouse models of heart disease. (A) Representative Western blot images of PCSK3, PCSK5, and PCSK6 proteins in the heart (H), liver (L), brown fat (B), and gastrocnemius muscle (M) of 16-day-old control αHet/γWT mice. (B) Expression of *Pcsk3*, *Pcsk5*, and *Pcsk6* in the hearts of control αHet/γWT and cardiac ERRα/γ KO (αKO/γKO) mice ($n = 6$ to 8). *, $P < 0.05$. (C) Representative Western blot images of GDF15, PCSK3, PCSK5, and PCSK6 proteins in the hearts of littermate control αHet/γWT and cardiac ERRα/γ KO mice ($n = 4$). (D) Diagram summarizing findings of pro-GDF15 cleavage by PCSK3, -5, and -6. β-Actin served as a loading control in panels A and C.

ditions, these results suggest that PCSK3, -5, and -6 can support GDF15 maturation in heart disease *in vivo*.

DISCUSSION

Like most hormones and many other TGF-β family member proteins, GDF15 is synthesized as a precursor protein and undergoes proteolytic processing to release the mature form as a secreted hormone. However, little is known about the protein enzymes that mediate this critical cleavage step. This issue becomes more important considering the current strong therapeutic interest in GDF15 for treating obesity and cachexia and its implication in cardiovascular disease. Although a recent report that focused on PCSK6 in prostate cancer touched on GDF15 as one of the substrates of PCSK6 (27), this study took a more systematic approach and identified three enzymes that effectively process pro-GDF15 to maturation. PCSK3, -5, and -6 (but not other PCSK proteins) can all recognize and cleave the canonical substrate sequence of pro-GDF15 *in vitro* and *in vivo* (Fig. 6D). We also showed that the catalytic triad Asp-His-Ser of PCSK3, -5, and -6 is essential for the members' enzymatic activities and GDF15 maturation. Together, these studies provided novel mechanistic insights into our understanding of GDF15 biology.

We showed that PCSK3, -5, and -6 can all cleave pro-GDF15 in multiple cell types *in vitro* and in the mouse heart *in vivo*. Whether they are essential for GDF15 *in vivo* maturation remains unclear at this moment, as inactivation of all three PCSK enzymes is likely needed to definitively address this question. It remains possible that one particular PCSK is critical for pro-GDF15 processing in certain cell types or tissues due to its much higher abundance than other PCSKs. In addition, it is also possible that in a complex organ (such as the heart) composed of many cell types,

TABLE 1 qPCR primer sequences

Gene	Species	Forward	Reverse
Pcsk1	Mouse	AGTTGGAGGCATAAGAATGCTG	GCCTTCTGGGCTAGTCTGC
Pcsk2	Mouse	AGAGAGACCCCAGGATAAAGATG	CTTGCCCAGTGTTGAACAGGT
Pcsk3	Mouse	TAGCAGGCAATTATGACCCTGG	TAAGCTACACCTACGCCACAG
Pcsk4	Mouse	CTTTCGCTCTCCTACAGCCG	AGTTGTTGTAGCCTTGGCCG
Pcsk5	Human	GAGGGACCCACAGTTTCATTTC	TGGGCACGACTGAAGTCATAA
Pcsk6	Mouse	CAGGCGCGAAGTGACTCTC	GACCGACAGCGACTGTTCTT
Pcsk7	Mouse	AGAGAGTCTGACGCAACAGG	TATGCCCAGTAGGCTGGACAA
Pcsk8	Mouse	CTGGTGGTTTTGCTCTGTGG	GGCTGTGAAGTATCCGTTGAAAG
Pcsk9	Mouse	GAGACCCAGAGGCTACAGATT	AATGTACTCCACATGGGGCAA
Gdf15	Mouse	CTGGCAATGCCTGAACAACG	GGTCGGGACTTGGTTCTGAG
36b4	Mouse	AGATGCAGCAGATCCGCAT	GTTCTTGCCCATCAGCACC

different PCSKs are essential for pro-GDF15 processing in distinct cell types. Future studies will address these possibilities. On the other hand, how cellular PCSK3, -5, and -6 activities are regulated remains little understood. It is possible that certain physiological stimuli or pathological conditions promote specific PCSK abundance and/or activity, thereby regulating mature GDF15 availability, as we showed for PCSK5 in heart disease.

MATERIALS AND METHODS

Animal studies and AAV injection. All animal studies were approved by and performed under the guidelines of the Institutional Animal Care and Use Committee of the Children's Hospital of Philadelphia (CHOP) and comply with the ARRIVE guidelines. The WT C57BL6/J mice were from the Jackson Laboratory. Cardiac ERRα/γ KO mice in the C57BL6/J background were previously described (26). Mice were maintained in a pathogen-free environment on a 12/12-h light/dark cycle with *ad libitum* access to food and water. Both sexes were included in studies. The mouse pups and dams were fed a breeder diet (LabDiet 5058), while weaned mice were fed a standard chow diet (LabDiet 5L0D). AAV9-cTnt-GFP, mouse pre-pro-GDF15, mouse PCSK3, human PCSK5, and mouse PCSK6 were generated at the CHOP Research Vector Core. Pericardial injection of mice at 3 to 5 days of age with 3×10^{11} vector genomes of AAV9 was performed as previously described (11). Mice were returned to their home cage after AAV injection and maintained for an additional 10 days before being euthanized.

Cell culture, plasmids, and transfection. HEK293 cells were cultured in Dulbecco's modified Eagle medium (DMEM) with L-glutamine, 4.5 g/liter of glucose, sodium pyruvate (Corning; 10013CV), and 10% fetal bovine serum (FBS; Sigma; F2442). HL1 cardiomyocytes were maintained in Claycomb medium (Sigma; 51800C) supplemented with FBS (Sigma; F2442), 0.1 mM L-(−)-norepinephrine bitartrate (Cayman Chemical; 16673), and 2 mM L-glutamine (Gibco; 25030) as previously described (26). Plasmid encoding mouse pre-pro-GDF15 was from Origene (MR204247). Plasmids encoding full-length mouse PCSK1 to -4 and PCSK7 to -9 were generated by PCR cloning from mouse cDNAs into the pcDNA3.1 vector. Plasmid encoding full-length human PCSK5 was from GeneCopoeia (Ex-T3161-M98). Plasmid encoding full-length mouse PCSK6 with FLAG tag was from Nanopro Biosciences (751729-1). The V5H6-tagged PCSK1 to -9 vectors were generated by PCR cloning into the pcDNA3.1D-V5H6 vector. The mutant plasmids GDF15 R188Q, PCSK3 H194L, S368A, and D153A, PCSK5 H212L, S386A, and D171A, and PCSK6 H236L, S410A, and D195A were generated by site-directed mutagenesis as previously described (26, 28, 29). HEK293 and HL1 cells were transfected using 1.5:1 and 5:1 ratios of FUGENE 6 (Promega), respectively.

Protease inhibitors and Western blot analysis. Protease inhibitors used in this study include E-64 (10 μM; Cayman Chemical; 10007963), pepstatin A (10 μM; Cayman Chemical; 9000469), GM-6001 (50 μM; Enzo Life Sciences; BML-EI300), benzamidine (5 mM; Sigma; B6506), and decanoyl-RVKR-CMK (25 μM; Cayman Chemical; 14965). Twenty-four hours after transfection, cells were treated with aforementioned protease inhibitors for 24 h. The culture medium was then collected and briefly centrifuged to remove cell debris; cells were lysed with radioimmunoprecipitation assay (RIPA) buffer supplemented with protease inhibitors (Roche; 4693159001). Western blot analysis was performed as previously described (26, 28, 29) using the following antibodies: GDF15 (Abcam; ab189358), PCSK3 (Santa Cruz; sc-133142), PCSK5 (Thermo Fisher; PA5-42378), PCSK6 (Abcam; AB151562), FLAG (Sigma; F1804), V5 (Thermo Fisher; MA1-81617), and β-actin (Cell Signaling; 4967). Image quantification was performed using ImageJ from films scanned at 1,200 dots per inch (dpi) in TIFF format by selecting uniform rectangles that enclose the bands. We separated peaks corresponding to different bands using ImageJ, which allowed accurate calculation of mature and pro-GDF15 band densities from closely located, nonspecific bands. Relative ratio was calculated by dividing the value of each band by that of its corresponding control band.

qRT-PCR. Quantitative reverse transcription-PCR (qRT-PCR) was performed as previously described (26, 30). Primers sequences are listed in Table 1.

ELISA. Mouse blood was collected using a lithium heparin-coated microvette (Sarstedt; CB300LH) and centrifuged at 3,000 $\times$ *g* for 5 min at 4°C. Plasma GDF15 levels were measured with an enzyme-linked immunosorbent assay (ELISA) kit (R&D; DY6385) by following the manufacturer's instructions.

Statistics. Data are presented means plus standard errors of the means (SEMs). Two-tailed, two-sample unequal-variance Student's *t* test was used to determine the statistical significance. A *P* value of <0.05 was considered statistically significant.

ACKNOWLEDGMENTS

We thank Douglas Wallace, Mitchell Lazar, Matthew Weitzman, Amita Sehgal, Michael Marks, and Mark Kahn for critical discussion of the project.

L.P. conceived and directed the project. J.J.L., J.L., and K.L. performed most experiments. X.L. and L.Z. generated AAV vectors. J.J.L. and L.P. wrote the manuscript, and all authors reviewed or edited the manuscript.

We and this work were supported by the Office of the Assistant Secretary of Defense for Health Affairs through the Peer Reviewed Medical Research Program under award no. W81XWH-16-1-0400 and by NIH grant DK111495 (L.P.). The AAV vector work was supported by the CHOP RVC internal operation fund.

We declare no conflict of interest.

REFERENCES

1. Bootcov MR, Bauskin AR, Valenzuela SM, Moore AG, Bansal M, He XY, Zhang HP, Donnellan M, Mahler S, Pryor K, Walsh BJ, Nicholson RC, Fairlie WD, Por SB, Robbins JM, Breit SN. 1997. MIC-1, a novel macrophage inhibitory cytokine, is a divergent member of the TGF-beta superfamily. Proc Natl Acad Sci U S A 94:11514–11519.
2. Hromas R, Hufford M, Sutton J, Xu D, Li Y, Lu L. 1997. PLAB, a novel placental bone morphogenetic protein. Biochim Biophys Acta 1354:40–44. https://doi.org/10.1016/S0167-4781(97)00122-X.
3. Lawton LN, Bonaldo MF, Jelenc PC, Qiu L, Baumes SA, Marcelino RA, de Jesus GM, Wellington S, Knowles JA, Warburton D, Brown S, Soares MB. 1997. Identification of a novel member of the TGF-beta superfamily highly expressed in human placenta. Gene 203:17–26. https://doi.org/10.1016/S0378-1119(97)00485-X.
4. Yokoyama-Kobayashi M, Saeki M, Sekine S, Kato S. 1997. Human cDNA encoding a novel TGF-beta superfamily protein highly expressed in placenta. J Biochem 122:622–626. https://doi.org/10.1093/oxfordjournals.jbchem.a021798.
5. Paralkar VM, Vail AL, Grasser WA, Brown TA, Xu H, Vukicevic S, Ke HZ, Qi H, Owen TA, Thompson DD. 1998. Cloning and characterization of a novel member of the transforming growth factor-beta/bone morphogenetic protein family. J Biol Chem 273:13760–13767. https://doi.org/10.1074/jbc.273.22.13760.
6. Böttner M, Laaff M, Schechinger B, Rappold G, Unsicker K, Suter-Crazzolara C. 1999. Characterization of the rat, mouse, and human genes of growth/differentiation factor-15/macrophage inhibiting cytokine-1 (GDF-15/MIC-1). Gene 237:105–111. https://doi.org/10.1016/S0378-1119(99)00309-1.
7. Baek SJ, Kim KS, Nixon JB, Wilson LC, Eling TE. 2001. Cyclooxygenase inhibitors regulate the expression of a TGF-beta superfamily member that has proapoptotic and antitumorigenic activities. Mol Pharmacol 59:901–908. https://doi.org/10.1124/mol.59.4.901.
8. Unsicker K, Spittau B, Krieglstein K. 2013. The multiple facets of the TGF-beta family cytokine growth/differentiation factor-15/macrophage inhibitory cytokine-1. Cytokine Growth Factor Rev 24:373–384. https://doi.org/10.1016/j.cytogfr.2013.05.003.
9. Baggen VJ, van den Bosch AE, Eindhoven JA, Schut AW, Cuypers JA, Witsenburg M, de Waart M, van Schaik RH, Zijlstra F, Boersma E, Roos-Hesselink JW. 2017. Prognostic value of N-terminal pro-B-type natriuretic peptide, troponin-T, and growth-differentiation factor 15 in adult congenital heart disease. Circulation 135:264–279. https://doi.org/10.1161/CIRCULATIONAHA.116.023255.
10. Wollert KC, Kempf T, Wallentin L. 2017. Growth differentiation factor 15 as a biomarker in cardiovascular disease. Clin Chem 63:140–151. https://doi.org/10.1373/clinchem.2016.255174.
11. Wang T, Liu J, McDonald C, Lupino K, Zhai X, Wilkins BJ, Hakonarson H, Pei L. 2017. GDF15 is a heart-derived hormone that regulates body growth. EMBO Mol Med 9:1150–1164. https://doi.org/10.15252/emmm.201707604.
12. Johnen H, Lin S, Kuffner T, Brown DA, Tsai VW, Bauskin AR, Wu L, Pankhurst G, Jiang L, Junankar S, Hunter M, Fairlie WD, Lee NJ, Enriquez RF, Baldock PA, Corey E, Apple FS, Murakami MM, Lin EJ, Wang C, During MJ, Sainsbury A, Herzog H, Breit SN. 2007. Tumor-induced anorexia and weight loss are mediated by the TGF-beta superfamily cytokine MIC-1. Nat Med 13:1333–1340. https://doi.org/10.1038/nm1677.
13. Mullican SE, Lin-Schmidt X, Chin CN, Chavez JA, Furman JL, Armstrong AA, Beck SC, South VJ, Dinh TQ, Cash-Mason TD, Cavanaugh CR, Nelson S, Huang C, Hunter MJ, Rangwala SM. 2017. GFRAL is the receptor for GDF15 and the ligand promotes weight loss in mice and nonhuman primates. Nat Med 23:1150–1157. https://doi.org/10.1038/nm.4392.
14. Yang L, Chang CC, Sun Z, Madsen D, Zhu H, Padkjaer SB, Wu X, Huang T, Hultman K, Paulsen SJ, Wang J, Bugge A, Frantzen JB, Norgaard P, Jeppesen JF, Yang Z, Secher A, Chen H, Li X, John LM, Shan B, He Z, Gao X, Su J, Hansen KT, Yang W, Jorgensen SB. 2017. GFRAL is the receptor for GDF15 and is required for the anti-obesity effects of the ligand. Nat Med 23:1158–1166. https://doi.org/10.1038/nm.4394.
15. Emmerson PJ, Wang F, Du Y, Liu Q, Pickard RT, Gonciarz MD, Coskun T, Hamang MJ, Sindelar DK, Ballman KK, Foltz LA, Muppidi A, Alsina-Fernandez J, Barnard GC, Tang JX, Liu X, Mao X, Siegel R, Sloan JH, Mitchell PJ, Zhang BB, Gimeno RE, Shan B, Wu X. 2017. The metabolic effects of GDF15 are mediated by the orphan receptor GFRAL. Nat Med 23:1215–1219. https://doi.org/10.1038/nm.4393.
16. Hsu JY, Crawley S, Chen M, Ayupova DA, Lindhout DA, Higbee J, Kutach A, Joo W, Gao Z, Fu D, To C, Mondal K, Li B, Kekatpure A, Wang M, Laird T, Horner G, Chan J, McEntee M, Lopez M, Lakshminarasimhan D, White A, Wang SP, Yao J, Yie J, Matern H, Solloway M, Haldankar R, Parsons T, Tang J, Shen WD, Alice Chen Y, Tian H, Allan BB. 2017. Non-homeostatic body weight regulation through a brainstem-restricted receptor for GDF15. Nature 550:255–259. https://doi.org/10.1038/nature24042.
17. Xiong Y, Walker K, Min X, Hale C, Tran T, Komorowski R, Yang J, Davda J, Nuanmanee N, Kemp D, Wang X, Liu H, Miller S, Lee KJ, Wang Z, Veniant MM. 2017. Long-acting MIC-1/GDF15 molecules to treat obesity: evidence from mice to monkeys. Sci Transl Med 9:eaan8732. https://doi.org/10.1126/scitranslmed.aan8732.
18. Kempf T, Horn-Wichmann R, Brabant G, Peter T, Allhoff T, Klein G, Drexler H, Johnston N, Wallentin L, Wollert KC. 2007. Circulating concentrations of growth-differentiation factor 15 in apparently healthy elderly individuals and patients with chronic heart failure as assessed by a new immunoradiometric sandwich assay. Clin Chem 53:284–291. https://doi.org/10.1373/clinchem.2006.076828.
19. Seidah NG, Mayer G, Zaid A, Rousselet E, Nassoury N, Poirier S, Essalmani R, Prat A. 2008. The activation and physiological functions of the proprotein convertases. Int J Biochem Cell Biol 40:1111–1125. https://doi.org/10.1016/j.biocel.2008.01.030.
20. Seidah NG, Sadr MS, Chretien M, Mbikay M. 2013. The multifaceted proprotein convertases: their unique, redundant, complementary, and opposite functions. J Biol Chem 288:21473–21481. https://doi.org/10.1074/jbc.R113.481549.
21. Horton JD, Cohen JC, Hobbs HH. 2007. Molecular biology of PCSK9: its role in LDL metabolism. Trends Biochem Sci 32:71–77. https://doi.org/10.1016/j.tibs.2006.12.008.
22. Sabatine MS, Giugliano RP, Keech AC, Honarpour N, Wiviott SD, Murphy SA, Kuder JF, Wang H, Liu T, Wasserman SM, Sever PS, Pedersen TR. 2017.

Evolocumab and clinical outcomes in patients with cardiovascular disease. N Engl J Med 376:1713–1722. https://doi.org/10.1056/NEJMoa1615664.
23. Dubois CM, Blanchette F, Laprise MH, Leduc R, Grondin F, Seidah NG. 2001. Evidence that furin is an authentic transforming growth factor-beta1-converting enzyme. Am J Pathol 158:305–316. https://doi.org/10.1016/S0002-9440(10)63970-3.
24. Susan-Resiga D, Essalmani R, Hamelin J, Asselin MC, Benjannet S, Chamberland A, Day R, Szumska D, Constam D, Bhattacharya S, Prat A, Seidah NG. 2011. Furin is the major processing enzyme of the cardiac-specific growth factor bone morphogenetic protein 10. J Biol Chem 286:22785–22794. https://doi.org/10.1074/jbc.M111.233577.
25. Bish LT, Morine K, Sleeper MM, Sanmiguel J, Wu D, Gao G, Wilson JM, Sweeney HL. 2008. Adeno-associated virus (AAV) serotype 9 provides global cardiac gene transfer superior to AAV1, AAV6, AAV7, and AAV8 in the mouse and rat. Hum Gene Ther 19:1359–1368. https://doi.org/10.1089/hum.2008.123.
26. Wang T, McDonald C, Petrenko NB, Leblanc M, Giguere V, Evans RM, Patel VV, Pei L. 2015. Estrogen-related receptor alpha (ERRalpha) and ERRgamma are essential coordinators of cardiac metabolism and function. Mol Cell Biol 35:1281–1298. https://doi.org/10.1128/MCB.01156-14.
27. Couture F, Sabbagh R, Kwiatkowska A, Desjardins R, Guay SP, Bouchard L, Day R. 2017. PACE4 undergoes an oncogenic alternative splicing switch in cancer. Cancer Res 77:6863–6879. https://doi.org/10.1158/0008-5472.CAN-17-1397.
28. Pei L, Mu Y, Leblanc M, Alaynick W, Barish GD, Pankratz M, Tseng TW, Kaufman S, Liddle C, Yu RT, Downes M, Pfaff SL, Auwerx J, Gage FH, Evans RM. 2015. Dependence of hippocampal function on ERRgamma-regulated mitochondrial metabolism. Cell Metab 21:628–636. https://doi.org/10.1016/j.cmet.2015.03.004.
29. Pei L, Leblanc M, Barish G, Atkins A, Nofsinger R, Whyte J, Gold D, He M, Kawamura K, Li HR, Downes M, Yu RT, Powell HC, Lingrel JB, Evans RM. 2011. Thyroid hormone receptor repression is linked to type I pneumocyte-associated respiratory distress syndrome. Nat Med 17:1466–1472. https://doi.org/10.1038/nm.2450.
30. Zhao J, Lupino K, Wilkins BJ, Qiu C, Liu J, Omura Y, Allred AL, McDonald C, Susztak K, Barish GD, Pei L. 2018. Genomic integration of ERRgamma-HNF1beta regulates renal bioenergetics and prevents chronic kidney disease. Proc Natl Acad Sci U S A 115:E4910–E4919. https://doi.org/10.1073/pnas.1804965115.

RESOURCE/METHODOLOGY

Single-nucleus transcriptomic survey of cell diversity and functional maturation in postnatal mammalian hearts

Peng Hu,[1,2,5] Jian Liu,[1,3,5] Juanjuan Zhao,[1,3,5] Benjamin J. Wilkins,[3,4] Katherine Lupino,[1,3] Hao Wu,[1,2] and Liming Pei[1,3,4]

[1]Center for Mitochondrial and Epigenomic Medicine, Children's Hospital of Philadelphia, Philadelphia, Pennsylvania 19104, USA; [2]Department of Genetics, Penn Epigenetics Institute, University of Pennsylvania, Philadelphia, Pennsylvania 19104, USA; [3]Department of Pathology and Laboratory Medicine, Children's Hospital of Philadelphia, Philadelphia, Pennsylvania 19104, USA; [4]Department of Pathology and Laboratory Medicine, Perelman School of Medicine, University of Pennsylvania, Philadelphia, Pennsylvania 19104, USA

A fundamental challenge in understanding cardiac biology and disease is that the remarkable heterogeneity in cell type composition and functional states have not been well characterized at single-cell resolution in maturing and diseased mammalian hearts. Massively parallel single-nucleus RNA sequencing (snRNA-seq) has emerged as a powerful tool to address these questions by interrogating the transcriptome of tens of thousands of nuclei isolated from fresh or frozen tissues. snRNA-seq overcomes the technical challenge of isolating intact single cells from complex tissues, including the maturing mammalian hearts; reduces biased recovery of easily dissociated cell types; and minimizes aberrant gene expression during the whole-cell dissociation. Here we applied sNucDrop-seq, a droplet microfluidics-based massively parallel snRNA-seq method, to investigate the transcriptional landscape of postnatal maturing mouse hearts in both healthy and disease states. By profiling the transcriptome of nearly 20,000 nuclei, we identified major and rare cardiac cell types and revealed significant heterogeneity of cardiomyocytes, fibroblasts, and endothelial cells in postnatal developing hearts. When applied to a mouse model of pediatric mitochondrial cardiomyopathy, we uncovered profound cell type-specific modifications of the cardiac transcriptional landscape at single-nucleus resolution, including changes of subtype composition, maturation states, and functional remodeling of each cell type. Furthermore, we employed sNucDrop-seq to decipher the cardiac cell type-specific gene regulatory network (GRN) of GDF15, a heart-derived hormone and clinically important diagnostic biomarker of heart disease. Together, our results present a rich resource for studying cardiac biology and provide new insights into heart disease using an approach broadly applicable to many fields of biomedicine.

[*Keywords*: single-nucleus RNA-seq; GDF15; ERRγ; postnatal heart maturation; mitochondrial cardiomyopathy]

Supplemental material is available for this article.

Received May 14, 2018; revised version accepted August 10, 2018.

Significant genetic and functional heterogeneity exist among individual cells and contribute to overall organ development, physiology, and plasticity (Altschuler and Wu 2010). For example, there are many different cell types, including cardiomyocytes, fibroblasts, endothelial cells (ECs), epicardial cells, blood cells, and others, in both developing and adult hearts, with significant anatomical, genetic, and functional heterogeneity among the same cell type (Paige et al. 2015; Potente and Makinen 2017; Tallquist and Molkentin 2017). Of particular interest are early postnatal hearts, in which the cell type composition and metabolic states undergo significant

[5]These authors contributed equally to this work.
Corresponding authors: lpei@pennmedicine.upenn.edu, haowu2@pennmedicine.upenn.edu
Article published online ahead of print. Article and publication date are online at http://www.genesdev.org/cgi/doi/10.1101/gad.316802.118.

changes and remodeling for functional maturation. However, the postnatal period is significantly underexplored compared with the embryonic period or adulthood. In addition, cell type-specific metabolic and transcriptional remodeling often occurs in the disease state. Many forms of heart disease, such as mitochondrial cardiomyopathy, a disease of heart muscle due to primary mitochondrial dysfunction, are well recognized to exhibit significant heterogeneity in disease genetics, symptoms, and outcomes (Meyers et al. 2013; Burke et al. 2016b; Ritterhoff and Tian 2017). However, the precise cell type composition and molecular underpinnings of such cellular and functional heterogeneity in maturing and diseased postnatal hearts remain poorly understood.

Single-cell RNA sequencing (RNA-seq) approaches empower genome-wide gene expression analysis at the single-cell resolution and have provided novel insights into many important biological questions, such as cellular identity and heterogeneity (Tanay and Regev 2017; Woodworth et al. 2017). Recent technological advances in droplet microfluidics have enabled massively parallel single-cell transcriptome analysis of tens of thousands of cells (Klein et al. 2015; Macosko et al. 2015) and nuclei (Lake et al. 2016; Habib et al. 2017; Hu et al. 2017). Although single-nucleus RNA-seq (snRNA-seq) often detects a lower number of RNA than single-cell RNA-seq, as it excludes transcripts outside the nucleus, it holds several technical advantages when applied to tissues that are difficult to dissociate, such as mammalian hearts. First, snRNA-seq bypasses preparation of intact single-cell suspension and thus can be used to study frozen and archived primary tissues. Second, snRNA-seq can minimize the bias of recovering only cells that are easily dissociated or cells of a certain size optimal for platform-specific cell capture and reduce the impact of aberrant transcriptional changes induced by enzymatic dissociation. To date, massively parallel snRNA-seq has been used only to study brain cell type compositions and functional states (Lake et al. 2016; Habib et al. 2017; Hu et al. 2017). Further applications of massively parallel snRNA-seq to study cardiac biology and disease will provide novel insights into physiologically and clinically significant questions that cannot be satisfactorily addressed with population-based genome-wide profiling methods.

Here we applied our recently developed massively parallel snRNA-seq method, sNucDrop-seq (Hu et al. 2017), to investigate the transcriptional landscape of postnatal mouse hearts in both healthy and disease states of mitochondrial cardiomyopathy. Our transcriptome analysis of nearly 20,000 nuclei offered new insights into several key questions in cardiac biology: cell type composition, and functional heterogeneity in normal postnatal hearts and changes of transcriptional landscape of each cell type in disease state. We also used our single-nucleus transcriptome data set to reveal cell type-specific gene regulatory networks (GRNs) exemplified by heart disease-associated *Gdf15* transcription. Our approach is applicable to study similar questions in many areas of biology and disease.

Results

sNucDrop-seq for single-nucleus transcriptome analysis of postnatal mouse hearts

We optimized a mouse heart nucleus isolation protocol based on sucrose gradient ultracentrifugation that helps minimize cytoplasmic contamination and protect nucleus integrity (Supplemental Fig. S1A; Hu et al. 2017). We performed sNucDrop-seq in normal developing postnatal hearts as well as hearts from a mouse model of pediatric mitochondrial cardiomyopathy. In this model, cardiac genetic inactivation of two transcription factors essential for normal cardiac metabolism and function (estrogen-related receptor α [ERRα] and ERRγ) results in rapid postnatal development of dilated mitochondrial cardiomyopathy, heart failure, and death within a month of birth (Wang et al. 2015). ERRα and ERRγ directly regulate expression of hundreds of genes important in mitochondrial fatty acid oxidation and oxidative phosphorylation (OxPhos) as well as cardiac contraction and conduction (Alaynick et al. 2007; Dufour et al. 2007; Huss et al. 2007; Wang et al. 2015). Cardiac *ERRα/γ* knockout (referred to here as knockout) mouse hearts exhibited loss of mitochondrial structure and function as well as defects of myocardial contraction and conduction, accompanied by significantly reduced expression of mitochondrial and cardiac function genes (Wang et al. 2015). To optimize and validate the sNucDrop-seq assay for postnatal heart tissues, we performed sNucDrop-seq analysis of dissected ventricles from control and knockout mice ($n = 3$ littermate pairs) of 9–10 d of age—an early stage of disease development in knockout, when significant gene expression and functional changes could be readily detected (Wang et al. 2015, 2017).

We performed sNucDrop-seq of both freshly isolated (control 1 and knockout 1) and frozen (control 2 and 3 and knockout 2 and 3) heart samples and obtained highly concordant results within the same genotype (Supplemental Fig. S1B,C). Overall, 78% of reads aligned to genomes, among which 77% mapped to exons, 16% mapped to introns, and 7% mapped to intergenic regions. This relatively lower percentage of reads mapped to the intronic region in the nuclear transcriptomic profiles of heart samples (compared with ~50% intronic reads in mouse brains) (Hu et al. 2017) suggests that the relative composition of nascent transcripts varies significantly among cell types and organs. After quality filtering (>500 genes detected per nucleus), >15,000 nuclei were retained from three pairs of control and knockout littermates (Supplemental Table S1) for further analysis (7760 nuclei for control and 7323 nuclei for knockout). We obtained similar numbers and distributions of transcripts and genes per nucleus between samples (Supplemental Fig. S1B; Supplemental Table S1). In addition, sNucDrop-seq results showed high concordance when compared with bulk RNA-seq from control and knockout hearts (Supplemental Fig. S1D), further validating the sNucDrop-seq approach. sNucDrop-seq also provided additional, previously inaccessible insights into these transcriptional changes at single-nucleus resolution: Differential gene expression changes (e.g.,

Nppa and *Cox7a1*) between control and knockout hearts could result from changes in both the percentage of positive-expressing cells and average gene expression per nucleus (Supplemental Fig. S1E).

Unbiased cell type identification and study of cellular heterogeneity in healthy postnatal hearts

We assigned 7760 nuclei from healthy hearts into 14 distinct clusters using principal component analysis (PCA) dimension reduction followed by graph-based clustering, which was visualized by spectral *t*-distributed stochastic neighbor embedding (tSNE) (Fig. 1A). Numbers of detected transcripts (unique molecular identifiers [UMIs]) and genes were comparable among all clusters (Supplemental Fig. S2A,B). Each cluster contained nuclei from all heart samples, indicating overall reproducible transcriptional identities across biological replicates. Each of these 14 clusters displayed distinct nuclear transcriptional signatures, including both protein-coding and noncoding RNAs (Fig. 1B; Supplemental Fig. S2C,D; Supplemental Table S2). Based on pathway analysis and cell type-specific markers (Fig. 1C,D), we identified all of the major cardiac cell types—including cardiomyocytes, fibroblasts, and ECs—that express cell type-specific marker genes and together constituted >90% of all nuclei. Cardiomyocytes

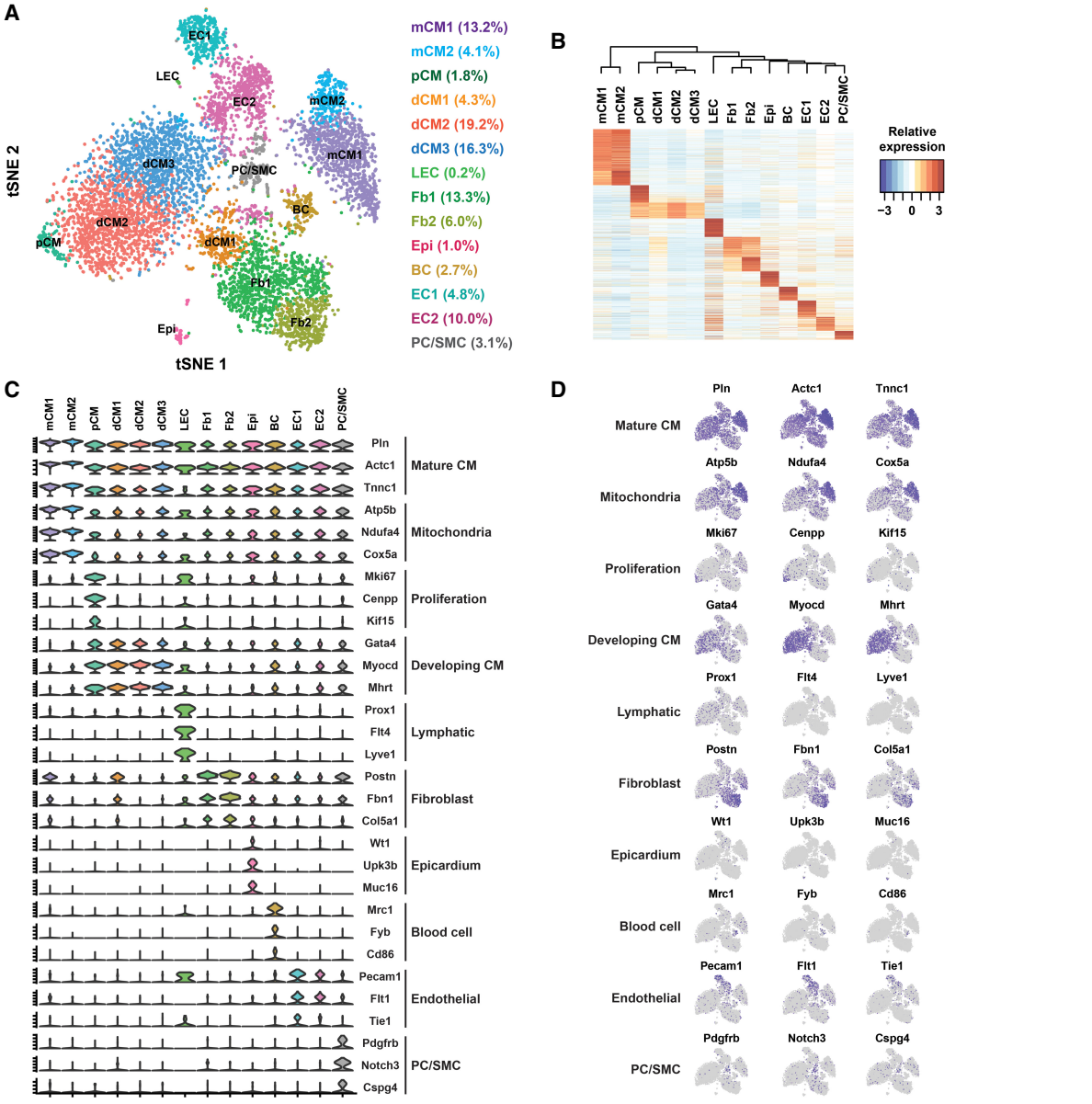

Figure 1. Unbiased cell type identification in the postnatal heart. (*A*) tSNE plot of 14 clusters of a P10 control heart. Cell identity and percentage are labeled. (*B*) Heat map showing clustering and gene expression of the 14 clusters. (*C*,*D*) Violin plot (*C*) and feature plot (*D*) illustrating the expression patterns of selected marker genes of each cluster. (pCM) Proliferating cardiomyocytes; (LEC) lymphatic ECs; (Fb) fibroblasts; (Epi) epicardial cells; (BC) blood cells; (PC/SMC) pericytes/smooth muscle cells.

could be divided into two major groups based on mitochondrial content, muscle fiber type, and key markers: less mature or developing cardiomyocytes (dCMs) with fewer mitochondria and positive for immature cardiomyoctye markers such as *Myocd* (also known as myocardin) and more mature cardiomyocytes (mCMs) with abundant mitochondria and positive for muscle fiber markers such as *Actc1* (also known as cardiac α-actin). Importantly, the relative cell type composition uncovered by sNucDrop-seq agreed well with the results defined by orthogonal approaches, including immunohistochemistry, FACS, and lineage tracing (Banerjee et al. 2007; Doppler et al. 2017). For instance, it was reported previously that 15-d-old (postnatal day 15 [P15]) mouse hearts contained 63% cardiomyocytes and 18% fibroblasts (Banerjee et al. 2007); we identified 59% cardiomyocytes and 19% fibroblasts in P10 mouse hearts.

Importantly, sNucDrop-seq revealed significant cellular heterogeneity within each major cell type. We were able to identify three populations of dCMs as well as two populations of mCMs, fibroblasts, and ECs. To determine whether these are distinct clusters, we performed differential expression tests to identify cell subtype-specific marker genes, which revealed subtle but significant differences between cell subtypes (Supplemental Table S3). Among dCM subpopulations, dCM3 was more mature, as it expressed more mitochondrial genes (e.g., *Cox6a2*, *Ndufa5*, and *Atp5j*), while dCM1 expressed fibroblast-enriched markers (e.g., *Col1a2*, *Col3a1*, and *Dcn*). Interestingly, some mCMs, such as those in the mCM1, also expressed these fibroblast-enriched markers. There was also a small population of presumably proliferating cardiomyocytes (pCMs) that expressed cell cycle genes (e.g., *Mki67*, *Cenpp*, and *Kif15*). Over 50% of these cells also expressed *Gata4* and *Myocd*, transcription factors critical for cardiomyocyte development (Fig. 1C,D). Indeed, *Gata4*$^+$ or *Myocd*$^+$ nuclei were significantly enriched only in dCMs (dCM1–3; odds ratio = 7.96; $P < 2.2 \times 10^{-16}$ by Fisher's exact test) but not in mCMs or nonmyocyte cells. Overall, these results reveal significant heterogeneity among dCMs, mCMs, and fibroblasts, with many subtypes that exhibited intermediate molecular signatures.

Through sNucDrop-seq analysis, we also identified two distinct EC populations not reported in previous single-cell RNA-seq studies of mouse embryonic (DeLaughter et al. 2016; Li et al. 2016) or adult (Gladka et al. 2018; Skelly et al. 2018) hearts. Analysis of subtype-enriched genes uncovered that EC2 expressed relatively more mitochondrial and muscle fiber genes (e.g., *Cox6a2*, *Mybpc3*, and *Mhrt*) (Supplemental Table S3). EC1-enriched genes included *Npr3* as well as *Tie1* and *Tie2* (receptors for angiopoietins critical for angiogenesis) (Supplemental Fig. S3A). As a proof of principle for using our cardiac cell atlas as a resource to identify and characterize these EC subtypes, we used immunohistochemistry to show that these EC subtypes represent anatomically distinct populations of cardiac ECs (Supplemental Fig. S3B). While general EC marker PECAM1 stained all ECs in the endocardium, arteries, veins, and capillaries, EC1-specific NPR3 marked only some capillary and endocardium but few arteries or veins. We also used confocal microscopy to examine these ECs with double immunostaining. PECAM1 and NPR3 double staining revealed that many NPR3 cells are PECAM1-positive and therefore ECs (Supplemental Fig. S3C). PECAM1 and cardiac troponin I (TNNI3) double staining revealed that there are some cells that coexpress PECAM1 and TNNI3 (Supplemental Fig. S3D), suggesting that a subpopulation of ECs can express muscle fiber genes.

The sNucDrop-seq analysis also identified relatively rare cell types. These included pericytes or smooth muscle cells, blood cells, epicardial cells, and pCMs, which express related specific marker genes and together constitute 8.8% of the total nuclei (Fig. 1A–D). Historically, these rare cardiac cell types were often defined by a few cell markers. Our unbiased approach not only validated known markers (Fig. 1C,D; Supplemental Table S2) but also revealed transcriptomic signatures based on the expression patterns of hundreds of genes for these cell types. Based on our sNucDrop-seq data, we identified unbiased lists of highly cell type-specific genes that can be used to classify cardiac pericytes/smooth muscle cells, epicardial cells, and lymphatic ECs (LECs), respectively (Supplemental Table S4). For example, although *Wt1* and *Tbx18* are well-established epicardium markers, our study uncovered >30 additional high-confidence markers for epicardial cells, including both known (e.g., *Upk3b* and *Upk1b*) and novel (e.g., *Il18r1* and *Msln*) genes (Supplemental Fig. S3E; Bochmann et al. 2010). Moreover, these new marker genes may reveal previously unrecognized biological functions of these less studied cell types; for example, mechanosensitive ion channel *Piezo2* and genes important in neurodevelopment (e.g., *Shank3* and *Reln*) were highly expressed and specifically enriched in LECs (Supplemental Fig. S3F). Indeed, 62% of the *Flt4*$^+$ (Vegfc receptor, which is a marker for lymphatic vessel) cells coexpressed *Piezo2*, suggesting potential functions of some LECs in sensing blood pressure or other mechanical signals. This significantly expanded list of potential marker genes highlights the value of our study as a resource for future research investigations of these relatively rare cardiac cells.

Transcriptomic dynamics of cardiomyocyte maturation in postnatal hearts

To investigate transcriptome dynamics during postnatal heart development, we also performed sNucDrop-seq in P6 control mouse ventricles ($n = 3$ mice) and compared the results with those of P10 control mice. Using the same analysis settings, we obtained 4560 nuclei with similar numbers of transcripts and genes per nucleus among the three biological replicates (Supplemental Table S1). Ten distinct clusters were identified based on their transcriptomic signatures (Fig. 2A; Supplemental Table S5). All of the cell types identified in P10 hearts were found in P6 hearts except for LEC, likely because it is relatively rare (0.2% or 19 nuclei in P10) and therefore harder to detect, with fewer total nuclei studied (4560 nuclei in P6

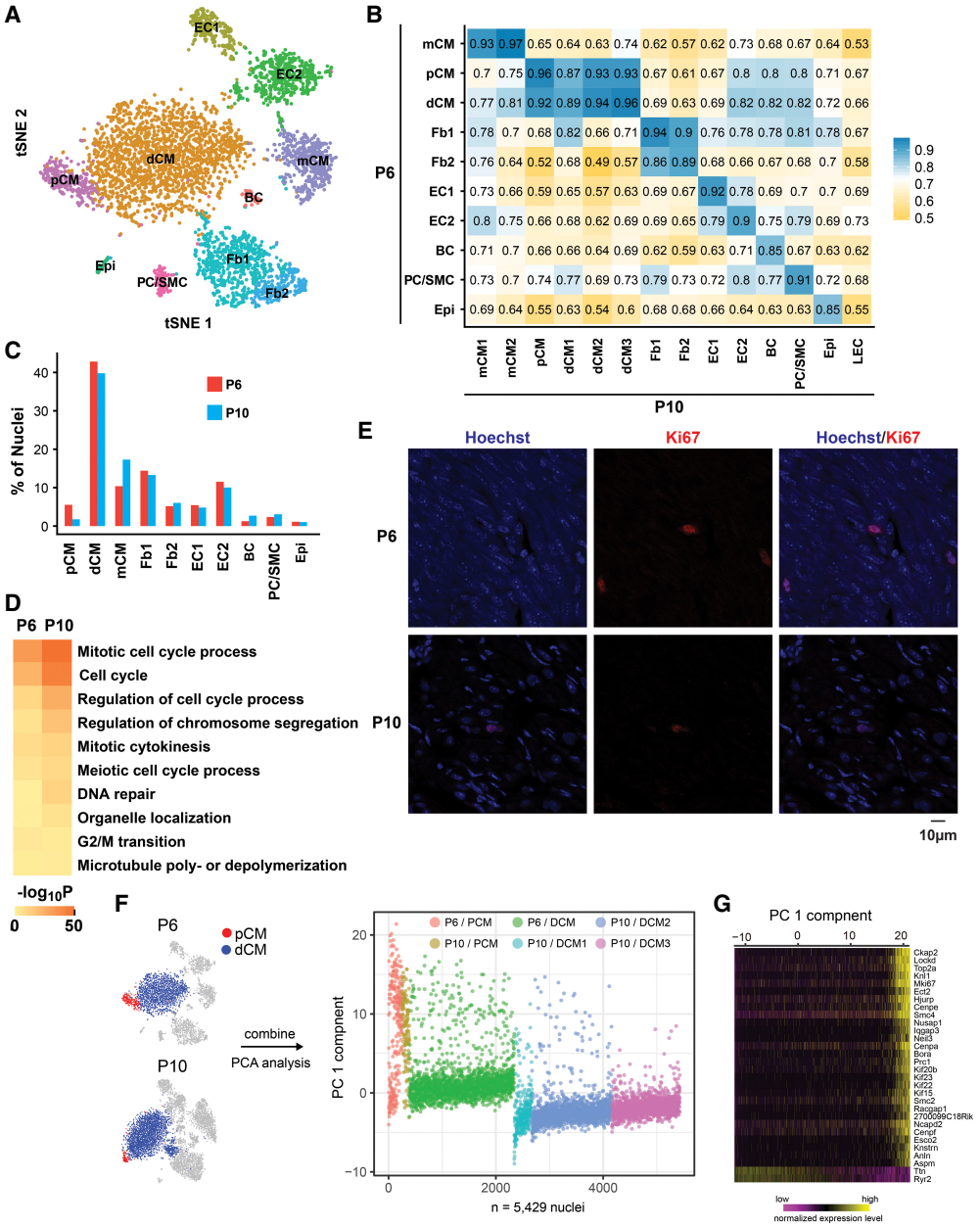

Figure 2. Transcriptomic dynamics of cardiomyocyte maturation in postnatal hearts. (*A*) tSNE plot of 10 clusters of a P6 control heart. Cell identities are labeled. (*B*) Pairwise comparison of all clusters between P6 and P10 control hearts. (*C*) Cell type compositions in P6 and P10 control hearts. (*D*) The top 10 enriched pathways in P6 and P10 pCMs. (*E*) Confocal microscopy shows that Ki67 staining (red) colocalizes with nucleus Hoechst staining (blue). (*F*, *left* panel) Workflow for PCA analysis. (*Right* panel) Plot of PC1 cell-loading scores (*Y*-axis). On the *X*-axis, cells are ordered by library size (largest to smallest) within each cell type (color-coded). (*G*) Heat map of the top loading genes. Nuclei are ordered by PC1. (Fb) Fibroblasts; (Epi) epicardial cells; (BC) blood cells; (PC/SMC) pericytes/smooth muscle cells.

vs. 7760 nuclei in P10). While two populations each of ECs and fibroblasts were also detected in P6 hearts, only one population each of dCMs and mCMs was found in P6 hearts. Pairwise comparison of all clusters between P6 and P10 hearts indicated that the cell types and subtypes identified in P6 hearts were counterparts of those in P10 hearts (Fig. 2B). Comparative analysis of cell type composition between P6 and P10 revealed that the biggest difference was the substantial decrease of pCMs and the corresponding increase of mCMs in P10 hearts, while the percentages of other cell types changed little (Fig. 2C). Notably, pCMs were much more abundant in P6 hearts than in P10 hearts (5.5% in P6 vs. 1.8% in P10). P6 and P10 pCM marker genes are highly overlapping, with 78% (101 out of 130) of P6 pCM marker genes also enriched in P10 pCMs. P6 and P10 pCMs exhibit similar gene signatures, dominated by essential cellular processes and pathways required for cell proliferation, such as

mitotic cell cycle and chromosome segregation, and, in particular, cytokinesis for cell division (Fig. 2D). Ki67 (a pCM and proliferating cell marker) immunostaining confirmed the existence of these pCMs in mouse hearts, and their percentage declined during postnatal development (Fig. 2E), consistent with our sNucDrop-seq data. These results suggest that cardiomyocyte differentiation and/or maturation represents a major biological event during this period of postnatal heart development in mice (between P6 and P10).

To further dissect the developmental/transitional transcriptional changes within pCMs and dCMs, we performed PCA analysis on 5429 cardiomyocyte nuclei combined from |P6 (2205 nuclei) and P10 (3224 nuclei) using 1276 highly variable genes (Fig. 2F, left panel). The top PCA component, which accounted for 3.99% of total variation, separated all nuclei into overlapping stepwise clusters ordered by age (from P6 to P10) and cell type (from pCMs to dCMs), indicating the temporally progressive maturation of cardiomyocytes (Fig. 2F, right panel). We identified the top genes associated with PC1. These included cell cycle markers (i.e., *Ckap2*, *Top2a*, and *Mki67*) highly expressed in pCMs and muscle contraction genes (i.e., *Ttn* and *Ryr2*) highly enriched in dCMs (Fig. 2G). These results suggest that these pCM and dCM clusters may represent different stages along the postnatal cardiomyocyte maturation process.

Cell type-specific transcriptional remodeling of pediatric mitochondrial cardiomyopathy

We next applied sNucDrop-seq to investigate the cell type-specific transcriptional landscape in the cardiac *ERRα/γ* knockout mouse model of pediatric mitochondrial cardiomyopathy. Analysis of the 7323 nuclei from three P10 knockout hearts revealed 13 clusters (Fig. 3A) with largely comparable numbers of detected transcripts and genes for each cluster (Supplemental Fig. S4A). As in control hearts, each cluster contained a unique transcriptome, including protein-coding and noncoding RNA signatures (Fig. 3B, C; Supplemental Fig. S4B,C; Supplemental Table S6). Pathway analysis and marker genes revealed the identities of these clusters (Fig. 3A–C; Supplemental Table S6). Pairwise comparison of all control and knockout clusters showed that there was generally a one-to-one correlation of the same subtype of cardiac cells between control and knockout (Fig. 3D).

While knockout hearts retained most of the major and rare cell types except pCMs and LECs, their relative abundance exhibited cell type-specific changes (Fig. 4A). There remained significant heterogeneity among cardiomyocytes, fibroblasts, and ECs. However, each knockout cell type or subtype exhibited significant transcriptome-level changes (Fig. 4B). Subtypes of cardiomyocytes, fibroblasts, and ECs exhibited larger transcriptional changes than epicardial cells, pericytes/smooth muscle cells, or blood cells, suggesting that distinct cardiac cell types undergo differential levels of transcriptional remodeling during heart disease progression. Pathway enrichment analysis revealed that mitochondrial OxPhos and TCA cycle (e.g., *Cox7a1*, *Ndufa1*, *Sdha*), fatty acid degradation/oxidation (e.g., *Acadm* and *Hadh*), extracellular matrix associated with fibrosis (e.g., *Post* and *Fbn1*), and ribosome genes (e.g., *Rplp1* and *Rps3*) were among the most affected pathways in knockout hearts (Fig. 4C,D). However, they also displayed cell type-specific and subtype-specific pathway changes. This suggests that individual cell types or subtypes adopted differential metabolic and functional adaptations to disease state.

It has often been observed that mitochondrial functions and gene expression are decreased in mitochondrial cardiomyopathy and many other forms of heart disease, including our knockout mouse model (Huss and Kelly 2005; Abel and Doenst 2011; Harvey and Leinwand 2011; Wang et al. 2015). However, previous RNA-seq studies were based on whole hearts/chambers or focused only on cardiomyocytes that possess the most abundant mitochondria. Our sNucDrop-seq analysis revealed cell type-specific mitochondrial gene expression changes in diseased hearts for all major cell types at the single-nucleus resolution. Consistent with bulk RNA-seq and our previous report (Wang et al. 2015), most subtypes of dCMs and mCMs exhibited significantly decreased expression of mitochondrial OxPhos genes (Fig. 4C,D), reflecting the direct effects of loss of ERRα/γ in these cells. Reduced OxPhos gene expression was also observed in fibroblasts and the EC1 subtype of ECs in knockout hearts but not in blood cells, pericytes/smooth muscle cells, or epicardial cells. In contrast, expression of mitochondrial OxPhos genes was significantly increased in a putative population of activated fibroblasts, consistent with a metabolic profile of increased mitochondrial respiration reported recently in these cells (Bernard et al. 2015; Negmadjanov et al. 2015). These mitochondrial gene expression changes in noncardiomyocytes are likely secondary due to the progression of mitochondrial cardiomyopathy.

It is generally appreciated that the heart switches from mainly catabolizing fat in the healthy state to predominantly using glucose in the heart failure stage (Huss and Kelly 2005). In addition, defective branched chain amino acid (BCAA) catabolism has been identified recently as a metabolic hallmark of heart failure and contributes to disease development (Sun et al. 2016; Li et al. 2017). Our sNucDrop-seq results revealed that only mCMs, not dCMs or other cell types, showed a significant decrease in gene expression related to fatty acid oxidation, BCAA catabolism, and associated pyruvate metabolism (Fig. 4C,D; Li et al. 2017). This was in contrast to a more universal decrease in mitochondrial TCA and OxPhos. Therefore, the general concept of mitochondrial dysfunction in heart disease occurs in a more intricate cell type-specific manner: Defective fatty acid oxidation and BCAA catabolism are mCM-specific, but a decrease in mitochondrial OxPhos takes place in a broader spectrum of cardiac cell types. These results suggest that targeting metabolic remodeling for heart disease treatment needs to consider these cell type-specific mitochondrial pathways.

Increased expression of fibrosis-associated extracellular matrix genes (e.g., *Postn* and *Fbn1*) was observed across most cell types in knockout hearts compared with wild-

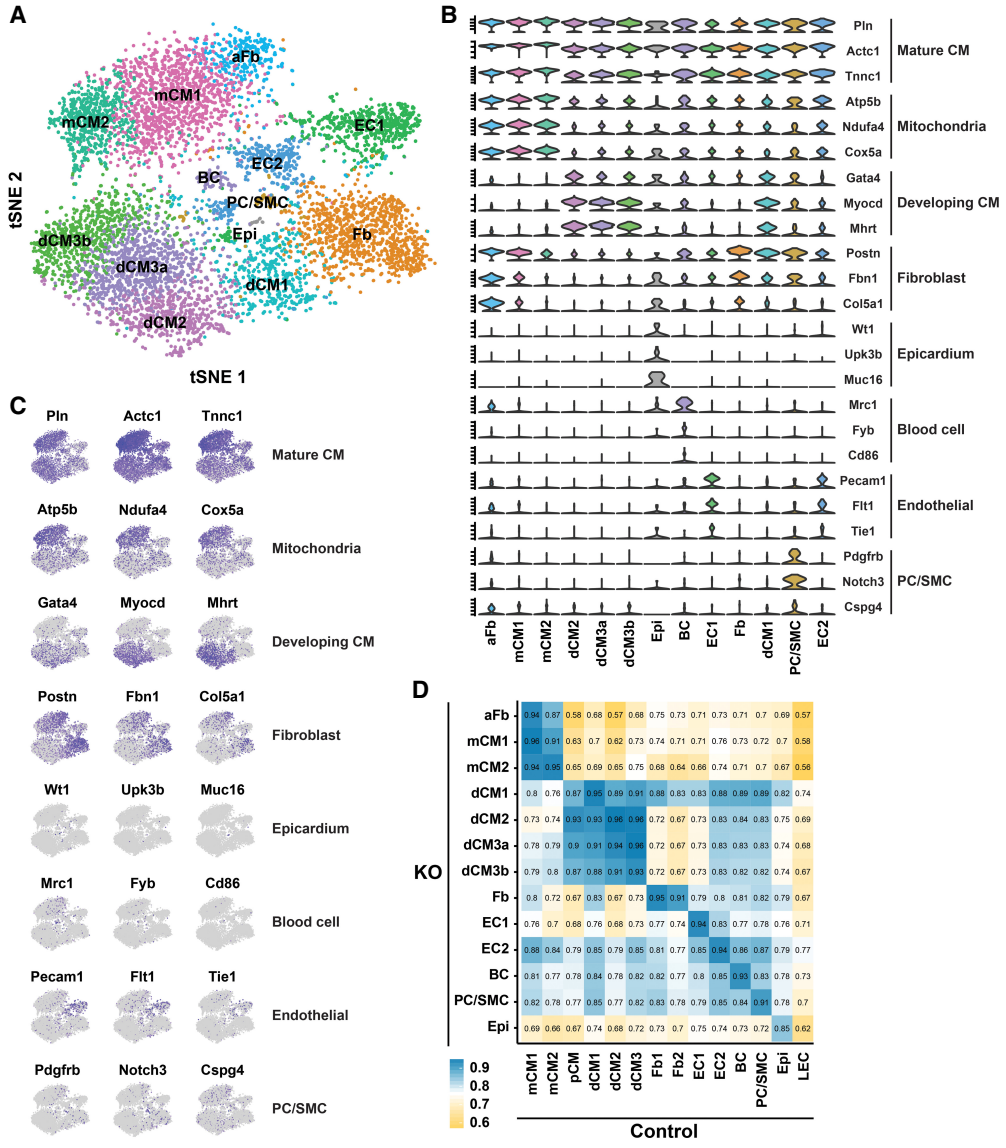

Figure 3. Cell type identification and correlation in a mouse model of pediatric mitochondrial cardiomyopathy. (*A*) tSNE plot of 13 clusters of P10 knockout hearts. (*B*,*C*) Violin plot (*B*) and feature plot (*C*) illustrating the expression patterns of selected marker genes of each cluster. (*D*) Pairwise comparison of all clusters between P10 control and knockout hearts. (aFb) Activated fibroblasts; (Fb) fibroblasts; (Epi) epicardial cells; (BC) blood cells; (PC/SMC) pericytes/smooth muscle cells.

type hearts (Fig. 4C,D). This suggests that cardiac fibrosis may occur in a much broader scope than generally believed: It affects the whole heart and is not limited to fibroblasts. Notably, we also observed an increase of ribosome genes expression in many cell types of diseased hearts. Increased protein synthesis or ribosome RNA abundance was reported previously in animal models of dilated or hypertrophic cardiomyopathy (Moroz 1967; Morgan et al. 1985; Burke et al. 2016a). Our results suggest that such a potentially compensatory response in protein synthesis occurs in mitochondrial cardiomyopathy and involves all major cardiac cell types.

Increased fibrosis is a hallmark of many forms of heart disease, including mitochondrial cardiomyopathy. Although knockout hearts retained a comparable percentage of total fibroblasts, a putative population of activated fibroblasts was identified based on known fibrosis marker genes in addition to the inactive fibroblast population. Activated fibroblasts exhibited transcriptional profiles of enriched fibrosis-related extracellular matrix as well as endoplasmic reticulum and mitochondrial OxPhos pathways, consistent with known phenotypes of activated fibroblasts (Supplemental Table S5; Bernard et al. 2015; Negmadjanov et al. 2015; Tallquist and Molkentin 2017). Indeed, a significantly increased level of fibrosis was observed in knockout hearts at this age, as revealed by Sirius Red staining (Fig. 4E). Detailed examination of the activated fibroblast transcriptional signature revealed

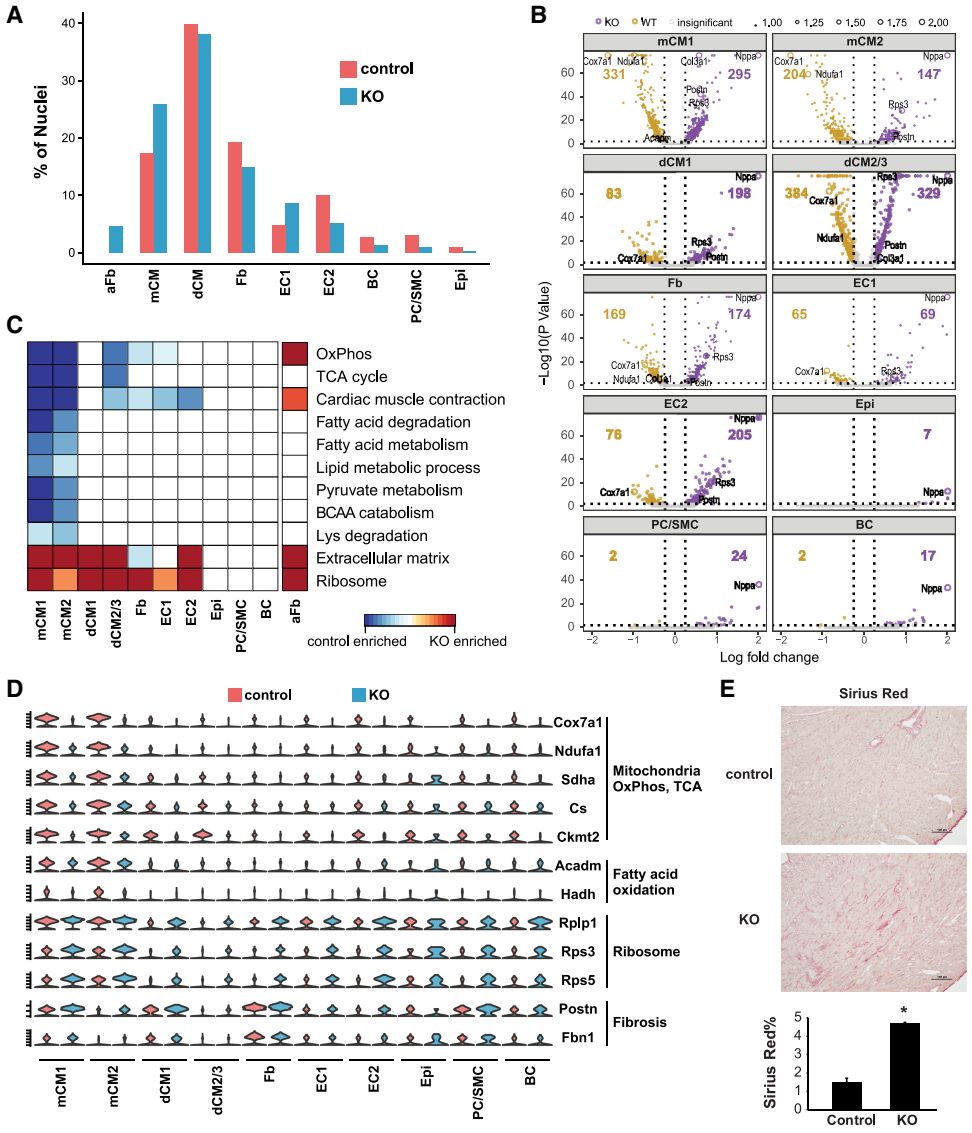

Figure 4. Cell type-specific transcriptional remodeling of pediatric mitochondrial cardiomyopathy. (*A*) Cell type compositions in P10 control and knockout hearts. (*B*) Volcano plot showing differentially expressed genes in correlated clusters of control and knockout hearts. (*C*) Cellular pathways significantly changed in knockout versus control hearts between correlating clusters. (*D*) Violin plot showing representative gene expression changes across different cell types. (*E*) Sirius Red stain of fibrosis in control and knockout hearts and quantification. $n = 2$ mice per genotype. Bar, 100 µm. (*) $P < 0.05$ by *t*-test. (Fb) Fibroblasts; (aFb) activated fibroblasts; (Epi) epicardial cells; (BC) blood cells; (PC/SMC) pericytes/smooth muscle cells; (BCAA) branched chain amino acid.

that they contained few genes involved in cell proliferation (Supplemental Table S6). Considering that knockout hearts contained similar percentages of total fibroblasts (fibroblasts and activated fibroblasts) (Fig. 4A) and lacked distinct populations of proliferating cells, this suggests that the increased fibrosis in knockout hearts results from fibroblast activation rather than proliferation.

While knockout hearts retained two EC populations (EC1 and EC2) and the total percentage of ECs remained unchanged between control and knockout, the relative composition of these EC subtypes likely changed in response to disease states. EC1 showed a significant expansion (8.6% compared with 4.8% in control) in knockout hearts, which was validated by immunostaining of the EC1-specific marker NPR3 (Supplemental Fig. S5A). Expression of *Tie1* and *Tie2* remained higher in EC1 than in EC2 (Supplemental Fig. S5B), suggesting that EC1 abundance might increase in knockout hearts due to increased angiogenesis.

GRNs associated with the transcriptional activation of Gdf15

GRN refers to a network of molecular regulators that functionally interact to modulate a gene expression program critical to specific cellular states and functions

(Wyrick and Young 2002). Single-cell transcriptome analysis enables the inference of cell type-specific or developmental stage-specific GRNs (Moignard et al. 2015; Wagner et al. 2016). Based on sNucDrop-seq results, we next investigated the GRNs underlying the transcriptional activation of *Gdf15* in heart disease. GDF15 (also known as MIC-1, NAG-1, PLAB, or PTGFB) is a protein of the transforming growth factor β (TGFβ) family with pleiotropic functions (Unsicker et al. 2013). GDF15 has recently gathered strong interest for its pharmaceutical potential in treating obesity and its implication in cardiovascular disease. GDF15 suppresses appetite through activating its receptor, GFRAL, in the brain stem (Johnen et al. 2007; Emmerson et al. 2017; Hsu et al. 2017; Mullican et al. 2017; Xiong et al. 2017; Yang et al. 2017) and is currently being investigated as a potential therapeutic agent/target for obesity, metabolic disease, anorexia, and cachexia. In addition, many clinical studies have found that plasma GDF15 is significantly elevated in various heart diseases and is associated with increased morbidity and mortality; it is therefore used as an independent biomarker for heart disease, especially heart failure (Baggen et al. 2017; Wollert et al. 2017). However, how GDF15 level is regulated at the molecular level in heart disease remains unclear (Wollert et al. 2017).

We demonstrated recently that cardiac *Gdf15* transcription is markedly activated during the progression of heart failure in our cardiac ERRα/γ knockout mouse model, and, in the pediatric period, GDF15 acts as a heart-derived hormone to inhibit liver growth hormone signaling, thereby coordinating cardiac function and postnatal body growth (Wang et al. 2017). Our previous quantitative PCR (qPCR) analysis showed that average *Gdf15* mRNA level increased ~10-fold in P10 ERRα/γ knockout mouse hearts (Wang et al. 2017). GDF15 protein immunostaining and quantification further showed that, in contrast to very few GDF15$^+$ cells in control mouse hearts, ~1.5% of cells in knockout mouse hearts express detectable GDF15 protein at 10 d of age (Fig. 5A,B). However, the exact cell types expressing *Gdf15* and how *Gdf15* transcription is activated in these specific cell types remain incompletely understood.

sNucDrop-seq allowed us to address these questions in a cell type-specific manner. Overall, there was a 10-fold increase in the number of *Gdf15*$^+$ nuclei reaching ~3% in P10 knockout hearts (Fig. 5C,D). The majority (72%) of *Gdf15*$^+$ nuclei was cardiomyocytes (mCMs and dCMs) (Fig. 5E; Supplemental Table S7). This is consistent with our previous immunostaining result showing that GDF15 protein colocalizes with TNNI3 (Wang et al. 2017). Small numbers of *Gdf15*$^+$ nuclei were also found

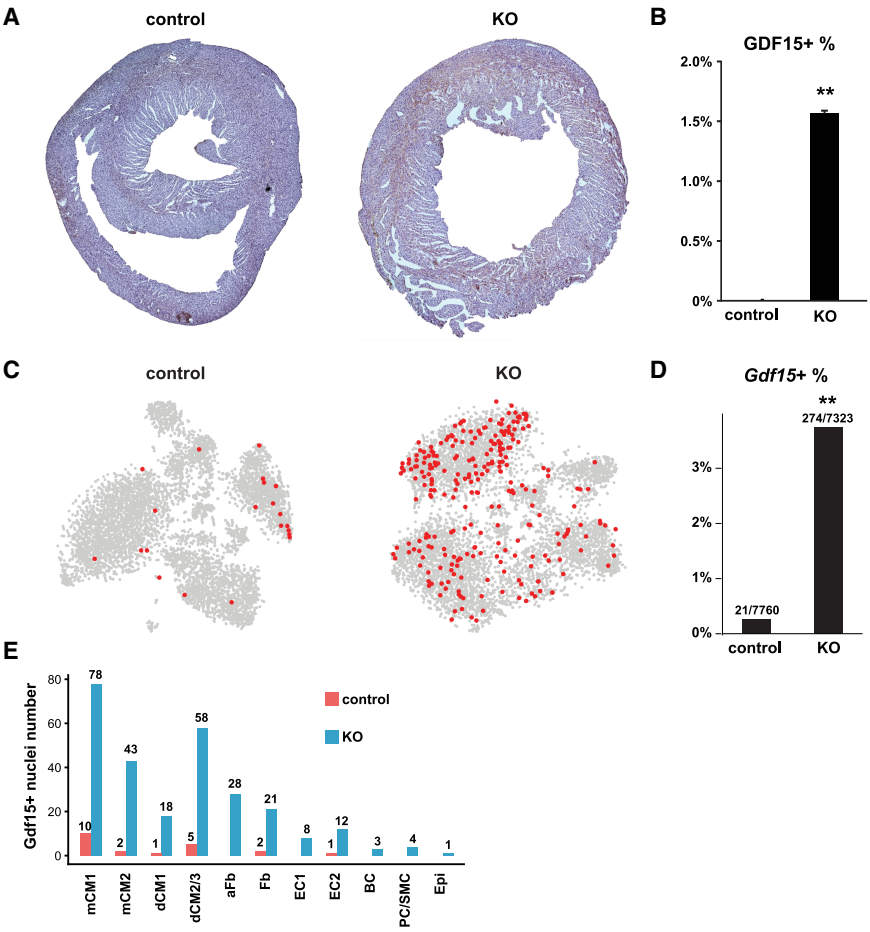

Figure 5. *Gdf15* expression in control and knockout hearts. (*A*) Representative pictures of GDF15 immunostaining in P10 hearts. (*B*) Quantification of *Gdf15*$^+$ cells based on immunostaining in *A*. $n = 2$ mice per genotype. (*C*) Feature plot showing *Gdf15*$^+$ nucleus distribution in P10 hearts. (*D*) Quantification of *Gdf15*$^+$ nuclei in control and knockout hearts based on sNucDrop-seq. (*E*) Distribution of *Gdf15*$^+$ nuclei in each cell type. (**) $P < 2.2 \times 10^{-16}$ by χ^2 test in *B* and *D*.

in other cell types, notably fibroblasts (both fibroblasts and activated fibroblasts) and ECs. This raises the question of cell type specificity of GRNs that control *Gdf15* expression.

To define cell type-specific GRNs that activate *Gdf15* transcription in knockout hearts, we reasoned that the core network components (i.e., transcription factors, cofactors, and chromatin modifiers) should be coexpressed in *Gdf15*$^+$ cells. We therefore searched for transcription factor, cofactor, and chromatin-modifying genes that (1) were statistically enriched in *Gdf15*$^+$ nuclei compared with *Gdf15*$^-$ nuclei in either control or knockout hearts in the same cell type and (2) showed strong positive correlation of expression with *Gdf15* in the same cell type. This analysis resulted in a list of candidate genes that constitute cell type-specific GRNs of *Gdf15* (Fig. 6A; Supplemental Table S8). Expression of *Gdf15* and these cell type-specific candidate GRN genes are highly correlated in cell types where both are present (Supplemental Fig. S6). For example, *Gata4* was revealed as a candidate cardiomyocyte and fibroblast GRN component, and *Gata4* and *Gdf15* expression was positively correlated in both cardiomyocytes and fibroblasts. Notably, *Gata4* is well known for its essential role in embryonic heart development, and mutations of the *Gata4* gene are known to cause congenital heart disease in humans. In addition, the transcriptional activity of *Gata4* is enhanced by pressure overload, angiotensin, and other signals that induce adult cardiomyopathy or heart failure through post-translational modification or increased expression (Oka et al. 2007). We next screened the mouse *Gdf15* promoter (within 2 kb upstream of the transcription start site) and candidate enhancer regions (high H3K4me1 and H3K27ac histone marks close to the *Gdf15* gene locus) and found that there were canonical binding motifs for almost all of the transcription factors of the candidate *Gdf15* GRNs (Supplemental Table S9). Therefore, these transcription factors may directly bind to the *Gdf15* promoter or enhancer to activate its transcription. Further analysis revealed the subset of genes with extensive known physical and functional interactions. Together, these genes form the nodes of the cell type-specific cardiac *Gdf15* GRNs (Fig. 6B).

As a proof of principle, we next validated the biological significance of these findings by focusing on *Gata4*. We found that adenoviral-mediated *Gata4* overexpression

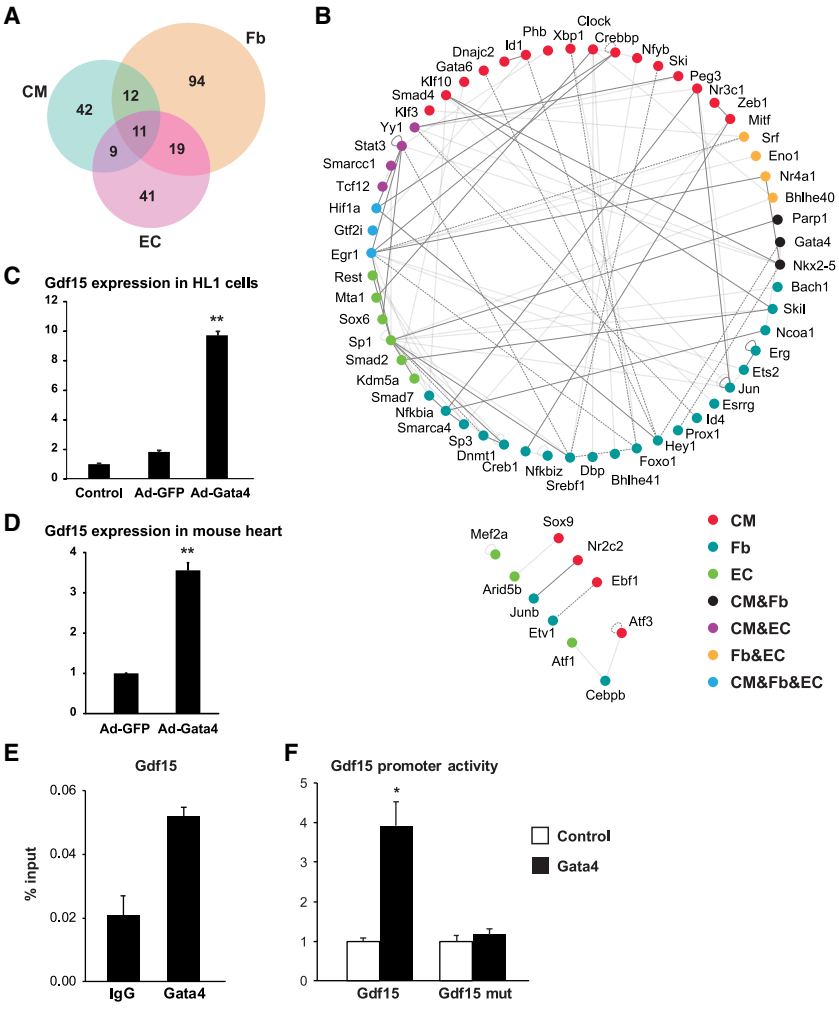

Figure 6. Cardiac cell type-specific GRNs of *Gdf15*. (*A*) Venn diagram showing the number of transcriptional regulators that constitute cell type-specific GRNs. (*B*) Cardiac *Gdf15* GRNs that include cell type-specific transcriptional regulators. Only genes of the key node status are shown. (*C*) Adenoviral-mediated overexpression of *Gata4* induces *Gdf15* expression in HL1 cells. (*D*) *Gata4* activates *Gdf15* expression in wild-type mouse hearts. (*E*) Increased binding of GATA4 to the mouse *Gdf15* promoter by chromatin immunoprecipitation (ChIP). (*F*) Luciferase reporter assay showing that GATA4 activates the mouse *Gdf15* promoter but not one with a mutant GATA4-binding site. The fibroblasts in *A* and *B* include both fibroblast and activated fibroblast cell populations. (*) $P < 0.05$; (**) $P < 0.01$ by *t*-test.

induced *Gdf15* expression in HL-1 cardiomyocytes in vitro (Fig. 6C) and, importantly, in wild-type postnatal mouse hearts in vivo (Fig. 6D). Chromatin immunoprecipitation (ChIP) studies showed that GATA4 bound to a canonical GATA site in the mouse *Gdf15* promoter (Fig. 6E). GATA4 increased activity of the *Gdf15* promoter but not one with the GATA site mutated (Fig. 6F). Together, these results reveal the molecular mechanism of *Gdf15* induction in heart disease and demonstrate the utility of snRNA-seq analysis in inferring cell type-specific GRNs.

Discussion

Here we applied massively parallel snRNA-seq to interrogate the transcriptional landscape in postnatal mouse hearts associated with either healthy or mitochondrial cardiomyopathy disease states. By resolving in vivo cellular heterogeneity in hearts with sNucDrop-seq, our study provided novel insights into several areas of cardiac biology that were underexplored. First, we showed that our unbiased approach could identify almost all cell types (abundant or rare), determine cell type composition of the heart, and resolve significant cellular heterogeneity associated with different developmental stages or functions in healthy postnatal hearts. Second, we investigated a pediatric mitochondrial cardiomyopathy mouse model, revealing distinct changes in organ composition and cell type-specific transcriptional remodeling with functional implications. Finally, we used the single-nucleus transcriptome results to uncover cell type-specific GRNs associated with transcriptional activation of *Gdf15* in heart disease. Importantly, our approach is generally applicable to studying many areas of cardiac biology and disease.

The high throughput of sNucDrop-seq enabled transcriptomic analysis of ~20,000 cardiac nuclei isolated from maturing postnatal hearts. Recent single-cell RNA-seq methods based on Fluidigm or flow cytometry platforms studied single heart cell transcriptome ranging from tens to ~1000 cells per age/developmental stage during mouse embryonic heart development (DeLaughter et al. 2016; Li et al. 2016; Gladka et al. 2018). Another report also used the Fluidigm platform for snRNA-seq analysis of isolated adult cardiomyocytes with 13–64 nuclei per sample (See et al. 2017). Our study complemented these previous studies by focusing on the early postnatal period, when the heart is rapidly maturing. In addition, sNucDrop-seq overcame the technical challenges associated with isolating intact single cells from mammalian hearts, thus empowering many new insights: (1) We identified several relatively rare cell types, including blood cells, pericytes/smooth muscle cells, LECs, epicardial cells, and pCMs, and determined their relative abundance in postnatal hearts. (2) We discovered significant heterogeneity within cardiomyocytes, fibroblasts, and ECs. Previous single-cell RNA-seq studies identified in mouse embryonic hearts heterogeneous cardiomyocyte populations, with one cardiomyocyte subpopulation that expressed fibroblast genes (DeLaughter et al. 2016). Our results suggest an even broader degree of cellular heterogeneity, possibly due to higher throughput and the nature of the postnatal stage. (3) We revealed the transcriptome-wide changes of all cell types and subtypes in the disease state of mitochondrial cardiomyopathy, which exhibited significant subtype-specific remodeling.

The transcriptome-wide insights obtained by sNucDrop-seq also informed new insights into cardiac biology in both healthy and disease states. For example, we uncovered numerous new marker genes for rare cell types or heterogeneous cell subtypes. Compared with previous methods that depended on a few cell markers, our method is likely more accurate because it is based on transcriptome-level information. These new gene signatures are potentially associated with previously unrecognized functions of these cells and will facilitate future studies. We also resolved distinct transcriptional signatures between cell subtypes, such as EC1 and EC2, and validated the result by immunostaining. Our results presented here as a resource should assist future endeavors to investigate potential functional, anatomical, or developmental differences between cardiac cell subtypes. sNucDrop-seq also has the ability to capture ongoing transcriptional events compared with steady-state transcriptome analysis by whole-cell RNA-seq.

We identified populations of presumable pCMs in both P6 and P10 control hearts. It is thought that mouse hearts continues to grow by means of cardiomyocyte proliferation in the early postnatal period (Eschenhagen et al. 2017). These two pCM populations are enriched for cardiomyocyte development genes such as *Gata4*$^+$ or *Myocd*$^+$, suggesting that they are cardiomyocytes. In addition, these two pCM populations share the same transcriptional signature of cell proliferation: mitosis, G2/M transition, chromosome segregation, and, in particular, cytokinesis for cell division (Fig. 2D). Ki67 immunostaining corroborated the presence of these pCMs in mouse hearts (Fig. 2E). Furthermore, the abundance of these pCMs declines from P6 (5.5%) to P10 (1.8%), consistent with the notion that mouse cardiomyocytes progressively lose their ability to proliferate shortly after birth. However, it remains possible that at least some of these cells are simply undergoing DNA synthesis and mitosis without cell division, such as multinucleation. Therefore, caution is warranted regarding the exact nature of these cells, and additional studies are needed to definitively address the question of to what extent these pCMs are proliferating.

We were able to reveal cell type-specific and subtype-specific transcriptional remodeling in a mouse model of mitochondrial cardiomyopathy. Overall, cardiomyocytes, fibroblasts, and ECs exhibited profound metabolic and functional changes, while fewer changes were observed in other cardiac cell types. A common theme to most cells is the down-regulation of the mitochondrial OxPhos pathway (but more limited for fatty acid oxidation and BCAA catabolism pathways) and an increase of ribosome related genes. Increased fibrosis gene expression was also observed in many nonfibroblast cells, suggesting that tissue fibrosis might involve a broader range of cell types than simply fibroblast activation—at least at the

transcriptional level. Intriguingly, we could not find signs of a distinct pCM population in knockout hearts any more. It is possible that mitochondrial cardiomyopathy had more profound impacts on cardiac health by impairing postnatal cardiomyocyte proliferation capacity (Naqvi et al. 2014; Eschenhagen et al. 2017).

The sNucDrop-seq data set allowed us to deduce candidate cell type-specific GRNs that activate *Gdf15* transcription in heart disease, and we experimentally validated key nodes of these GRNs. Intriguingly, different cell types seem to use both overlapping (i.e., *Gata4* for cardiomyocytes and fibroblasts) and cell type-specific (i.e., *Gata6* for cardiomyocytes) transcription factors to regulate *Gdf15* expression. One explanation is that these transcription factors exhibit cell type-specific expression patterns or their expression is induced only in specific cell types during heart disease progression. This raises the question of how these upstream regulators are transcriptionally activated in a cell type-specific manner (i.e., cell type-specific *Gata4* GRNs). Based on our current study of *Gdf15* GRNs, we anticipate that future time-course snRNA-seq studies covering multiple stages of heart disease progression will help address this question and shed light on the molecular underpinnings of heart disease progression. In summary, while future studies are needed to continue validating our current findings, our results demonstrate the value of large-scale snRNA-seq analysis in studying multiple areas of cardiac biology and disease.

Materials and methods

Animal studies

All animal studies were approved by and performed under the guidelines of the Institutional Animal Care and Use Committee of the Children's Hospital of Philadelphia (CHOP). All mice were in the C57BL6/J background. Cardiac ERRα/γ knockout mice were described previously (Wang et al. 2015).

snRNA-seq and data analysis

We performed sNucDrop-seq and data analysis as described previously (Hu et al. 2017) with optimizations for the heart tissue. Detailed methods and analysis are in the Supplemental Material. The data were deposited in the Gene Expression Omnibus (GEO) database under accession number GSE118545.

Whole-heart RNA-seq

RNA-seq of hearts from P16 littermate control and knockout was as described previously (Wang et al. 2017). The data were deposited in the GEO database (GSE88761).

RNA and protein analysis

qRT–PCR, luciferase reporter assay, and immunohistochemistry were performed as described previously (Pei et al. 2006, 2011, 2015; Wang et al. 2017; Zhao et al. 2018). We isolated total RNA from mouse tissues or HL-1 cells using RNAzol RT (Molecular Research Center) following the manufacturer's instructions. The antibodies used were PECAM1 (Santa Cruz Biotechnology, sc-46694; and BD Biosciences, 550274), NPR3 (Santa Cruz Biotechnology, sc-515449), TNNI3 (Abcam, ab47003), Ki67 (Vector Laboratories, vp-RM04), and GDF15 (Abcam, ab189358). Sirius Red staining was performed using the Picrosirius Red stain kit (Polysciences). Adenovirus construction and pericardial injection were performed as described previously (Pei et al. 2006, 2011; Wang et al. 2017).

Statistical analysis

Fishers' exact test, χ^2 test, correlation test, and Student's *t*-test were performed in R to determine the statistical significance, with $P < 0.05$ deemed as statistically significant.

See the Supplemental Material for additional Materials and Methods.

Acknowledgments

We are grateful to Dr. Douglas Wallace, Dr. Mitchell Lazar, Dr. Matthew Weitzman, Dr. Amita Sehgal, Dr. Michael Marks, Dr. Mark Kahn, Dr. Zoltan Arany, and Dr. Rajan Jain for critical discussion of the project. We thank Jing Jing Li, Xiangjin Kang, Qi Qiu, Deborah Kwon, and Emily Fabyanic for their technical help. The authors and this work were supported by the Office of the Assistant Secretary of Defense for Health Affairs through the Peer Reviewed Medical Research Program under award number W81XWH-16-1-0400; National Institutes of Health DK111495 to L.P., R00HG007982 and DP2HL142044 to H.W., and K08 DK099379 to B.J.W.; and W.W. Smith Charitable Trust grants H1407 to L.P. and H1703 to H.W.

Author contributions: L.P. conceived and directed the project. P.H., J.L., J.Z., H.W., and L.P. performed the experiments and analyzed the data. P.H. carried out bioinformatics analysis of single-nucleus data. B.J.W. is a pathologist who examined the histological and immunohistochemistry studies and captured microscopic images. K.L. provided technical assistance. P.H., J.L., H.W., and L.P. wrote the manuscript, and all authors reviewed and/or edited the manuscript.

References

Abel ED, Doenst T. 2011. Mitochondrial adaptations to physiological vs. pathological cardiac hypertrophy. *Cardiovasc Res* **90:** 234–242.

Alaynick WA, Kondo RP, Xie W, He W, Dufour CR, Downes M, Jonker JW, Giles W, Naviaux RK, Giguere V, et al. 2007. ERRγ directs and maintains the transition to oxidative metabolism in the postnatal heart. *Cell Metab* **6:** 13–24.

Altschuler SJ, Wu LF. 2010. Cellular heterogeneity: do differences make a difference? *Cell* **141:** 559–563.

Baggen VJ, van den Bosch AE, Eindhoven JA, Schut AW, Cuypers JA, Witsenburg M, de Waart M, van Schaik RH, Zijlstra F, Boersma E, et al. 2017. Prognostic value of N-terminal pro-B-type natriuretic peptide, troponin-T, and growth-differentiation factor 15 in adult congenital heart disease. *Circulation* **135:** 264–279.

Banerjee I, Fuseler JW, Price RL, Borg TK, Baudino TA. 2007. Determination of cell types and numbers during cardiac development in the neonatal and adult rat and mouse. *Am J Physiol Heart Circ Physiol* **293:** H1883–H1891.

Bernard K, Logsdon NJ, Ravi S, Xie N, Persons BP, Rangarajan S, Zmijewski JW, Mitra K, Liu G, Darley-Usmar VM, et al. 2015. Metabolic reprogramming is required for myofibroblast contractility and differentiation. *J Biol Chem* **290:** 25427–25438.

Bochmann L, Sarathchandra P, Mori F, Lara-Pezzi E, Lazzaro D, Rosenthal N. 2010. Revealing new mouse epicardial cell markers through transcriptomics. *PLoS One* **5:** e11429.

Burke MA, Chang S, Wakimoto H, Gorham JM, Conner DA, Christodoulou DC, Parfenov MG, DePalma SR, Eminaga S, Konno T, et al. 2016a. Molecular profiling of dilated cardiomyopathy that progresses to heart failure. *JCI Insight* **1:** e86898.

Burke MA, Cook SA, Seidman JG, Seidman CE. 2016b. Clinical and mechanistic insights into the genetics of cardiomyopathy. *J Am Coll Cardiol* **68:** 2871–2886.

DeLaughter DM, Bick AG, Wakimoto H, McKean D, Gorham JM, Kathiriya IS, Hinson JT, Homsy J, Gray J, Pu W, et al. 2016. Single-cell resolution of temporal gene expression during heart development. *Dev Cell* **39:** 480–490.

Doppler SA, Carvalho C, Lahm H, Deutsch MA, Dressen M, Puluca N, Lange R, Krane M. 2017. Cardiac fibroblasts: more than mechanical support. *J Thorac Dis* **9:** S36–S51.

Dufour CR, Wilson BJ, Huss JM, Kelly DP, Alaynick WA, Downes M, Evans RM, Blanchette M, Giguere V. 2007. Genome-wide orchestration of cardiac functions by the orphan nuclear receptors ERRα and γ. *Cell Metab* **5:** 345–356.

Emmerson PJ, Wang F, Du Y, Liu Q, Pickard RT, Gonciarz MD, Coskun T, Hamang MJ, Sindelar DK, Ballman KK, et al. 2017. The metabolic effects of GDF15 are mediated by the orphan receptor GFRAL. *Nat Med* **23:** 1215–1219.

Eschenhagen T, Bolli R, Braun T, Field LJ, Fleischmann BK, Frisen J, Giacca M, Hare JM, Houser S, Lee RT, et al. 2017. Cardiomyocyte regeneration: a consensus statement. *Circulation* **136:** 680–686.

Gladka MM, Molenaar B, de Ruiter H, van der Elst S, Tsui H, Versteeg D, Lacraz GPA, Huibers MMH, van Oudenaarden A, van Rooij E. 2018. Single-cell sequencing of the healthy and diseased heart reveals Ckap4 as a new modulator of fibroblasts activation. *Circulation* **138:** 166–180.

Habib N, Avraham-Davidi I, Basu A, Burks T, Shekhar K, Hofree M, Choudhury SR, Aguet F, Gelfand E, Ardlie K, et al. 2017. Massively parallel single-nucleus RNA-seq with DroNc-seq. *Nat Methods* **14:** 955–958.

Harvey PA, Leinwand LA. 2011. The cell biology of disease: cellular mechanisms of cardiomyopathy. *J Cell Biol* **194:** 355–365.

Hsu JY, Crawley S, Chen M, Ayupova DA, Lindhout DA, Higbee J, Kutach A, Joo W, Gao Z, Fu D, et al. 2017. Non-homeostatic body weight regulation through a brainstem-restricted receptor for GDF15. *Nature* **550:** 255–259.

Hu P, Fabyanic E, Kwon DY, Tang S, Zhou Z, Wu H. 2017. Dissecting cell-type composition and activity-dependent transcriptional state in mammalian brains by massively parallel single-nucleus RNA-seq. *Mol Cell* **68:** 1006–1015.e7.

Huss JM, Kelly DP. 2005. Mitochondrial energy metabolism in heart failure: a question of balance. *J Clin Invest* **115:** 547–555.

Huss JM, Imahashi K, Dufour CR, Weinheimer CJ, Courtois M, Kovacs A, Giguere V, Murphy E, Kelly DP. 2007. The nuclear receptor ERRα is required for the bioenergetic and functional adaptation to cardiac pressure overload. *Cell Metab* **6:** 25–37.

Johnen H, Lin S, Kuffner T, Brown DA, Tsai VW, Bauskin AR, Wu L, Pankhurst G, Jiang L, Junankar S, et al. 2007. Tumor-induced anorexia and weight loss are mediated by the TGF-β superfamily cytokine MIC-1. *Nat Med* **13:** 1333–1340.

Klein AM, Mazutis L, Akartuna I, Tallapragada N, Veres A, Li V, Peshkin L, Weitz DA, Kirschner MW. 2015. Droplet barcoding for single-cell transcriptomics applied to embryonic stem cells. *Cell* **161:** 1187–1201.

Lake BB, Ai R, Kaeser GE, Salathia NS, Yung YC, Liu R, Wildberg A, Gao D, Fung HL, Chen S, et al. 2016. Neuronal subtypes and diversity revealed by single-nucleus RNA sequencing of the human brain. *Science* **352:** 1586–1590.

Li G, Xu A, Sim S, Priest JR, Tian X, Khan T, Quertermous T, Zhou B, Tsao PS, Quake SR, et al. 2016. Transcriptomic profiling maps anatomically patterned subpopulations among single embryonic cardiac cells. *Dev Cell* **39:** 491–507.

Li T, Zhang Z, Kolwicz SC Jr, Abell L, Roe ND, Kim M, Zhou B, Cao Y, Ritterhoff J, Gu H, et al. 2017. Defective branched-chain amino acid catabolism disrupts glucose metabolism and sensitizes the heart to ischemia-reperfusion injury. *Cell Metab* **25:** 374–385.

Macosko EZ, Basu A, Satija R, Nemesh J, Shekhar K, Goldman M, Tirosh I, Bialas AR, Kamitaki N, Martersteck EM, et al. 2015. Highly parallel genome-wide expression profiling of individual cells using nanoliter droplets. *Cell* **161:** 1202–1214.

Meyers DE, Basha HI, Koenig MK. 2013. Mitochondrial cardiomyopathy: pathophysiology, diagnosis, and management. *Tex Heart Inst J* **40:** 385–394.

Moignard V, Woodhouse S, Haghverdi L, Lilly AJ, Tanaka Y, Wilkinson AC, Buettner F, Macaulay IC, Jawaid W, Diamanti E, et al. 2015. Decoding the regulatory network of early blood development from single-cell gene expression measurements. *Nat Biotechnol* **33:** 269–276.

Morgan HE, Siehl D, Chua BH, Lautensack-Belser N. 1985. Faster protein and ribosome synthesis in hypertrophying heart. *Basic Res Cardiol* **80:** 115–118.

Moroz LA. 1967. Protein synthetic activity of heart microsomes and robosomes during left ventricular hypertrophy in rabbits. *Circ Res* **21:** 449–459.

Mullican SE, Lin-Schmidt X, Chin CN, Chavez JA, Furman JL, Armstrong AA, Beck SC, South VJ, Dinh TQ, Cash-Mason TD, et al. 2017. GFRAL is the receptor for GDF15 and the ligand promotes weight loss in mice and nonhuman primates. *Nat Med* **23:** 1150–1157.

Naqvi N, Li M, Calvert JW, Tejada T, Lambert JP, Wu J, Kesteven SH, Holman SR, Matsuda T, Lovelock JD, et al. 2014. A proliferative burst during preadolescence establishes the final cardiomyocyte number. *Cell* **157:** 795–807.

Negmadjanov U, Godic Z, Rizvi F, Emelyanova L, Ross G, Richards J, Holmuhamedov EL, Jahangir A. 2015. TGF-β1-mediated differentiation of fibroblasts is associated with increased mitochondrial content and cellular respiration. *PLoS One* **10:** e0123046.

Oka T, Xu J, Molkentin JD. 2007. Re-employment of developmental transcription factors in adult heart disease. *Semin Cell Dev Biol* **18:** 117–131.

Paige SL, Plonowska K, Xu A, Wu SM. 2015. Molecular regulation of cardiomyocyte differentiation. *Circ Res* **116:** 341–353.

Pei L, Waki H, Vaitheesvaran B, Wilpitz DC, Kurland IJ, Tontonoz P. 2006. NR4A orphan nuclear receptors are transcriptional regulators of hepatic glucose metabolism. *Nat Med* **12:** 1048–1055.

Pei L, Leblanc M, Barish G, Atkins A, Nofsinger R, Whyte J, Gold D, He M, Kawamura K, Li HR, et al. 2011. Thyroid hormone receptor repression is linked to type I pneumocyte-associated respiratory distress syndrome. *Nat Med* **17:** 1466–1472.

Pei L, Mu Y, Leblanc M, Alaynick W, Barish GD, Pankratz M, Tseng TW, Kaufman S, Liddle C, Yu RT, et al. 2015. Dependence of hippocampal function on ERRγ-regulated mitochondrial metabolism. *Cell Metab* **21:** 628–636.

Potente M, Makinen T. 2017. Vascular heterogeneity and specialization in development and disease. *Nat Rev Mol Cell Biol* **18:** 477–494.

Ritterhoff J, Tian R. 2017. Metabolism in cardiomyopathy: every substrate matters. *Cardiovasc Res* **113:** 411–421.

See K, Tan WLW, Lim EH, Tiang Z, Lee LT, Li PYQ, Luu TDA, Ackers-Johnson M, Foo RS. 2017. Single cardiomyocyte nuclear transcriptomes reveal a lincRNA-regulated de-differentiation and cell cycle stress-response in vivo. *Nat Commun* **8:** 225.

Skelly DA, Squiers GT, McLellan MA, Bolisetty MT, Robson P, Rosenthal NA, Pinto AR. 2018. Single-cell transcriptional profiling reveals cellular diversity and intercommunication in the mouse heart. *Cell Rep* **22:** 600–610.

Sun H, Olson KC, Gao C, Prosdocimo DA, Zhou M, Wang Z, Jeyaraj D, Youn JY, Ren S, Liu Y, et al. 2016. Catabolic defect of branched-chain amino acids promotes heart failure. *Circulation* **133:** 2038–2049.

Tallquist MD, Molkentin JD. 2017. Redefining the identity of cardiac fibroblasts. *Nat Rev Cardiol* **14:** 484–491.

Tanay A, Regev A. 2017. Scaling single-cell genomics from phenomenology to mechanism. *Nature* **541:** 331–338.

Unsicker K, Spittau B, Krieglstein K. 2013. The multiple facets of the TGF-β family cytokine growth/differentiation factor-15/macrophage inhibitory cytokine-1. *Cytokine Growth Factor Rev* **24:** 373–384.

Wagner A, Regev A, Yosef N. 2016. Revealing the vectors of cellular identity with single-cell genomics. *Nat Biotechnol* **34:** 1145–1160.

Wang T, McDonald C, Petrenko NB, Leblanc M, Giguere V, Evans RM, Patel VV, Pei L. 2015. Estrogen-related receptor α (ERRα) and ERγ are essential coordinators of cardiac metabolism and function. *Mol Cell Biol* **35:** 1281–1298.

Wang T, Liu J, McDonald C, Lupino K, Zhai X, Wilkins BJ, Hakonarson H, Pei L. 2017. GDF15 is a heart-derived hormone that regulates body growth. *EMBO Mol Med* **9:** 1150–1164.

Wollert KC, Kempf T, Wallentin L. 2017. Growth differentiation factor 15 as a biomarker in cardiovascular disease. *Clin Chem* **63:** 140–151.

Woodworth MB, Girskis KM, Walsh CA. 2017. Building a lineage from single cells: genetic techniques for cell lineage tracking. *Nat Rev Genet* **18:** 230–244.

Wyrick JJ, Young RA. 2002. Deciphering gene expression regulatory networks. *Curr Opin Genet Dev* **12:** 130–136.

Xiong Y, Walker K, Min X, Hale C, Tran T, Komorowski R, Yang J, Davda J, Nuanmanee N, Kemp D, et al. 2017. Long-acting MIC-1/GDF15 molecules to treat obesity: evidence from mice to monkeys. *Sci Transl Med* **9:** eaan8732.

Yang L, Chang CC, Sun Z, Madsen D, Zhu H, Padkjaer SB, Wu X, Huang T, Hultman K, Paulsen SJ, et al. 2017. GFRAL is the receptor for GDF15 and is required for the anti-obesity effects of the ligand. *Nat Med* **23:** 1158–1166.

Zhao J, Lupino K, Wilkins BJ, Qiu C, Liu J, Omura Y, Allred AL, McDonald C, Susztak K, Barish GD, et al. 2018. Genomic integration of ERRγ-HNF1β regulates renal bioenergetics and prevents chronic kidney disease. *Proc Natl Acad Sci* **115:** E4910–E4919.

Genomic integration of ERRγ-HNF1β regulates renal bioenergetics and prevents chronic kidney disease

Juanjuan Zhao[a,b], Katherine Lupino[a,b], Benjamin J. Wilkins[b,c], Chengxiang Qiu[d,e], Jian Liu[a,b], Yasuhiro Omura[f], Amanda L. Allred[f], Caitlin McDonald[a,b], Katalin Susztak[d,e], Grant D. Barish[f], and Liming Pei[a,b,c,1]

[a]Center for Mitochondrial and Epigenomic Medicine, Children's Hospital of Philadelphia, Philadelphia, PA 19104; [b]Department of Pathology and Laboratory Medicine, Children's Hospital of Philadelphia, Philadelphia, PA 19104; [c]Department of Pathology and Laboratory Medicine, Perelman School of Medicine, University of Pennsylvania, Philadelphia, PA 19104; [d]Renal Electrolyte and Hypertension Division, Department of Medicine, Perelman School of Medicine, University of Pennsylvania, Philadelphia, PA 19104; [e]Department of Genetics, Perelman School of Medicine, University of Pennsylvania, Philadelphia, PA 19104; and [f]Department of Medicine, Division of Endocrinology, Metabolism and Molecular Medicine, Northwestern University Feinberg School of Medicine, Chicago, IL 60611

Edited by Bert W. O'Malley, Baylor College of Medicine, Houston, TX, and approved April 11, 2018 (received for review March 21, 2018)

Mitochondrial dysfunction is increasingly recognized as a critical determinant of both hereditary and acquired kidney diseases. However, it remains poorly understood how mitochondrial metabolism is regulated to support normal kidney function and how its dysregulation contributes to kidney disease. Here, we show that the nuclear receptor estrogen-related receptor gamma (ERRγ) and hepatocyte nuclear factor 1 beta (HNF1β) link renal mitochondrial and reabsorptive functions through coordinated epigenomic programs. ERRγ directly regulates mitochondrial metabolism but cooperatively controls renal reabsorption via convergent binding with HNF1β. Deletion of ERRγ in renal epithelial cells (RECs), in which it is highly and specifically expressed, results in severe renal energetic and reabsorptive dysfunction and progressive renal failure that recapitulates phenotypes of animals and patients with HNF1β loss-of-function gene mutations. Moreover, ERRγ expression positively correlates with renal function and is decreased in patients with chronic kidney disease (CKD). REC-ERRγ KO mice share highly overlapping renal transcriptional signatures with human patients with CKD. Together these findings reveal a role for ERRγ in directing independent and HNF1β-integrated programs for energy production and use essential for normal renal function and the prevention of kidney disease.

nuclear receptor | ERRγ | mitochondria | kidney | renal reabsorption

Mitochondria are organelles that generate the majority of cellular energy through oxidative phosphorylation (OxPhos) and fatty acid oxidation (FAO). Their optimal function is central to health. Mutations of mitochondrial DNA and proteins directly cause mitochondrial disease, with severe defects often observed in organs of high mitochondrial content and energetic demand, including the kidney (1–3). Mitochondrial dysfunction in general has been recognized to broadly contribute to heart disease, obesity, diabetes, neurodegeneration, aging, and many kidney diseases including acute kidney injury, polycystic kidney disease, and chronic kidney disease (CKD) (1, 4–8). CKD is characterized by gradual loss of kidney function with various etiologies, incompletely understood pathophysiology, and no cure. CKD features both glomerular and tubular cell dysfunction as well as metabolic dysregulation (9). Transcriptomic and metabolomic studies have implicated impaired mitochondrial OxPhos in many kidney diseases including CKD (10, 11). A recent study also shows that renal mitochondrial OxPhos and FAO are among the top dysregulated cellular pathways in both patients with CKD and animal models (12).

Among all kidney cells, the tubule and collecting duct renal epithelial cells (RECs) have a very high density of mitochondria. The main physiological function of RECs is to maintain whole-body homeostasis of osmolality, acid-base balance, and extracellular fluid volume through reabsorption of water, critical nutrients, and electrolytes. Mechanistically, these reabsorptive functions are achieved by the work of many membrane transporters and channels specific for water, glucose, amino acids, sodium, chloride, bicarbonate, and other biomolecules on the REC apical and basolateral surfaces, using cellular ATP as the ultimate energy source. Accordingly, RECs are densely packed with mitochondria and depend on mitochondrial OxPhos and FAO to generate energy to support their reabsorptive functions. However, it remains poorly understood how mitochondrial metabolism is coordinated with kidney reabsorptive functions, and how mitochondrial dysfunction contributes to kidney disease.

Recent work has revealed nuclear receptor estrogen-related receptor gamma (ERRγ) as a critical transcriptional regulator of mitochondrial OxPhos and FAO (13–15). Studies using cell type-specific ERRγ KO mice bypassed the perinatal lethality of whole-body ERRγ KO mice and provided definitive evidence for an essential role of ERRγ in neuronal metabolism and learning/memory, cardiac metabolism and contraction/conduction, functional maturation of pancreatic β cells, brown adipocyte thermogenic function, and skeletal muscle fiber type determination and function (16–22). Genomic studies show that ERRγ directly

Significance

Renal epithelial cells (RECs) contain abundant mitochondria that are essential to support renal reabsorption of electrolytes, glucose, and amino acids. However, it remains poorly understood how mitochondrial metabolism is coordinated with kidney reabsorptive functions. Here we show that deletion of estrogen-related receptor gamma (ERRγ) in RECs results in severe renal mitochondrial and reabsorptive dysfunction with fluid-filled cysts. ERRγ directly regulates mitochondrial metabolism and cooperates in regulating renal reabsorption genes with hepatic nuclear factor 1 beta (HNF1β), mutations of which cause strikingly similar renal dysfunction and cysts in animals and humans. These findings reveal a role for ERRγ in simultaneously coordinating a transcriptional program of renal energy-generating mitochondrial and energy-consuming reabsorptive functions relevant to kidney disease.

Author contributions: J.Z. and L.P. designed research; J.Z., K.L., B.J.W., J.L., Y.O., A.L.A., C.M., G.D.B., and L.P. performed research; C.Q. and K.S. contributed new reagents/analytic tools.; J.Z., K.L., B.J.W., C.Q., J.L., C.M., K.S., G.D.B., and L.P. analyzed data; and J.Z., G.D.B., and L.P. wrote the paper.

The authors declare no conflict of interest.

This article is a PNAS Direct Submission.

Data deposition: Microarray data were deposited in ArrayExpress database (E-MTAB-2502). RNA-Seq, ChIP-Seq, and ChIP-reChIP-Seq data were deposited in the GEO database (GSE104907).

[1]To whom correspondence should be addressed. Email: lpei@pennmedicine.upenn.edu.

This article contains supporting information online at www.pnas.org/lookup/suppl/doi:10.1073/pnas.1804965115/-/DCSupplemental.

binds to and activates the transcription of hundreds of genes important in mitochondrial OxPhos in neurons, and OxPhos, FAO, and cardiac contraction genes in heart cells (17, 23). In addition, ERRγ is highly expressed in the kidney and is essential for normal embryonic kidney development (24). Notably, human genetic studies reveal that a de novo reciprocal translocation at *t*(1, 2)(q41; p25.3) involving the ERRγ locus is associated with bilateral renal agenesis/hypoplasia/dysplasia (25).

Here we generated REC-ERRγ KO mice and show that they develop renal mitochondrial and reabsorption dysfunction. Genomic studies suggest that ERRγ regulates mitochondrial metabolism and renal reabsorption through distinct mechanisms: although ERRγ alone regulates mitochondrial OxPhos/FAO functions, ERRγ cooperates with HNF1β to activate the expression of renal reabsorption genes. In addition, human patients with CKD show decreased kidney ERRγ expression and share highly overlapping renal transcriptional signatures with REC-ERRγ KO mice. Together, these results uncover a mechanism for coordinated regulation of renal mitochondrial and reabsorption functions and identify ERRγ signaling as an important link to mitochondrial dysfunction associated with kidney disease.

Results

Loss of ERRγ in RECs Results in Kidney Disease with Cysts. We first determined where ERRγ is expressed in postnatal kidneys by analyzing an ERRγ heterozygous mouse strain in which LacZ was knocked into the ERRγ locus (16). X-gal staining revealed that ERRγ was highly and specifically expressed in the RECs of all of the segments of tubules and collecting ducts, but barely detectable in any other cells, including those in the glomeruli (*SI Appendix*, Fig. S1*A*). Furthermore, ERRγ protein was found exclusively in the nucleus but not in mitochondria or cytosol, in line with its function as a nuclear transcription factor (*SI Appendix*, Fig. S1*B*).

To determine the importance of ERRγ in postnatal kidney biology and disease, we generated REC-ERRγ KO mice by crossing mice harboring a floxed allele of ERRγ (17) with Sim1-Cre strain. Strong renal Cre expression occurred at birth and resulted in rapid postnatal loss of kidney ERRγ expression with only 15% ERRγ mRNA remaining by 1 wk of age (*SI Appendix*, Fig. S1*C*). Using a double fluorescent Cre reporter mouse strain (26), we further found that this Sim1-Cre line mediated recombination specifically in all segments of the tubule and collecting duct epithelium within the kidney (*SI Appendix*, Fig. S1*D*), exactly where ERRγ is normally expressed (*SI Appendix*, Fig. S1*A*). We used both male and female REC-ERRγ KO mice for all subsequent studies.

Both male and female REC-ERRγ KO mice (Cre^+) were born and survived perinatally at the expected Mendelian ratio. Their kidneys were of normal weight and histological appearance at birth and at 3 wk of age, suggesting no developmental defects (Fig. 1 *A*–*C*). Consistent with the histological observations, electron microscopy showed that renal ultrastructure, including mitochondria in the glomeruli, proximal tubules, and distal tubules, was comparable to controls at 3 wk of age (*SI Appendix*, Fig. S2). Subsequently, however, both male and female REC-ERRγ KO mice developed progressive renal abnormalities (Fig. 1*A*). Kidneys of REC-ERRγ KO mice were significantly heavier than controls by 1 mo of age, and threefold heavier by 3 mo of age (Fig. 1 *B* and *D*). Histological examination showed that REC-ERRγ KO mouse kidneys contained multiple fluid-filled cysts of variable sizes (Fig. 1*E*), resulting in the disruption of overall kidney organization and structure. Glomeruli were present and appeared histologically normal based on H&E staining. The carbohydrate-rich basement membranes of glomeruli including capillary loops responsible for renal filtration function also remained intact, as evaluated by periodic acid-Schiff staining (Fig. 1*E*). These findings suggest that ERRγ is critical for maintaining normal kidney structure and function in vivo.

ERRγ Directly Regulates Mitochondrial Metabolic and Renal Reabsorptive Function. To further understand the molecular mechanisms underlying the observed kidney disease phenotype, we used RNA-Seq to quantify the transcriptomic changes between control and REC-ERRγ KO mouse kidneys ($n = 4$ each) at 3 wk of age, just before morphological abnormalities became observable. We found that expression levels of 1,018 genes were significantly decreased and 1,406 genes were significantly increased in REC-ERRγ KO mouse kidneys (Fig. 2*A*; $P < 0.01$; fold change $> \pm 1.5$). Pathway analysis revealed that the down-regulated 1,018 genes were enriched for two cellular functions: mitochondrial metabolism (OxPhos, FAO, etc.) and transmembrane transport associated with renal reabsorption (Fig. 2*B*). Decreased mitochondrial metabolism (OxPhos, FAO and amino acid metabolism) was recently identified as a genetic signature of human CKD (12). Pathways enriched in the up-regulated 1,406 genes included inflammatory response (*SI Appendix*, Fig. S3*A*), which has also been implicated in human CKD (12). We validated expression changes for many of these genes, using qRT-PCR. For example, renal expression of genes important in OxPhos (*CS*, *Ndufa4*, *Sdhb*, *Cox5b*, and *Atp5b*) and FAO (*Cpt1b*, *Cpt2*, *Acadm*, and *Hadha*) were reduced in REC-ERRγ KO mice (Fig. 2*C*). Further, transcripts implicated in renal reabsorption were significantly decreased in REC-ERRγ KO kidneys, including *Slc5a2*/*Sglt2* (Na^+/glucose cotransporter), *Atp1a1*, and *Atp1b1* (Na^+/K^+ ATPases, genetic variations of which are associated with hypertension), *Slc34a1* (Na^+/phosphate cotransporter, mutations of which cause Fanconi Renotubular Syndrome 2 in humans), *Slc12a1* ($Na^+/K^+/Cl^-$ cotransporter, mutations of which cause Bartter syndrome type 1 featuring renal tubular hypokalemic alkalosis), *Slc6a19* (neutral amino acid transporter, mutations of which cause Hartnup Disease because of blocked reabsorption of neutral amino acids in humans), *Sgk2* (a regulator of renal transport), and *Pkd2* (mutations of which cause autosomal dominant polycystic kidney disease in humans; Fig. 2*C*).

We next investigate whether the renal transcriptome changes in REC-ERRγ KO mice are gender-dependent. Both male and female REC-ERRγ KO mice exhibited similar pathway changes for both down- and up-regulated genes (*SI Appendix*, Fig. S3*B*). This is consistent with the fact that both sexes of REC-ERRγ KO mice develop kidney disease. To determine whether these molecular defects of mitochondrial and renal functions persisted in the later stage of kidney disease, we performed RNA-Seq analysis in 3-mo-old male control and REC-ERRγ KO mice and compared it with RNA-Seq data of 3-wk-old male mice. All the down-regulated and most of the up-regulated cellular pathways were maintained in 3-mo-old REC-ERRγ KO mice (*SI Appendix*, Fig. S3*C*). A few additional up-regulated cellular pathways were found at 3 mo of age, likely reflecting secondary changes at the later stage of kidney disease.

To determine whether expression of these genes was directly regulated by ERRγ, we performed chromatin immunoprecipitation sequencing (ChIP-Seq) of ERRγ, using two biological replicates of WT mouse kidney samples. Because ERRγ is specifically expressed in RECs, this effectively mapped the ERRγ cistrome in RECs. ERRγ binding peaks were distributed mainly in introns, intergenic and promoter regions (*SI Appendix*, Fig. S4*A*). Eighty-six percent (7,463/8,702) of the ERRγ peaks contain the consensus ERR binding motif (AAGGTCA). Pathway analysis revealed that mitochondrial metabolism, including OxPhos pathway genes that comprise most of the lists for Huntington's disease and Alzheimer disease, and renal reabsorption are among the most enriched pathways of genes annotated to the kidney ERRγ cistrome (Fig. 2*D*). This is nearly the same pattern seen among down-regulated RNA-Seq pathways in REC-ERRγ KO kidneys (Fig. 2*B*). We validated these ERRγ ChIP-Seq results

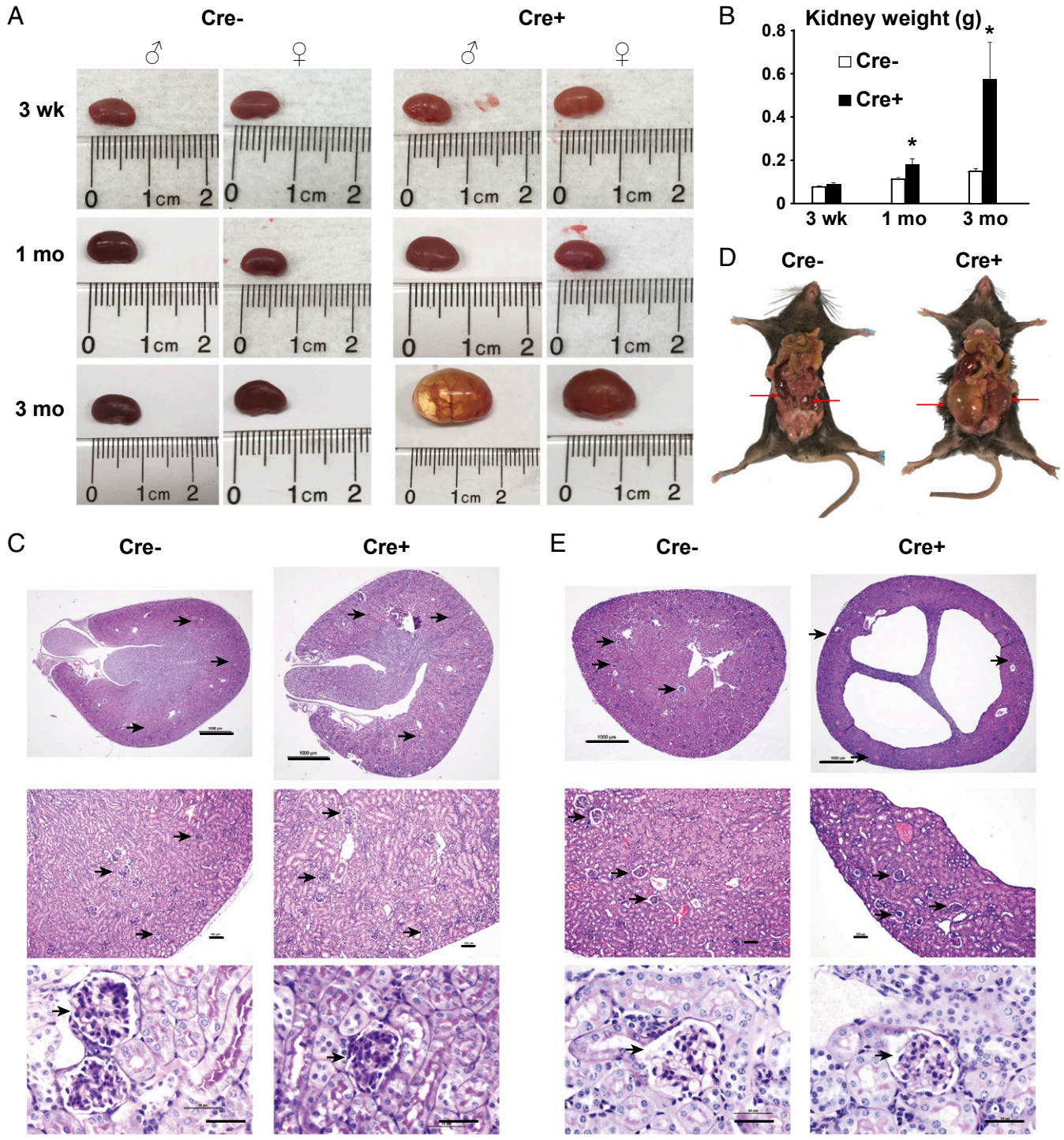

Fig. 1. REC-ERRγ KO mice develop kidney disease with fluid-filled cysts. (*A* and *B*) Representative pictures (*A*) and weight (*B*) of control and REC-ERRγ KO kidneys at different ages (n = 12–19). (*C*) Three-week-old control and REC-ERRγ KO kidney morphology. (*Top*) H&E stain. (Scale bar, 1,000 μm.) (*Middle*) H&E stain. (Scale bar, 100 μm.) (*Bottom*) Periodic acid-Schiff stain (Scale bar, 100 μm.) Arrowheads point to glomeruli. (*D*) Kidneys (red arrows) of 3-mo-old control and REC-ERRγ KO mice, illustrating their relative sizes to the body. (*E*) Three-month-old control and REC-ERRγ KO kidney morphology. Staining and scale bars are the same as in *C*. Error bar indicates SEM. $*P < 0.05$ between Cre^- and Cre^+ by t test. Both male and female mice were included.

using ChIP-qPCR which showed that ERRγ directly bound to the same set of OxPhos, FAO, and renal reabsorption genes (Fig. 2*E*). By comparing the ChIP-Seq and RNA-Seq datasets, we found that 53% (537 of 1,018) of the genes down-regulated in REC-ERRγ KO mice were bound by ERRγ (Fig. 2*F*). These genes are again highly enriched for mitochondrial metabolism (OxPhos, FAO, etc.) and renal reabsorption pathways (Fig. 2*G*). In contrast, only 19% (271 of 1,406) of the up-regulated genes were bound by ERRγ (*SI Appendix*, Fig. S4*B*). Inflammatory pathway was again enriched in this list, but to a lesser extent than was observed in the ERRγ transcriptome as a whole (*SI Appendix*, Fig. S4*C*). These results suggest that the major biological function of ERRγ in RECs is transcriptional activation of mitochondrial metabolism and renal reabsorption.

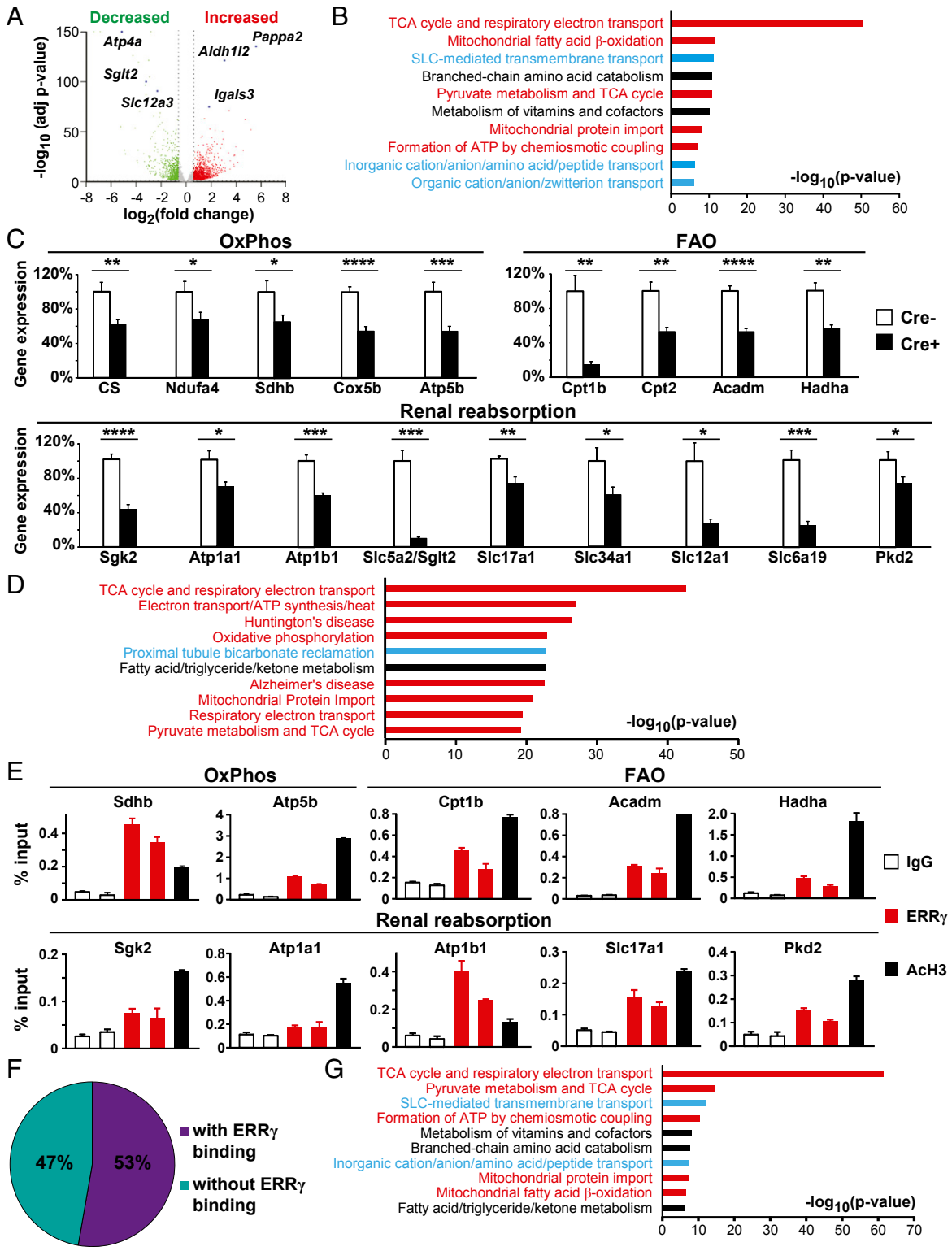

Fig. 2. ERRγ is essential for maintaining normal expression of REC mitochondrial metabolic and renal reabsorptive genes. (*A*) Volcano plot showing genes differentially expressed in 3-wk-old control and REC-ERRγ KO kidneys by RNA-Seq ($n = 4$). Filtering criteria is fold change $>\pm1.5$ and $P < 0.01$ (dotted lines). (*B*) Top 10 enriched pathways of down-regulated genes. (*C*) Gene expression in 3-wk-old control ($n = 7$) and REC-ERRγ KO ($n = 10$) kidneys by qPCR. (*D*) Top 10 ranked pathways of genes with nearby ERRγ ChIP-Seq peaks. (*E*) ChIP-qPCR shows that ERRγ binds to OxPhos, FAO, and renal reabsorption genes. (*F*) Pie graph of down-regulated genes with or without annotated ERRγ binding peaks. (*G*) Top enriched pathways of down-regulated genes with annotated ERRγ binding peaks. Error bar indicates SEM. $^*P < 0.05$; $^{**}P < 0.01$; $^{***}P < 0.001$; $^{****}P < 0.0001$ between Cre^- and Cre^+ by *t* test. Both male and female mice were included.

Next we investigated whether mitochondrial metabolism and renal reabsorption function were impaired in REC-ERRγ KO mice. Enzymatic activities of multiple mitochondrial electron transport chain complexes were found decreased in 3-wk-old REC-ERRγ KO kidneys (Fig. 3*A*), consistent with their reduced RNA expression. In addition, mtDNA content was significantly reduced (Fig. 3*B*), despite normal mitochondrial ultrastructures, indicating mitochondrial dysfunction. Importantly, all these mitochondrial metabolic defects were present at 3 wk of age, before any morphological or functional renal defects were observed, suggesting that mitochondrial dysfunction is a genesis for renal defects in REC-ERRγ KO mice.

The Sim1-Cre line also mediates recombination in nonrenal tissues such as the hypothalamus (27). We next studied whether ERRγ regulates REC mitochondrial functions in a cell-autonomous manner. We found that adenoviral-mediated ERRγ overexpression increased expression of mitochondrial metabolic genes (Fig. 3*C*), leading to increase in both basic and stimulated mitochondrial respiration in human tubular REC HKC-8 cells (Fig. 3*D*). In addition, siRNA-mediated knockdown of ERRγ resulted in decreased mitochondrial respiration, which was rescued by reintroduction of ERRγ (*SI Appendix*, Fig. S4*D*). These results indicate that the mitochondrial defects in REC-ERRγ KO mice occur as a result of kidney intrinsic functions of ERRγ.

A central function of the kidney is the reabsorption of water, essential nutrients, and electrolytes. For example, in normal health, almost all urine glucose is reabsorbed, mostly through the high-capacity sodium-glucose cotransporter 2 (SGLT2/Slc5a2) on the apical membrane of the proximal tubule RECs. Loss or inhibition of SGLT2 in humans leads to significant loss of glucose reabsorption and glucosuria (28). The almost complete dependence of renal Sglt2 expression on ERRγ is particularly interesting because a new class of SGLT2 inhibitors (Gliflozins) have become the latest class of potent, FDA-approved medications to treat type 2 diabetes (29, 30). We found that ERRγ increased Sglt2 expression (Fig. 3*E*) and significantly elevated cellular glucose uptake in human RECs (Fig. 3*F*).

SGLT2 inhibitors are clinically used to treat diabetes through inhibiting renal glucose reabsorption, resulting in glucosuria. Although REC-ERRγ KO mice showed similar, very low urine glucose levels compared with controls under normal conditions (*SI Appendix*, Fig. S4*E*), likely because of a small amount of remaining SGLT2, they decompensated in the setting of streptozotocin (STZ)-induced diabetes. In this model, STZ induced acute diabetes with very high plasma glucose and low plasma insulin levels in both control and REC-ERRγ KO mice (Fig. 3*G*). However, as seen in patients with diabetes treated with SGLT2 inhibitors, REC-ERRγ KO mice exhibited strong glucosuria with urine glucose levels soaring more than 100-fold above controls because of the loss of SGLT2 and renal glucose reabsorption function. Together, these results demonstrate that ERRγ is an essential regulator of renal glucose reabsorption through control of Sglt2 transcription.

ERRγ Regulates Mitochondrial and Renal Reabsorption Genes Through Distinct Mechanisms. Genomic approaches including ChIP-Seq and ChIP-on-chip have been used to unambiguously demonstrate that ERRγ activates mitochondrial metabolic genes by directly binding to their promoters or enhancers in neurons and hearts (17, 23). It is therefore not surprising that ERRγ binds to and regulates mitochondrial metabolic genes in the kidney, another organ with abundant mitochondria and high energetic demand. It is, however, unexpected that ERRγ also directly binds to and activates the transcription of reabsorption genes, which was not the case in neurons or heart cells (17, 23). To understand whether these two sets of molecular signatures are regulated by ERRγ via similar mechanisms, we further examined the ERRγ binding patterns around mitochondrial and renal reabsorption genes. Notably, de novo motif analysis of kidney ERRγ binding peaks revealed that the second most enriched motif after ERR is HNF1β (Fig. 4*A*), a homeodomain-containing transcription factor known to cause maturity onset diabetes of the young (MODY5) (31). HNF1β is highly expressed in both tubule and collecting duct RECs and is critical for kidney development and function (32–34). Mutations of HNF1β are the most frequent monogenic cause of developmental kidney disease. The most common features of HNF1β-associated kidney disease include fluid-filled renal cysts, renal hypoplasia, and electrolyte abnormalities (34), the very same symptoms seen in humans with chromosome translocation mapped to ERRγ locus (25) or in our REC-ERRγ KO mice. In addition, perinatal deletion of HNF1β in mouse kidneys results in similar cystic renal disease (33, 35). The common pathological features of HNF1β and ERRγ loss-of-function prompted us to investigate further a possible role for HNF1β in ERRγ's regulation of kidney metabolism and function.

We performed HNF1β ChIP-Seq in biological duplicate WT mouse kidney samples and compared these results with our ERRγ genome-wide binding datasets. The renal ERRγ and HNF1β cistromes shared 1,109 common peaks, representing about 13% of the total ERRγ peaks and 9% of the total HNF1β peaks (Fig. 4*B*). Pathway analysis showed that ERRγ-only peaks annotate to mitochondrial metabolic pathways (OxPhos, FAO, and neurodegenerative diseases in which mitochondrial dysfunction is known to contribute), but are not associated with any renal reabsorption pathway (Fig. 4*C*). In sharp contrast, ERRγ/HNF1β overlapping peaks had stronger representation of the renal absorption pathway compared with ERRγ- or HNF1β-only peaks (Fig. 4*C* and *SI Appendix*, Fig. S5*A*), and importantly, lacked association with mitochondrial metabolic pathways (Fig. 4*C*). This complete separation of mitochondrial metabolism and renal reabsorption through pathway analysis was further confirmed by visualization of ChIP-Seq peaks near these genes (Fig. 4*D* and *SI Appendix*, Fig. S5*B*) and validated by ChIP-qPCR (Fig. 4*E* and *SI Appendix*, Fig. S5*C*). These results suggest that ERRγ regulates the transcription of mitochondrial and renal reabsorption genes through distinct mechanisms: mitochondrial metabolic genes are bound by ERRγ, as seen in neurons and heart cells (17, 23), whereas renal reabsorption genes are bound by both ERRγ and HNF1β.

ERRγ and HNF1β Functionally Cooperate to Regulate Renal Reabsorption Genes. Our ChIP-Seq results clearly suggest that ERRγ and HNF1β bind to a common set of genes important in renal reabsorption. However, it could not yet be excluded that ERRγ and HNF1β may bind to these genes in different cells or, rarely, occupy their common binding regions at the same time in the same cell because ChIP-Seq results represent an average binding signal from millions of cells. To address this, we next used HNF1β ChIP-ERRγ reChIP-Seq to determine whether ERRγ and HNF1β bind to any of these common peaks simultaneously in the same cells. By applying similar statistical and filtering parameters used in our ChIP-Seq studies, ChIP-reChIP-Seq identified a total of 1,892 peaks (Fig. 5*A*). Of these peaks, 1,725 (91%) colocalize with HNF1β ChIP-Seq peaks (related to the first ChIP step of the ChIP-reChIP-Seq), validating the reproducibility of our ChIP and sequencing assay. Importantly, 20% (341) of these peaks colocalize to previously found ERRγ/HNF1β overlapping peaks. This 20% is a significantly higher percentage than would be expected by the overlap of single ERRγ and HNF1β ChIP-seq results (9%, $P = 5 \times 10^{-56}$ by hypergeometric test). These 341 peaks are highly likely to be simultaneously bound by both ERRγ and HNF1β in the same cells, and they annotate to many renal reabsorption genes, including Atp1b1. These peaks are enriched for renal reabsorption-related pathways compared with the other 1,384 peaks, but not for any mitochondrial metabolic pathways (Fig. 5*A*). We validated this

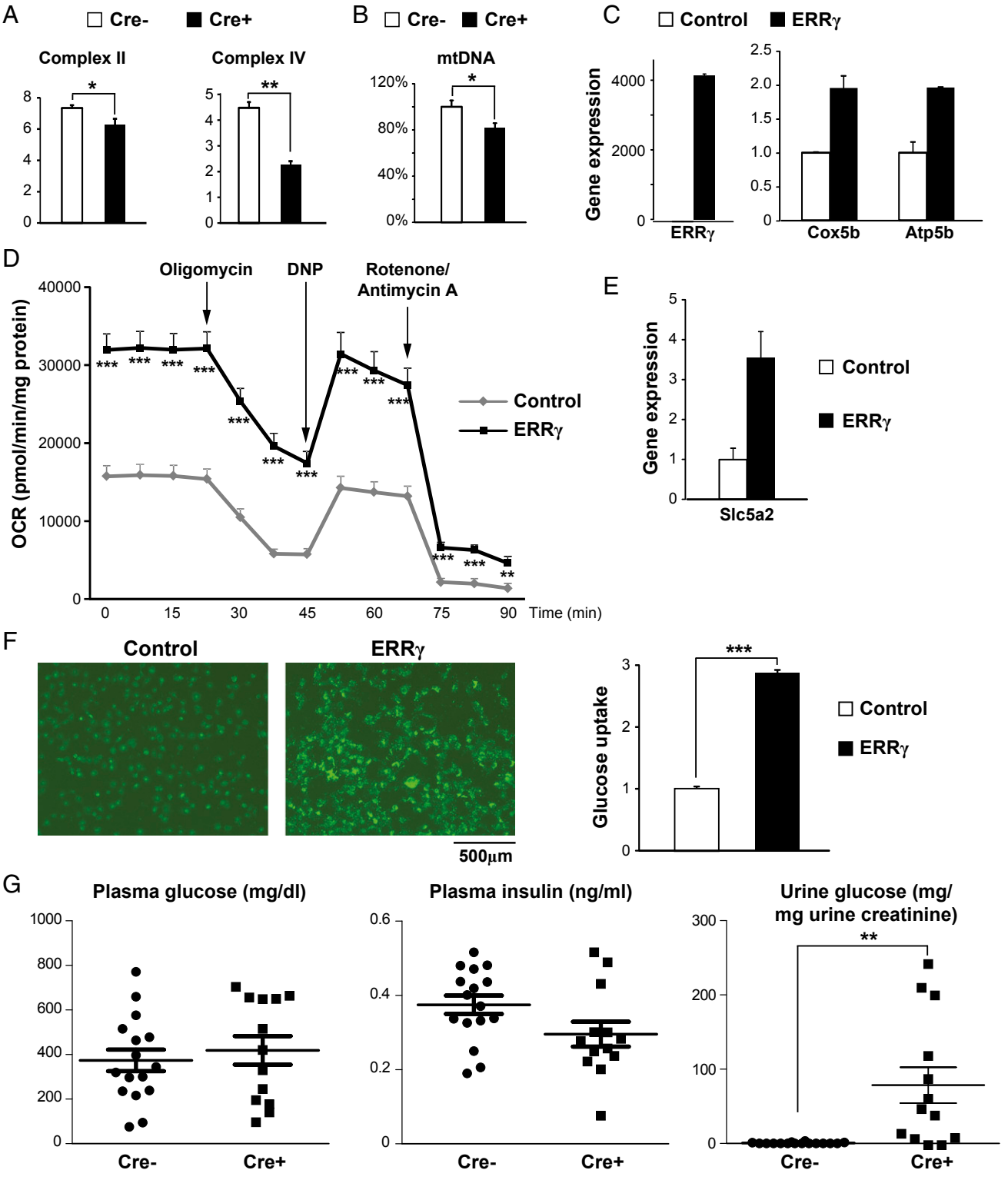

Fig. 3. ERRγ regulates REC mitochondrial and reabsorptive functions. (*A*) Enzymatic activities (μmol/min/mg tissue) of mitochondrial electron transport chain complexes in 3-wk-old control ($n = 3$) and REC-ERRγ KO ($n = 6$) kidneys. (*B*) Relative mitochondrial DNA content in 3-wk-old control ($n = 13$) and REC-ERRγ KO ($n = 12$) kidneys. (*C*) ERRγ and mitochondrial OxPhos genes expression in HKC-8 cells by qPCR. (*D*) Oxygen consumption rate (OCR) in HKC-8 cells measured by Seahorse XF24 analyzer. $n = 7$ for control and $n = 8$ for ERRγ. (*E*) Slc5a2/Sglt2 expression in HKC-8 cells by qPCR. (*F*) Glucose transport into HKC-8 cells. (*F*, *Left*) Representative pictures visualizing fluorescent 2-NBDG uptake. (*F*, *Right*) Quantification ($n = 10$). (*G*) Plasma and urine glucose and plasma insulin levels in 10–13-wk-old control ($n = 16$) and REC-ERRγ KO ($n = 13$) mice 2 wk after STZ treatment. Error bar indicates SEM. $^*P < 0.05$; $^{**}P < 0.01$; $^{***}P < 0.001$ by *t* test. Both male and female mice were included.

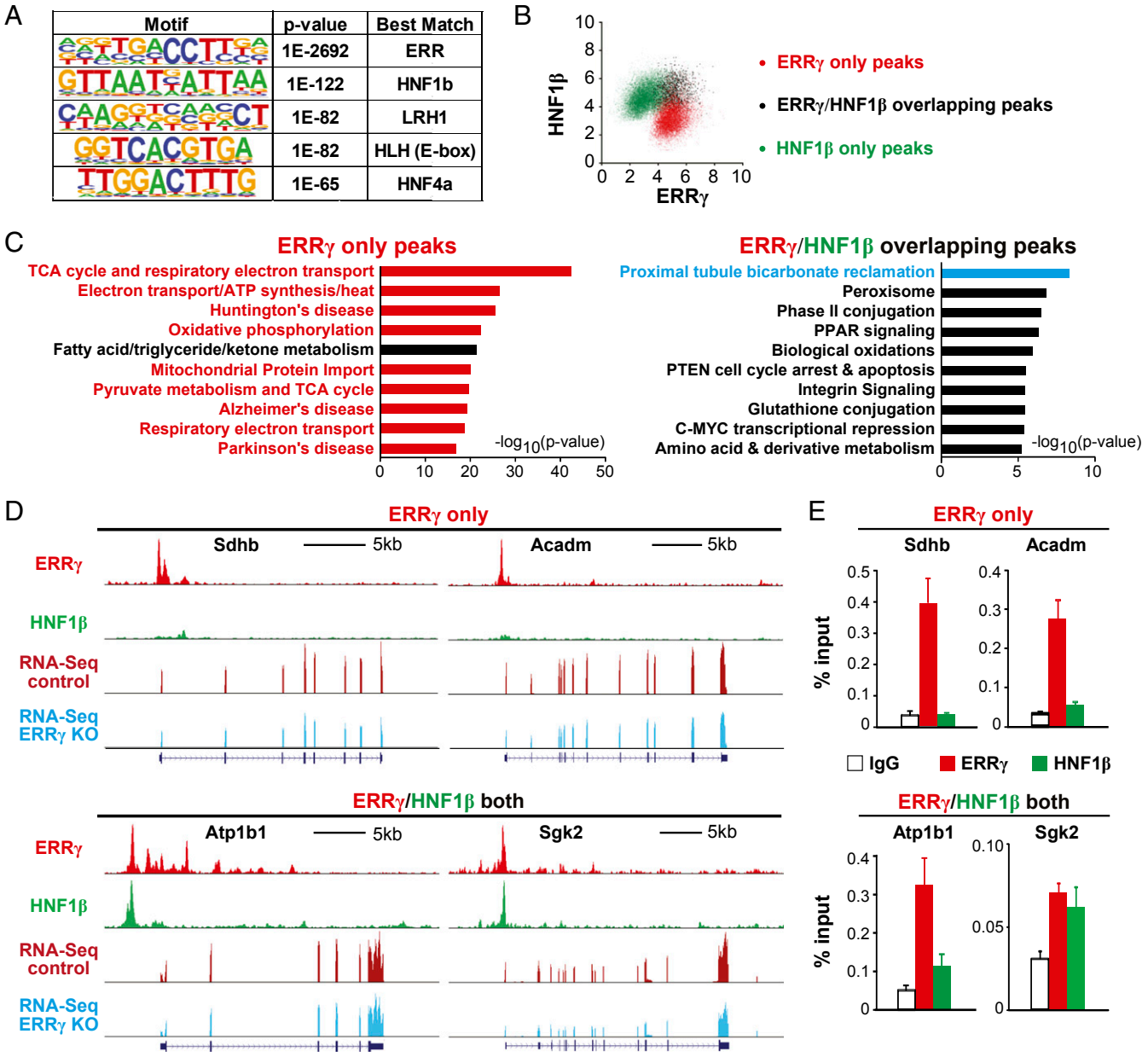

Fig. 4. ERRγ cooperates with HNF1β to regulate the transcription of renal reabsorptive genes. (*A*) Top 5 de novo motifs near ERRγ ChIP-Seq peaks. (*B*) Overlap of renal ERRγ and HNF1β ChIP-Seq peaks. Axis is $\log_2$ tags/10^7 reads. (*C*) Top 10 pathways of genes annotated to ERRγ and/or HNF1β ChIP-Seq peaks. (*D*) Representative ERRγ and HNF1β ChIP-Seq peaks. *y* axis is peak reads. Same scale for control and ERRγ KO RNA-Seq tracks. (*E*) Binding of ERRγ and/or HNF1β near OxPhos, FAO and renal reabsorption genes by ChIP.

result on Atp1b1 using reciprocal ERRγ and HNF1β ChIP-reChIP-qPCR (Fig. 5*B*).

We next investigated whether ERRγ and HNF1β functionally cooperate to regulate the transcription of renal reabsorption genes. We were unable to detect a physical interaction between ERRγ and HNF1β in lysates from kidney cells or mouse kidneys, using coimmunoprecipitation followed by Western blot (*SI Appendix*, Fig. S5*D*). This suggests that they either do not interact directly or their interaction is not strong enough to be detected by this method, as previously reported in cases of transcription factor tethering (36). The expression of ERRγ and HNF1β cobound genes such as Atp1b1 was activated by either ERRγ or HNF1β, and further increased with both ERRγ and HNF1β (Fig. 5*C*). Together, these results suggest that ERRγ and HNF1β functionally cooperate to regulate renal reabsorption genes.

Human Patients with CKD Show Decreased Kidney ERRγ Expression and Share Highly Overlapping Renal Transcriptional Signatures with REC-ERRγ KO Mice. To relate these findings of ERRγ to human kidney diseases beyond congenital disorders (25), we measured renal ERRγ expression in 95 human kidney tubule samples from patients with CKD and control cohorts. We found that ERRγ expression positively correlated with glomerular filtration rate (GFR), a well-established clinical index for kidney function (Fig. 6*A*). In addition, kidney ERRγ expression was significantly reduced in patients with CKD (GFR < 60) compared with healthy controls (GFR > 60; Fig. 6*B*). We next compared the renal transcriptomes between REC-ERRγ KO mice and human patients with CKD (12). About 25% of down-regulated and 19% of up-regulated genes in REC-ERRγ KO mice were shared in human patients with CKD (Fig. 6 *C* and *D*). There is a significant

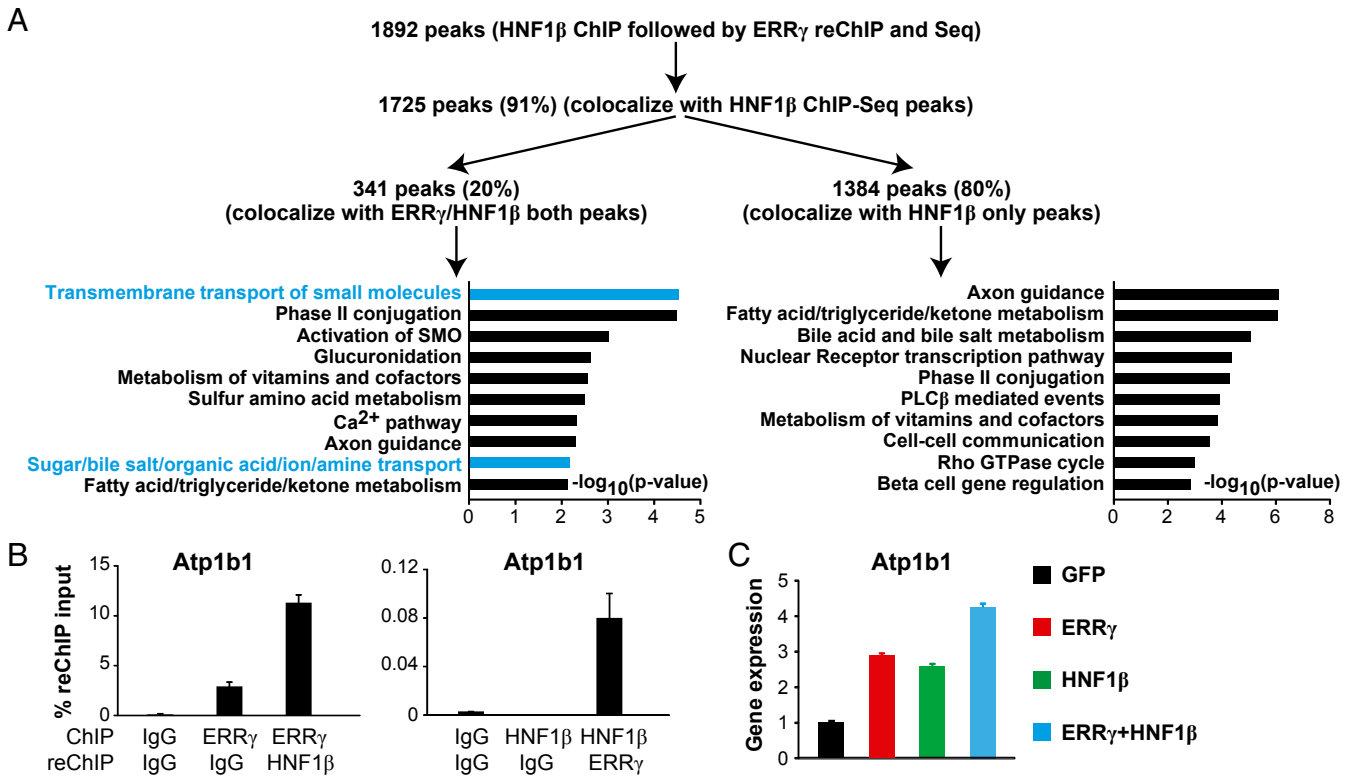

Fig. 5. Functional cooperation between ERRγ and HNF1β in regulating renal function. (*A*) HNF1β ChIP-ERRγ reChIP-Seq and data analysis. (*B*) Atp1b1 is cobound by ERRγ and HNF1β in the same cells by ChIP-reChIP-qPCR. (*C*) Enhanced activation of Atp1b1 expression by both ERRγ and HNF1β.

overlap of affected pathways between REC-ERRγ KO mice and human patients with CKD. In particular, pathways down-regulated are nearly identical in mouse and human and include many mitochondrial function and renal reabsorption pathways that are regulated by ERRγ. These results suggest a broad and critical role for ERRγ in human kidney disease.

Discussion

Mitochondrial dysfunction has been increasingly recognized as an important determinant of kidney diseases including CKD (4–7, 10, 11). ERRγ has recently emerged as a key transcriptional regulator of mitochondrial biogenesis and function, and human genetic studies have linked ERRγ to kidney disease (13–15, 25). However, definitive evidence linking regulation of mitochondrial function and kidney biology/disease is still missing. Here we show that ERRγ is an essential transcriptional coordinator of kidney mitochondrial and reabsorptive functions relevant to human kidney disease. Renal ERRγ expression correlates with kidney function in humans. Mice lacking REC ERRγ develop kidney mitochondrial and reabsorptive dysfunction with similar signs and molecular signatures as seen in human CKD. Mechanistically, we demonstrate that ERRγ directly regulates mitochondrial metabolism and renal reabsorption, but through distinct mechanisms. The functional cooperation between ERRγ and HNF1β, another transcriptional regulator important in kidney biology and disease, further uncovers the transcriptional network optimized to coordinate kidney mitochondrial and reabsorptive functions. Together, these results improve our understanding of how mitochondrial function is coordinately regulated to support normal kidney function and how its dysregulation contributes to kidney disease (Fig. 6*E*).

The near complete dependence of SGLT2 expression and renal glucose reabsorption on ERRγ is particular noteworthy because of the recent clinical use and efficacy of SGLT2 inhibitors in treating type 2 diabetes, and their therapeutic potential in treating obesity, kidney disease, and cardiovascular disease. We further demonstrated that ERRγ can increase Sglt2 expression and REC glucose uptake in a cell-autonomous manner. Under STZ-induced diabetic conditions, REC-ERRγ KO mice faithfully recapitulated glucosuria seen in patients treated with SGLT2 inhibitors. However, this did not result in lower blood glucose, as observed clinically. One possible explanation for this is there remains a small amount of SGLT2 and intact SGLT1 in the REC-ERRγ KO animals. This incomplete glucose excretion phenomenon has also been observed in Sglt2 KO mice (37), as well as in SGLT2 inhibitor-treated patients with diabetes in whom only 40–50% of the expected glucose reabsorption inhibition can be achieved with a full dose (30). Another possible explanation is that STZ destroys pancreatic β cells, causing type 1 diabetes and very high plasma glucose levels. Loss of insulin production and incomplete glucose excretion may explain the lack of blood glucose normalization in REC-ERRγ mice, similar to what was reported in Sglt2 KO mice (37). Notably, SGLT2 inhibitors are not currently approved for type 1 diabetes.

ERRγ has been shown to promote energy-generating mitochondrial functions in several energy-demanding cell types, including neurons, cardiomyocytes, skeletal myocytes, brown adipocytes, and now in RECs (17–23, 38). In three of these cell types (neurons, cardiomyocytes, and RECs) ChIP-Seq or ChIP-on-chip has been used to demonstrate that ERRγ directly binds near mitochondrial OxPhos genes (17, 23). However, ERRγ cistromes also exhibit cell-type-specific features that match the metabolic profile and energy-intensive cellular functions of individual cell types. Neurons depend on aerobic catabolism of glucose, including OxPhos as an energy source, and they cannot metabolize fat. Accordingly, the neuronal ERRγ cistrome includes many glycolysis and OxPhos genes but is depleted of FAO genes (17). Cardiomyocytes, in contrast, use both glucose and fat

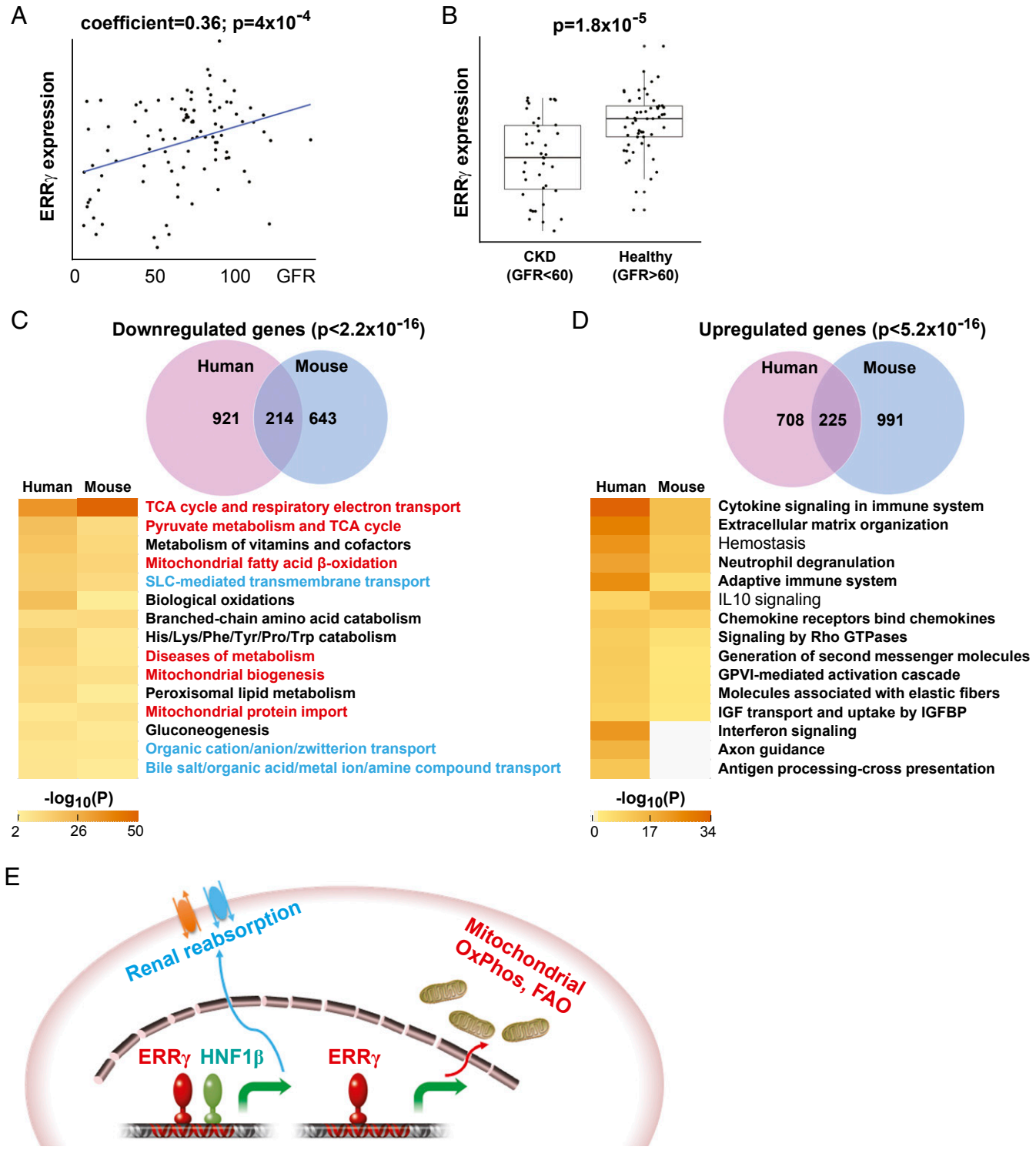

Fig. 6. Human patients with CKD show decreased kidney ERRγ expression and share highly overlapping renal transcriptional signatures with REC-ERRγ KO mice. (*A*) ERRγ expression positively correlates with GFR across 95 human kidney tubule samples, by Pearson correlation. (*B*) ERRγ expression is significantly reduced in human CKD kidney tubules, by *t* test. (*C* and *D*) Venn diagram and heat map comparison of top enriched pathways of down-regulated (*C*) or up-regulated (*D*) kidney genes between 3-wk-old REC-ERRγ KO mice and human patients with CKD. Statistical analysis was performed using Fisher's exact test. (*E*) Model illustrating that ERRγ coordinates energy-generating mitochondrial metabolism and energy-consuming renal reabsorption functions through distinct mechanisms.

as fuel. As a consequence, cardiac ERRγ binds to and activates the transcription of FAO genes in addition to OxPhos genes (23). Here in RECs, we demonstrate that ERRγ directly regulates both OxPhos and FAO, key metabolic pathways used by these cells (12). Therefore, ERRγ is a key transcriptional regulator of cell-type specific metabolic functions. In addition, ERRγ has been shown to directly bind to and activate genes for cardiac contraction and conduction, two major cellular energy utilization

processes specific to the heart (18, 23). Here, we show that ERRγ directly regulates the major energy consumption process in another cell type; namely, reabsorption in RECs, via functional cooperation with the REC-related transcription factor HNF1β. Together these studies reveal a common theme of cellular metabolic regulation: cellular energy production and consumption must be coordinated because most cells do not have an extensive capacity to fully store energy. Our studies thus demonstrate that ERRγ is a central transcriptional coordinator of cell-type specific energy production and utilization.

Materials and Methods

All mouse studies were approved by and performed under the guidelines of the Institutional Animal Care and Use Committee of the Children's Hospital of Philadelphia. Adenoviruses were generated as previously described (39, 40). Transmission electron microscopy, gene expression, Western blot, cellular oxygen consumption measurement, mitochondrial DNA, and enzyme activity analysis were performed as previously described (18, 41). Please see *SI Appendix, SI Materials and Methods* for detailed description of mouse studies, cell culture, glucose uptake, histological analysis, RNA-Seq, ChIP-Seq, and ChIP-reChIP-Seq experiments. Statistical analysis was performed using Student's *t* test, Pearson correlation, or Fisher's exact test. Microarray data were deposited in ArrayExpress database (E-MTAB-2502). RNA-Seq, ChIP-Seq, and ChIP-reChIP-Seq data were deposited in the GEO database (GSE104907).

ACKNOWLEDGMENTS. We thank Dr. Douglas Wallace, Dr. Mitchell Lazar, Dr. Matthew Weitzman, Dr. Amita Sehgal, Dr. Michael Marks, and Dr. Mark Kahn for critical discussion of the project. We thank Dr. Biao Zuo, Dr. Ray Meade, and the UPenn Electron Microscopy Resource Laboratory core facility for technical support. The authors and this work were supported by the Office of the Assistant Secretary of Defense for Health Affairs through the Peer Reviewed Medical Research Program under Award W81XWH-16-1-0400, and pilot awards from the Diabetes Research Center at the University of Pennsylvania from a grant sponsored by the NIH (DK19525; DK111495 to L.P.; DK099379 to B.J.W.; DK108987 to G.D.B.; and DK087635 and DP3 DK108220 to K.S.).

1. Wallace DC (2013) A mitochondrial bioenergetic etiology of disease. *J Clin Invest* 123: 1405–1412.
2. van den Ouweland JM, Maechler P, Wollheim CB, Attardi G, Maassen JA (1999) Functional and morphological abnormalities of mitochondria harbouring the tRNA(Leu)(UUR) mutation in mitochondrial DNA derived from patients with maternally inherited diabetes and deafness (MIDD) and progressive kidney disease. *Diabetologia* 42:485–492.
3. Dinour D, Mini S, Polak-Charcon S, Lotan D, Holtzman EJ (2004) Progressive nephropathy associated with mitochondrial tRNA gene mutation. *Clin Nephrol* 62:149–154.
4. Che R, Yuan Y, Huang S, Zhang A (2014) Mitochondrial dysfunction in the pathophysiology of renal diseases. *Am J Physiol Renal Physiol* 306:F367–F378.
5. Emma F, Montini G, Parikh SM, Salviati L (2016) Mitochondrial dysfunction in inherited renal disease and acute kidney injury. *Nat Rev Nephrol* 12:267–280.
6. Bhargava P, Schnellmann RG (2017) Mitochondrial energetics in the kidney. *Nat Rev Nephrol* 13:629–646.
7. Ishimoto Y, et al. (2017) Mitochondrial abnormality facilitates cyst formation in autosomal dominant polycystic kidney disease. *Mol Cell Biol*, MCB.00337-17.
8. Pei L, Wallace DC (2018) Mitochondrial etiology of neuropsychiatric disorders. *Biol Psychiatry* 83:722–730.
9. Breyer MD, Susztak K (2016) The next generation of therapeutics for chronic kidney disease. *Nat Rev Drug Discov* 15:568–588.
10. Granata S, et al. (2009) Mitochondrial dysregulation and oxidative stress in patients with chronic kidney disease. *BMC Genomics* 10:388.
11. Sharma K, et al. (2013) Metabolomics reveals signature of mitochondrial dysfunction in diabetic kidney disease. *J Am Soc Nephrol* 24:1901–1912.
12. Kang HM, et al. (2015) Defective fatty acid oxidation in renal tubular epithelial cells has a key role in kidney fibrosis development. *Nat Med* 21:37–46.
13. Eichner LJ, Giguère V (2011) Estrogen related receptors (ERRs): A new dawn in transcriptional control of mitochondrial gene networks. *Mitochondrion* 11:544–552.
14. Hock MB, Kralli A (2009) Transcriptional control of mitochondrial biogenesis and function. *Annu Rev Physiol* 71:177–203.
15. Misra J, Kim DK, Choi HS (2017) ERRγ: A junior orphan with a senior role in metabolism. *Trends Endocrinol Metab* 28:261–272.
16. Alaynick WA, et al. (2007) ERRgamma directs and maintains the transition to oxidative metabolism in the postnatal heart. *Cell Metab* 6:13–24.
17. Pei L, et al. (2015) Dependence of hippocampal function on ERRγ-regulated mitochondrial metabolism. *Cell Metab* 21:628–636.
18. Wang T, et al. (2015) Estrogen-related receptor α (ERRα) and ERRγ are essential coordinators of cardiac metabolism and function. *Mol Cell Biol* 35:1281–1298.
19. Yoshihara E, et al. (2016) ERRγ is required for the metabolic maturation of therapeutically functional glucose-responsive β cells. *Cell Metab* 23:622–634.
20. Gan Z, et al. (2013) Nuclear receptor/microRNA circuitry links muscle fiber type to energy metabolism. *J Clin Invest* 123:2564–2575.
21. Gantner ML, Hazen BC, Eury E, Brown EL, Kralli A (2016) Complementary roles of estrogen-related receptors in brown adipocyte thermogenic function. *Endocrinology* 157:4770–4781.
22. Ahmadian M, et al. (2018) ERRγ preserves brown fat innate thermogenic activity. *Cell Rep* 22:2849–2859.
23. Dufour CR, et al. (2007) Genome-wide orchestration of cardiac functions by the orphan nuclear receptors ERRalpha and gamma. *Cell Metab* 5:345–356.
24. Berry R, et al. (2011) Esrrg functions in early branch generation of the ureteric bud and is essential for normal development of the renal papilla. *Hum Mol Genet* 20: 917–926.
25. Harewood L, et al. (2010) Bilateral renal agenesis/hypoplasia/dysplasia (BRAHD): Postmortem analysis of 45 cases with breakpoint mapping of two de novo translocations. *PLoS One* 5:e12375.
26. Muzumdar MD, Tasic B, Miyamichi K, Li L, Luo L (2007) A global double-fluorescent Cre reporter mouse. *Genesis* 45:593–605.
27. Balthasar N, et al. (2005) Divergence of melanocortin pathways in the control of food intake and energy expenditure. *Cell* 123:493–505.
28. van den Heuvel LP, Assink K, Willemsen M, Monnens L (2002) Autosomal recessive renal glucosuria attributable to a mutation in the sodium glucose cotransporter (SGLT2). *Hum Genet* 111:544–547.
29. Chao EC, Henry RR (2010) SGLT2 inhibition–A novel strategy for diabetes treatment. *Nat Rev Drug Discov* 9:551–559.
30. Vallon V (2015) The mechanisms and therapeutic potential of SGLT2 inhibitors in diabetes mellitus. *Annu Rev Med* 66:255–270.
31. Anık A, Çatlı G, Abacı A, Böber E (2015) Maturity-onset diabetes of the young (MODY): An update. *J Pediatr Endocrinol Metab* 28:251–263.
32. Lazzaro D, De Simone V, De Magistris L, Lehtonen E, Cortese R (1992) LFB1 and LFB3 homeoproteins are sequentially expressed during kidney development. *Development* 114:469–479.
33. Gresh L, et al. (2004) A transcriptional network in polycystic kidney disease. *EMBO J* 23:1657–1668.
34. Clissold RL, Hamilton AJ, Hattersley AT, Ellard S, Bingham C (2015) HNF1B-associated renal and extra-renal disease-an expanding clinical spectrum. *Nat Rev Nephrol* 11: 102–112.
35. Verdeguer F, et al. (2010) A mitotic transcriptional switch in polycystic kidney disease. *Nat Med* 16:106–110.
36. Zhang Y, et al. (2016) HNF6 and Rev-erbα integrate hepatic lipid metabolism by overlapping and distinct transcriptional mechanisms. *Genes Dev* 30:1636–1644.
37. Vallon V, et al. (2011) SGLT2 mediates glucose reabsorption in the early proximal tubule. *J Am Soc Nephrol* 22:104–112.
38. Narkar VA, et al. (2011) Exercise and PGC-1α-independent synchronization of type I muscle metabolism and vasculature by ERRγ. *Cell Metab* 13:283–293.
39. Pei L, et al. (2006) NR4A orphan nuclear receptors are transcriptional regulators of hepatic glucose metabolism. *Nat Med* 12:1048–1055.
40. Pei L, et al. (2011) Thyroid hormone receptor repression is linked to type I pneumocyte-associated respiratory distress syndrome. *Nat Med* 17:1466–1472.
41. Wang T, et al. (2017) GDF15 is a heart-derived hormone that regulates body growth. *EMBO Mol Med* 9:1150–1164.